

國立交通大學

材料科學與工程學研究所

博士論文

側鏈含有菲基-1,3-二氮雜茂之予體-受體結構規則之聚噻吩運用於異質接面太陽能電池上之合成



Synthesis and Characterization of Side Chain  
Tethered Donor-Acceptor Regioregular  
Polythiophene Presenting Phenanthrenyl-Imidazole  
Moieties for Heterojunction Solar Cell Applications

博士生:張耀德

指導教授:韋光華 博士

中華民國九十八年二月

側鏈含有菲基-1,3-二氮雜茂之予體-受體結構規則之聚  
噻吩運用於異質接面太陽能電池上之合成與研究

Synthesis and Characterization of Side Chain Tethered  
Donor-Acceptor Regioregular Polythiophene Presenting  
Phenanthrenyl-Imidazole Moieties for Heterojunction Solar  
Cell Applications

研究生：張耀德

Student : Yao-Te Chang

指導教授：韋光華


Advisor : Kung-Hwa Wei



A Thesis  
Submitted to Department of Materials Science and Engineering  
College of Engineering National Chiao Tung University  
in Partial Fulfillment of the Requirements  
for the Degree of  
Doctor of Philosophy  
In  
Materials Science and Engineering  
February 2009  
Hsinchu, Taiwan, Republic of China

中華民國九十八年二月

## *Table of Content*

Abstract	IX
摘要	XII
誌謝	XIV
<b>Chapter 1: Introduction</b>	<b>1</b>
<i>1-1 Introduction of Polymer Solar Cell</i>	1
<i>1-2 The Basis Principle of Polymer Solar Cell</i>	2
<i>1-3 Materials of Polymer Solar Cell</i>	6
<i>1-4 Motivation</i>	11
<b>Chapter 2 : Soluble Phenanthrenyl-Imidazole-Presenting Regioregular Poly(3-octylthiophene) Copolymers having Tunable Bandgaps for Solar Cell Applications</b>	<b>14</b>
<i>2-1. Introduction</i>	15
<i>2-2. Experimental</i>	20
<i>2-3. Results and Discussion</i>	29
<i>2-4. Conclusions</i>	45
	
<b>Chapter 3: Intramolecular Donor–Acceptor Regioregular Poly(3-hexylthiophene)s Presenting Octylphenanthrenyl-Imidazole Moieties Exhibit Enhanced Charge Transfer for Heterojunction Solar Cell Applications</b>	<b>46</b>
<i>3-1. Introduction</i>	47
<i>3-2. Experimental</i>	53
<i>3-3. Results and Discussion</i>	66
<i>3-4. Conclusions</i>	90
<b>Chapter 4: Intramolecular Donor–Acceptor Regioregular Poly(hexylphenanthrenyl-imidazole thiophene) Exhibits Enhanced Hole Mobility for Heterojunction Solar Cell Applications</b>	<b>91</b>

<i>4-1. Introduction</i>	92
<i>4-2. Experimental</i>	96
<i>4-3. Results and Discussion</i>	104
<i>4-4. Conclusions</i>	116
<b>Chapter 5. Conclusions</b>	117
<b>References</b>	120
<b>Publications</b>	136
<b>學經歷資料</b>	138



## *Figure Lists*

### **Chapter 1: Introduction**

**Figure 1-1.** Schematic drawing of the working principle and Current-Voltage characteristics of an organic photovoltaic cell. 4-5

**Figure 1-2.** Donor and acceptor materials used in polymer-fullerene bulk-heterojunction solar cells. 7

### **Chapter 2 : Soluble Phenanthrenyl-Imidazole-Presenting Regioregular Poly(3-octylthiophene) Copolymers having Tunable Bandgaps for Solar Cell Applications**

**Figure 2-1.** The  $^1\text{H}$  NMR spectra of **M2**, **P00**, **P37**, **P55**, and **P82**. 30

**Figure 2-2.** FTIR spectra of **M2**, **P00**, and **P37**. 31

**Figure 2-3.** The thermal degradation temperature of synthesized polymers 33

**Figure 2-4.** UV-Vis spectra of **P00** and **P82** recorded in THF solution. 34

**Figure 2-5.** The UV-Vis spectra of **P00** and **P82** recorded in the solid state. 36

**Figure 2-6.** PL spectra, normalized to the number of absorbed photons, of all seven polymers in solution state. 37

**Figure 2-7.** PL spectra, normalized to the number of absorbed photons, of synthesized polymers in the solid state. 38

**Figure 2-8.** Current density-voltage characteristics of illuminated (AM 1.5G,  $100 \text{ mW/cm}^2$ ) polymer solar cells incorporating **P00**, **P55**, **P73**, and **P82** and **PCBM**. 39

**Figure 2-9. (a)** The external quantum efficiency of **P00**, **P73** and **P82/PCBM** solar cells. 42

**Figure 2-9. (b)** The UV-Vis absorption of the copolymer/PCBM blends

experience the same annealing condition as that of the device. 44

### **Chapter 3: Intramolecular Donor–Acceptor Regioregular Poly(3-hexylthiophene)s Presenting Octylphenanthrenyl-Imidazole Moieties Exhibit Enhanced Charge Transfer for Heterojunction Solar Cell Applications**

**Figure 3-1.** The <sup>1</sup>H NMR spectra of **M2**, **P3HT**, **P46**, **P82**, and **P91**. 67

**Figure 3-2.** UV–Vis spectra of **P3HT** and **P91** in the solid state. 68

**Figure 3-3.** The chemical structure diagram of HT and octylphenanthrenyl-imidazole moiety. 70

**Figure 3-4.** PL spectra, normalized to the number of absorbed photons, of the synthesized polymers in the solid state. 72

**Figure 3-5.** Normalized fluorescence transients of (A) **P3HT** and (B) **P91** coated on quartz, recorded at values of  $t_{ex}$  and  $t_{em}$  at 440 and 600 nm, respectively. 76

**Figure 3-6.** Time-resolved transients of (A) **P3HT**, (B) the blend of **P3HT** and **PCBM**, (C) **P91**, and (D) the blend of **P91** and **PCBM** coated on quartz at values of  $t_{ex}$  and  $t_{em}$  of 440 and 600 nm, respectively. 77

**Figure 3-7.** Time-resolved transients of (A) **P3HT**, (B) the blend of **P3HT** and **PCBM**, (C) **P91**, and (D) the blend of **P91** and **PCBM** coated on quartz at values of  $t_{ex}$  and  $t_{em}$  of 440 and 620 nm, respectively. 77

**Figure 3-8.** Time-resolved transients of (A) **P3HT**, (B) the blend of **P3HT** and **PCBM**, (C) **P91**, and (D) the blend of **P91** and **PCBM** coated on quartz at values of  $t_{ex}$  and  $t_{em}$  of 440 and 660 nm, respectively. 78

**Figure 3-9.** External quantum efficiencies of the copolymer/**PCBM** solar cells. 78

**Figure 3-10.** Current density–voltage characteristics of illuminated (AM 1.5G, 100 mW/cm<sup>2</sup>) polymer solar cells incorporating self-made

**P3HT, P64, P82, and P91 and PCBM.** 84

**Figure 3-11.** The current density vs. wavelength diagram of self-made **P3HT/PCBM, P64/PCBM, P82/PCBM, and P91/PCBM** devices. 84

**Figure 3-12.** The atomic force microscopy images of a) self-made **P3HT/PCBM** and b) **P91/PCBM** films. 99

#### **Chapter 4: Intramolecular Donor–Acceptor Regioregular Poly(hexylphenanthrenyl-imidazole thiophene) Exhibits Enhanced Hole Mobility for Heterojunction Solar Cell Applications**

**Figure 4-1.** a) UV–Vis spectra of **P3HT/PCBM** as cast and **PHPIT/PCBM** annealed at 120 °C in the solid state, and the solar spectrum.  
b) CV bandgap data for **PHPIT, PEDOT, PCBM, Al, and ITO.** 105

**Figure 4-2.** Current–voltage characteristics of illuminated (AM 1.5G, 100 mW/cm<sup>2</sup>) polymer/PCBM (1:1, w/w) solar cells. 107

**Figure 4-3.** Photocurrents of diodes that were illuminated at AM 1.5G and 100 mW/cm<sup>2</sup> after annealing at various temperatures for 30 min. 108

**Figure 4-4.** Atomic force microscopy (AFM) images of **PHPIT/PCBM** films a) as cast and annealed at 120 °C for b) 20, c) 30, and d) 45 min. 110

**Figure 4-5.** EQEs of devices containing **PHPIT/PCBM** blends (1:1, w/w) annealed at 120 °C for various times. 112

**Figure 4-6.** Dark *J–V* curves for a) electron- and b) hole-dominated carrier devices incorporating **PHPIT/PCBM** (1:1, w/w) annealed at 120 °C for various times. 114

## *Schemes and Table Lists*

### **Chapter 1: Introduction**

**Scheme 1-1.** General mechanism for photoenergy conversion in excitonic solar cells. 3

**Scheme 1-2.** Elementary steps in the process of photoinduced charge separation for a donor (D) and an acceptor (A). 4

**Scheme 1-3.** The schematic draw of the five contributions of the bandgap of polyaromatic linear conjugated systems. 12

### **Chapter 2 : Soluble Phenanthrenyl-Imidazole-Presenting Regioregular Poly(3-octylthiophene) Copolymers having Tunable Bandgaps for Solar Cell Applications**

**Scheme 2-1.** The synthetic scheme of **M1** and **M2**; NBS: *N*-bromosuccinimide. 18

**Scheme 2-2.** The Grignard Metathesis polymerization of **M1** and **M2**; THF: tetrahydrofuran. 19

**Table 2-1.** Molecular weights and thermal properties of synthesized polymers. 33

**Table 2-2.** UV-Visible absorption peaks and optical bandgaps of synthesized polymers. 36

**Table 2-3.** Redox data, HOMO, LUMO energy levels, and band gap energies of our synthesized polymers. 36

**Table 2-4.** Photovoltaic properties of the polymer solar cells. 41



### **Chapter 3: Intramolecular Donor–Acceptor Regioregular Poly(3-hexylthiophene)s Presenting Octylphenanthrenyl-Imidazole Moieties Exhibit Enhanced Charge Transfer for Heterojunction Solar Cell Applications**

**Scheme 3-1.** Synthesis of **M1** and **M2**; NBS: *N*-bromosuccinimide. 51

**Scheme 3-2.** Grignard metathesis polymerization of **M1** and **M2**; THF: tetrahydrofuran. 52

**Table 3-1.** Molecular Weights and Thermal Properties of Synthesized Polymers. 68

**Table 3-2.** UV–Vis Absorption Peaks and Optical Bandgaps of Synthesized Polymers. 71

**Table 3-3.** Redox data, HOMO, LUMO energy levels, and band gap energies of our synthesized polymers. 71

**Table 3-4.** Rate Constants for the Polymer, its Blend with **PCBM**, and Electron Transfer for **P3HT** and **P91** at Different Wavelengths. 79

**Table 3-5.** Photovoltaic Properties of the Polymer Solar Cells. 85

**Table 3-6.** Redox data, HOMO, LUMO energy levels, and band gap energies of our synthesized polymers 88

### **Chapter 4: Intramolecular Donor–Acceptor Regioregular Poly(hexylphenanthrenyl-imidazole thiophene) Exhibits Enhanced Hole Mobility for Heterojunction Solar Cell Applications**

**Scheme 4-1.** Synthesis of the monomer and polymer; NBS: *N*-bromosuccinimide; THF: tetrahydrofuran; dppp: 1,3-bis(diphenylphosphino)propane. 95

**Table 4-1.** Photovoltaic properties of polymer solar cells annealed at 120 °C

for various lengths of time and of **P3HT/PCBM** annealed at 120 °C for 30 min. 107

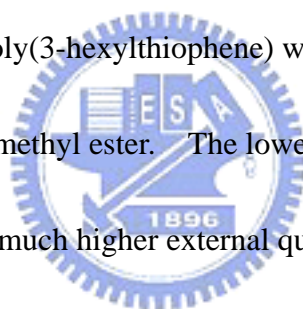
**Table 4-2.** Hole mobilities, electron mobilities, and hole-to-electron-mobility ratios of **P3HT/PCBM** annealed at 120 °C for 30 min and **PHPIT/PCBM** annealed at 120 °C for various lengths of time. 115



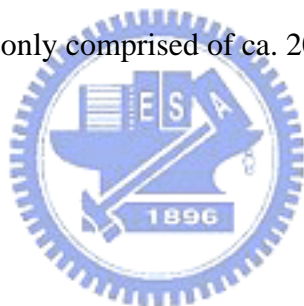
## Abstract

In this dissertation, a series of polythiophene copolymers have been synthesized to study to photovoltaic characteristics. First of all, we have used Grignard metathesis polymerization to successfully synthesize a series of regioregular polythiophene copolymers that contain electron-withdrawing and conjugated phenanthrenyl-imidazole moieties as side chains. The introduction of the phenanthrenyl-imidazole moieties onto the side chains of the regioregular polythiophenes increased their conjugation lengths and thermal stabilities and altered their band gap structures. The band gap energies, determined from the onset of optical absorption, could be tuned from 1.89 eV to 1.77 eV by controlling the number of phenanthrenyl-imidazole moieties in the copolymers. Moreover, the observed quenching in the photoluminescence of these copolymers increases with the number of phenanthrenyl-imidazole moieties in the copolymers, owing to the fast deactivation of the excited state by the electron-transfer reaction. Both the lowered bandgap and fast charge transfer contribute to the much higher external quantum efficiency of the poly(3-octylthiophene)-side-chain-tethered phenanthrenyl-imidazole than that of pure poly(3-octylthiophene), leading to much higher short circuit current density. In particular, the short circuit current densities of the device containing the copolymer having 80 mol % phenanthrenyl-imidazole, **P82**, improved to 14.2 mA/cm<sup>2</sup> from 8.7

mA/cm<sup>2</sup> for the device of pure poly(3-octylthiophene), **P00**, an increase of 62%. In addition, the maximum power conversion efficiency improves to 2.80% for **P82** from 1.22% for **P00** (pure **P3OT**). Second, intramolecular donor–acceptor structures prepared by binding conjugated octylphenanthrenyl-imidazole moieties covalently onto the side chains of regioregular poly(3-hexylthiophene)s exhibit lowered bandgaps and enhanced electron transfer. For instance, conjugating 90 mol% octylphenanthrenyl-imidazole moieties onto poly(3-hexylthiophene) chains reduced the optical bandgap from 1.91 to 1.80 eV, and the electron transfer probability was at least twice than that of pure poly(3-hexylthiophene) when blended with [6,6]-phenyl-C<sub>61</sub>-butyric acid methyl ester. The lowered bandgap and the fast charge transfer both contribute to the much higher external quantum efficiencies—and, thus, much higher short-circuit current densities—for the copolymers presenting octylphenanthrenyl-imidazole moieties, relative to those of pure poly(3-hexylthiophene)s. In particular, the short-circuit current density of a device containing the copolymer presenting 90 mol% octylphenanthrenyl-imidazole moieties improved to 13.7 mA/cm<sup>2</sup> from 8.3 mA/cm<sup>2</sup> for the device containing pure poly(3-hexylthiophene)—an increase of 65%. In addition, the maximum power conversion efficiency was 3.45% for the copolymer presenting 90 mol% octylphenanthrenyl-imidazole moieties. Finally, **PHPIT**, a new kind of



intramolecular D–A side-chain-tethered hexylphenanthrenyl-imidazole polythiophene has been synthesized. The visible light absorption of the **PHPIT/PCBM** blend is enhanced by the presence of the electron-withdrawing hexylphenanthrenyl-imidazole. The EQE of the device was maximized when the **PHPIT/PCBM** blend experienced annealing at 120 °C for 30 min. The more-balanced electron and hole mobilities and the enhanced visible and internal light absorptions in the devices consisting of annealed **PHPIT/PCBM** blends both contributed to a much higher short-circuit current density, which in turn led to a power conversion efficiency as high as 4.1%, despite the fact that **PHPIT** is only comprised of ca. 20 repeating units.



## 摘要

本論文乃研究探討利用 Grignard metathesis 來合成一系列聚噻吩高分子來探討高分子本身之光電效應。而論文的第一部份，是以合成出一系列聚(辛基-噻吩)(P3OT)衍生物，而在其側鏈上導入一菲基-1,3-二氮雜茂(phenanthrenyl-imidazole)，希望藉由導入此官能基之後可以增加高分子本身主鏈的共軛長度，不但可以將高分子本身的能隙(bandgap)降低，且具有電子傳輸的效果，而且在光激發光方面，因為隨呢導入菲基-1,3-二氮雜茂比例增加，發光淬息(quenching)現象就越來越明顯，也因為如此促使了高分子的製作成元件之後，外部量子效率(external quantum efficiencies)增加，相對的在含有比較高比例的菲基-1,3-二氮雜茂聚(辛基-噻吩)高分子之光電流(short-circuit current density)也提升了(由  $8.7 \text{ mA/cm}^2$  提升到  $14.2 \text{ mA/cm}^2$ ，提升了約 62%)，光電轉換效率也增加了(由 1.22% 提升到 2.80%)。第二部份則是，利用 Grignard metathesis 來合成一系列聚(己基-噻吩)(P3HT)高分子衍生物，然後將菲基-1,3-二氮雜茂末端作了修飾導入了兩個辛基長碳鏈提升溶解度，相同的，導入了辛基-菲基-1,3-二氮雜茂之後，高分子本身的能隙降低，發光淬息(quenching)現象就越來越明顯，而此系列之高分子開路光電流也提升了(由  $8.3 \text{ mA/cm}^2$  提升到  $13.7 \text{ mA/cm}^2$ ，提升了約 65%)，光電轉換效率改善到 3.45%。第三部份，則是合成一高分子，PHPIT，

在菲基-1,3-二氮雜茂末端修飾導入了三個己基官能基到單體本身之中，而此高分子與[6,6]-苯基-C<sub>61</sub>-丁酸甲酯 ([6,6]-phenyl-C<sub>61</sub>-butyric acid methyl ester) (PCBM) 摻混之後，對於可見光之吸光能力增強，而製作成元件之後發現，在迴火溫度為 120 °C，持續 30 分鐘的情況下，其外部量子效率最高，而在此條件下，也因為較為平衡的電子電動流動率也促使了較高的光電流密度，因此，此高分子在此條件下之光電轉換效率約為 4.1%。



## 誌謝

終於也輪到我寫誌謝了，一直以來看到數位實驗室先輩的博士論文的完成總是花上了一千多個日子，而我比較辛苦花了兩千多個日子來完成，當然期間的酸甜苦辣的往事也歷歷在目，激勵了我能夠在最後完成了這部論文。要感謝的人實在太多了，謹以此文表達我衷心的謝意。

首先我得感謝指導教授韋光華老師，沒有他提供舒適的研究環境，已及充分的經費已經儀器的支持，這部論文是無法完成的。而且他對於研究上的要求以及指導叮嚀，除了激勵我成長之外更讓我體會到做研究的酸甜苦辣，並且也給予我再外來發展上一些比較客觀的批與指教讓我學會了人生中做人做事的道理。也很感謝刁維光老師在論文研究過程中的幫忙與教導，以及碩士班時期諄諄教誨的許慶豐老師使我在有機合成這條路上可以研究比較平順。也因為有諸位師長朋友的幫助，讓我可以渡過諸多困難與挫折。以及最後能來參加我口試的各位口試委員們：黃華宗、林建村、陳文章、林宏洲以及郭宗枋諸位師長給予我的意見與鼓勵。

實驗室畢業的學長田運宜 (帥帥)、呂奇明 (Mickey)、翁錦成 (小豬)、葉孝蔚、李中斌學長，感謝他們讓我體會到做研究就是要一股作氣的完成，以及他們的不服輸人生觀。以及實驗室的夥伴們：我已畢業同窗室友兼實驗室夥伴嘉宏、比我早畢業的學弟清茂、擅於提供意見以及解決問題的旭生、快樂過生活的茂源、知識淵博以及籃球球友碩麟、阿彌佗佛的陳冠宇、製造歡樂的陳振平、認真開朗的李紹睿、實事求是積極進取的蘇明鑫、籃球狂熱紀傑元、陳紘揚、世紀帝國高手阿川、KTV 歌友璨丞、實驗室的諸、位美女們琬琪、靜宜、孟婷、慧玫、含章、世莉、姿吟、曉文、大姊頭級行事作風阿莎力的克瑤、熱心助人天真樂觀的美女助理克瑜、實驗室諸位碩士班的新生、林宏洲老師實驗室球友小吳、許慶豐老師實驗室的芳奕、冷翰與黃華宗老師實驗室的籃球夥伴們、系辦的諸位助理小姐琳婷、蕙馨、素瓊、印度博士後研究員 Dina 與 Dahna。

衷心的感謝你們，沒有你們一路上的陪伴，就沒有在這學校裡面的許多回憶以及感動。

最後，僅以本論文獻給我最親愛的母親以及家人，感謝他們在我求學過程中給予我的一些意見以及精神上與生活上的支持使我可以無後顧之憂得以順利完成這部論文得以畢業。

張耀德 2009. 2. 27



## Chapter 1: Introduction

### *1-1 Introduction of Polymer Solar Cell*

The development of conjugated polymers that possess extended delocalized  $\pi$ -electrons for use in organic optoelectronic devices has been an area of extensive investigation, with some studies having focused on solar cell devices based on bulk heterojunctions using conjugated polymers.<sup>[1-7]</sup> Recently, research into conjugated polymers containing electron donor–acceptor pairs has become quite active<sup>[8]</sup> because such materials exhibit specific optical, electrical, and electronic properties. Polymer solar cells have attracted considerable attention in the past few years owing to their potential of providing environmentally safe, flexible, lightweight, inexpensive, efficient solar cells. Especially, bulk-heterojunction solar cells consisting of a mixture of a conjugated donor polymer with a methanofullerene acceptor are considered as a promising approach. Here a brief introduction and overview is given of the field of polymer solar cells. In the more than 20 years since the seminal work of Tang,<sup>[2]</sup> organic solar cells have undergone a gradual evolution that has led to energy conversion efficiencies ( $\eta$ , see Figure 1) of about 5%.<sup>[3-8]</sup> Two main approaches have been explored in the effort to develop viable devices: the donor–acceptor bilayer,<sup>[8-10]</sup> commonly achieved by vacuum deposition of molecular components,<sup>[11]</sup> and the so-called bulk heterojunction (BHJ),<sup>[12, 13]</sup> which is represented in the ideal case as a

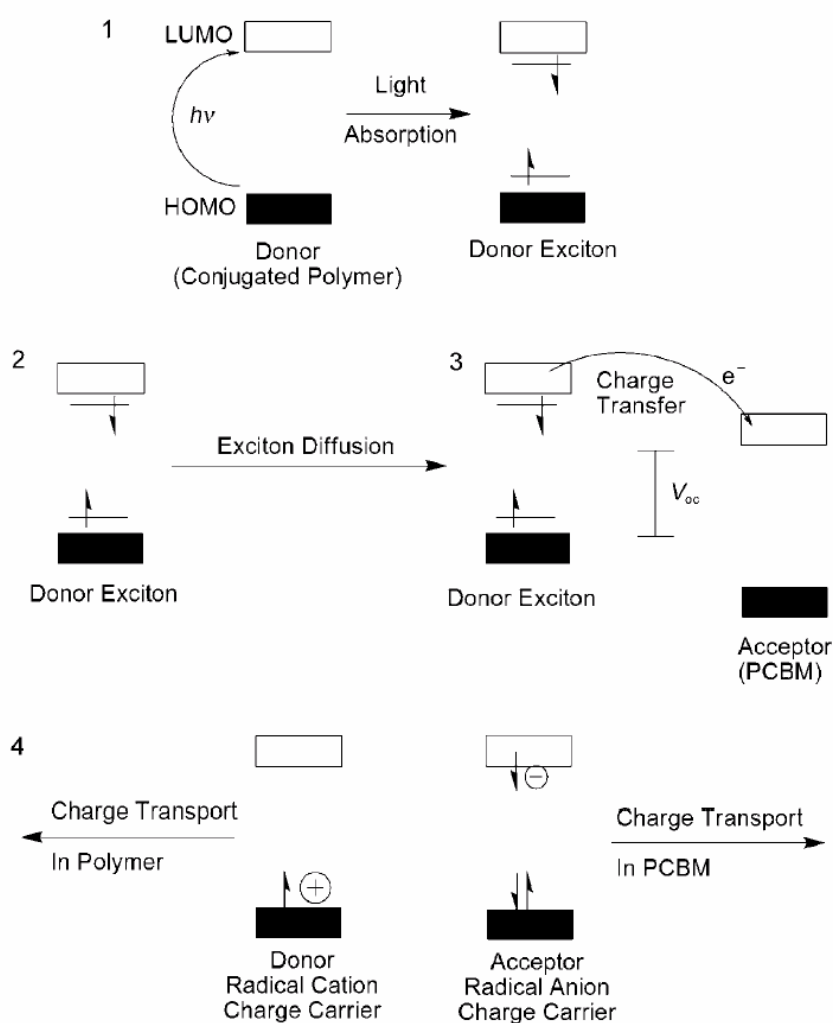
bicontinuous composite of donor and acceptor phases, thereby maximizing the all-important interfacial area between the donors and acceptors.

### ***1-2 The Basis Principle of Polymer Solar Cell***

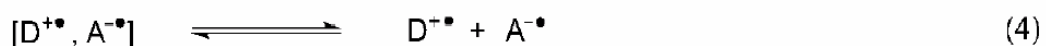
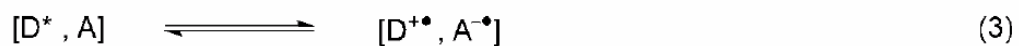
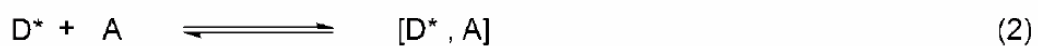
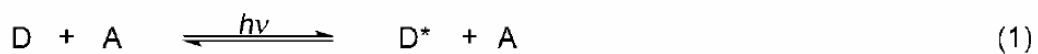
Efforts to optimize the performance of organic solar cells should find their basis in the fundamental mechanism of operation. Scheme 1-1 illustrates the mechanism by which light energy is converted into electrical energy in the devices. The energy conversion process has four fundamental steps in the commonly accepted mechanism:<sup>[14]</sup> 1) Absorption of light and generation of excitons, 2) diffusion of the excitons, 3) dissociation of the excitons with generation of charge, and 4) charge transport and charge collection. Figure 1-1 shows a schematic representation of a typical BHJ solar cell, illustrating the components involved in the mechanistic steps as well as a current–voltage curve defining the primary quantities used to validate the performance of a solar cell. The elementary steps involved in the pathway from photoexcitation to the generation of free charges are shown in Scheme 1-2.<sup>[15, 16]</sup>

The processes can also occur in an analogous fashion in the case of an excited acceptor, and the details of these mechanistic steps have been described extensively in the literature.<sup>[16]</sup> The key point is that electron transfer is not as simple as depicted in Scheme 1-1. The process must be energetically favorable to form the geminate pair in step 3 of Scheme 1-2 and an energetic driving force must exist to separate this

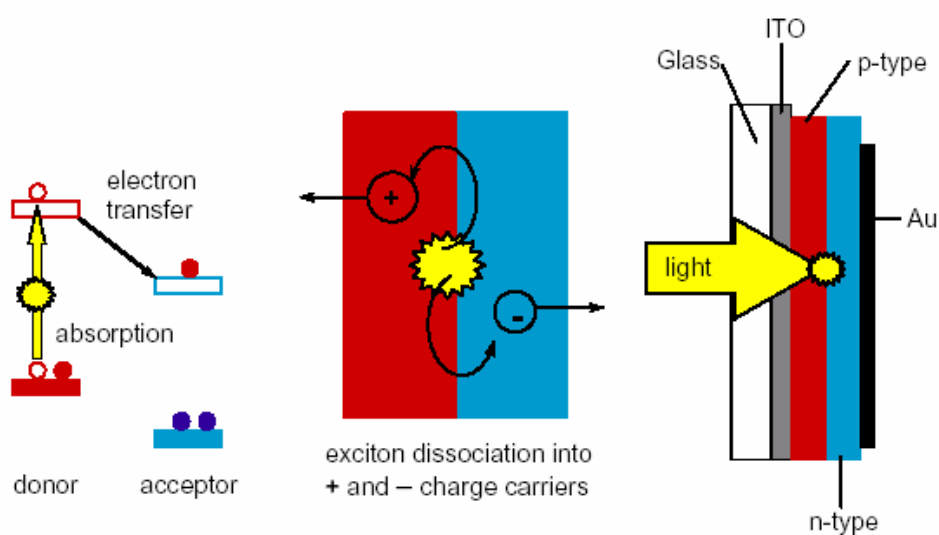
electron–hole pair. The open circuit voltage ( $V_{oc}$ ) is also governed by the energetic relationship between the donor and the acceptor (Scheme 1-1) rather than the work functions of the cathode and anode, as would be expected from a simplistic view of these diode devices. Specifically, the energy difference between the HOMO of the donor and the LUMO of the acceptor is found to most closely correlate with the  $V_{oc}$  value.<sup>[18, 19]</sup>



**Scheme 1-1.** General mechanism for photoenergy conversion in excitonic solar cells.



**Scheme 1-2.** Elementary steps in the process of photoinduced charge separation for a donor (D) and an acceptor (A): 1) Photoexcitation of the donor; 2) diffusion of the exciton and formation of an encounter pair; 3) electron transfer within the encounter pair to form a geminate pair; 4) charge separation.



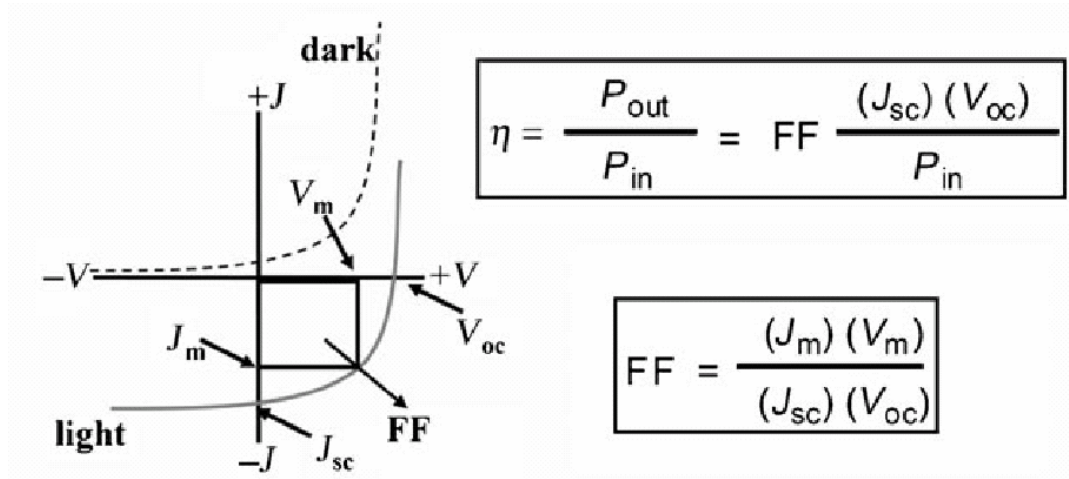
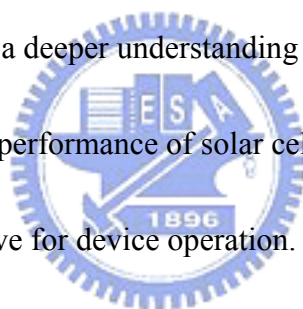


**Figure 1-1.** Schematic drawing of the working principle of an organic photovoltaic cell. Illumination of donor (in red) through a transparent electrode (ITO) results in the photoexcited state of the donor, in which an electron is promoted from the highest occupied molecular orbital (HOMO) to the lowest unoccupied molecular orbital (LUMO) of the donor. The typical current–voltage characteristics for dark and light current in a solar cell illustrate the important parameters for such devices:  $J_{sc}$  is the short-circuit current density,  $V_{oc}$  is the open circuit voltage,  $J_m$  and  $V_m$  are the current and voltage at the maximum power point, and FF is the fill factor. The efficiency ( $\eta$ ) is defined, both simplistically as the ratio of power out ( $P_{out}$ ) to power in ( $P_{in}$ ), as well as in terms of the relevant parameters derived from the current–voltage relationship.

### ***1-3 Literature Review of Polymer Solar Cell Materials***

In combining electron donating (*p*-type) and electron accepting (*n*-type) materials in the active layer of a solar cell, care must be taken that excitons created in either material can diffuse to the interface, to enable charge separation. Due to their short lifetime and low mobility, the diffusion length of excitons in organic semiconductors is limited to about ~10 nm only. While the best currently available devices are composed of P3HT/PCBM and MDMO-PPV/PCBM composites as shown in Figure 1-2, <sup>[20-22]</sup> much effort is being devoted to enhancing the efficiency of BHJ solar cells by developing a deeper understanding of the processes and interactions that dominate the performance of solar cells and developing new materials that are more effective for device operation. In the following sections, several key areas that have been examined in an attempt to improve solar energy conversion will be discussed along with key concepts that ought to be considered in the search for high efficiency. The prototypical polymer solar cells based on MDMO-PPV/PCBM and P3HT/PCBM composites discussed above show the extent of optimization that is required to generate efficient polymer–fullerene solar cells. However, a variety of other approaches have been used in attempts to overcome some of the inherent limitations of these typical examples. These limitations can largely be gleaned directly by a consideration of the fundamental mechanism for



photoconversion in these excitonic solar cells (Scheme 1-1), which begins with light absorption.

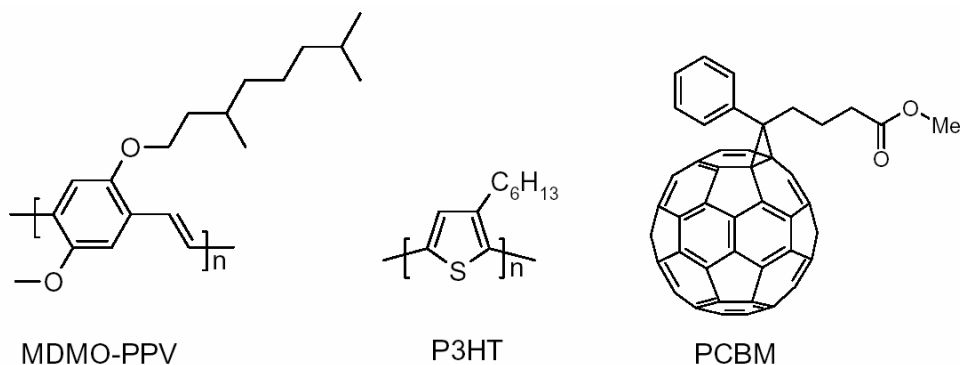


**Figure 1-2.** Donor and acceptor materials used in polymer-fullerene

bulk-heterojunction solar cells. Donors: MDMO-PPV =

poly[2-methoxy-5-(3',7'-dimethyloctyloxy)-*p*-phenylene vinylene]; P3HT=

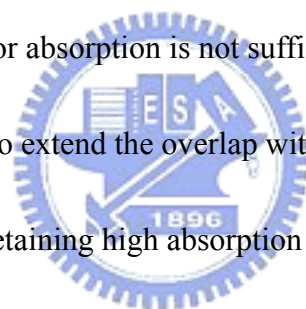
poly(3-hexylthiophene); Acceptors: PCBM: [6,6]-phenyl-C<sub>61</sub>-butyric acid methyl ester.

The photon flux reaching the surface of the earth from the sun occurs at a maximum of approximately 1.8 eV (700 nm); however, neither MDMOPPV (E<sub>g</sub>=2.2 eV) nor P3HT (E<sub>g</sub>=1.9 eV) can effectively harvest photons from the solar spectrum.

It is calculated that P3HT is only capable of absorbing about 46% of the available solar photons<sup>[23]</sup> and only in the wavelength range between 350 nm and 650 nm.

The limitation in the absorption is primarily due to limited spectral breadth rather than the absorption coefficient, as conjugated polymers typically have extremely high

absorption coefficients on the order of  $10^5 \text{ cm}^{-1}$ .<sup>[24]</sup> Developing a polymer that could capture all of the solar photons down to 1.1 eV would allow absorption of 77% of all the solar photons.<sup>[25]</sup> Expanding the spectral breadth of absorption in polymer–fullerene composites has most commonly been pursued by extending (or shifting) the polymer absorption spectrum into the near-infrared region. This is primarily achieved through the use of low-bandgap polymers, which has led to efficiencies as high as 3.5%<sup>[23]</sup> in polymer–fullerene composite solar cells. While low-bandgap polymers have often been touted as the solution of this problem, merely having a lower energy onset for absorption is not sufficient to harvest more solar photons. What is needed is to extend the overlap with the solar spectrum to gain broader coverage while also retaining high absorption coefficients at relevant wavelengths and suitable energy levels for interaction with PCBM.



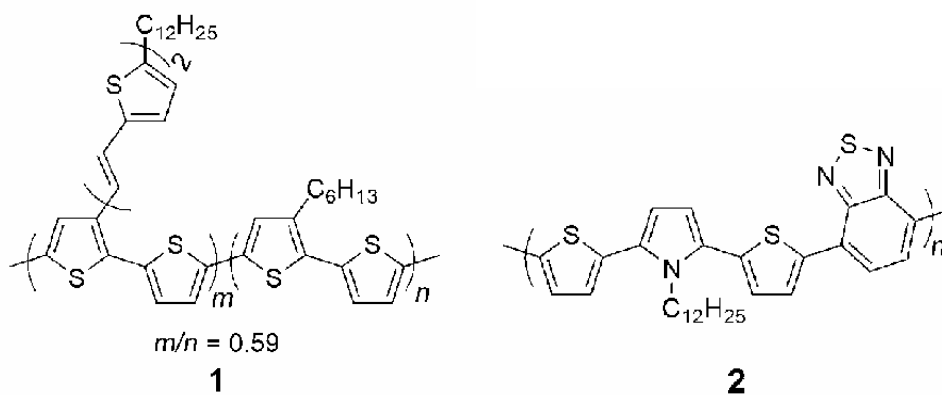
The first approach towards these goals focused on broadening the absorption of known polymers through the UV and visible regions. An excellent example is afforded by poly(3-vinylthiophenes), such as **1**.<sup>[26]</sup> The incorporation of chromophores that are conjugated to the backbone through the 3-vinyl linkage leads to a broadening of the wavelengths at which high photoconversion efficiencies can be achieved. In a direct comparison with P3HT/PCBM devices, cells with polymer **1** afforded 3.2% efficiency versus 2.4% with P3HT under the same conditions. The enhanced

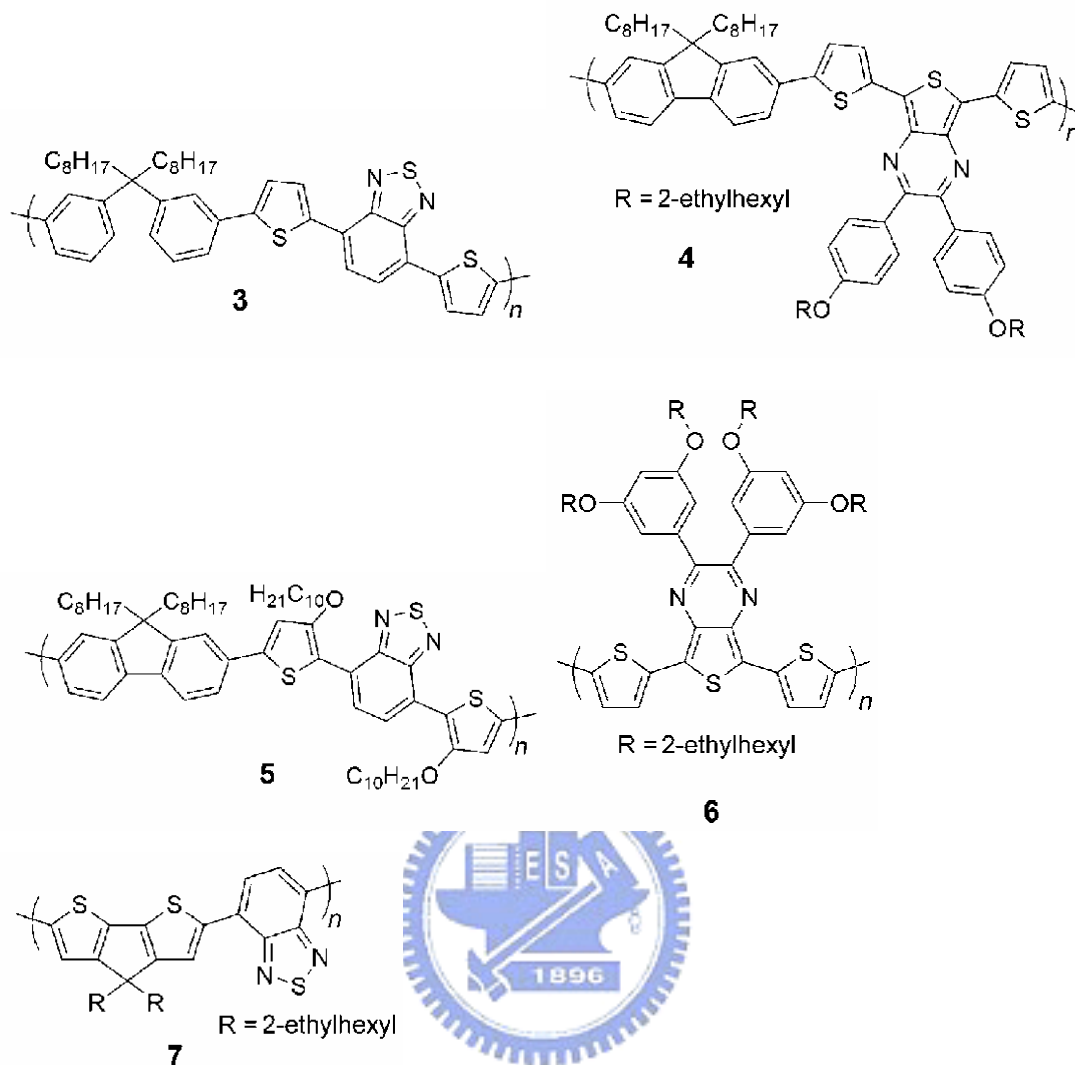


performance of polymer **1** can be attributed to the increased photocurrent in the 400–500 nm range.

The second approach to increase the spectral breadth of the absorbed photons is to synthesize the so-called low-bandgap polymers;<sup>[27]</sup> which is loosely defined as polymers with a bandgap less than 1.5 eV. Compounds **2–7**<sup>[28–33]</sup> represent a few of the more successful polymers employed to-date. The most common synthetic technique used to achieve low-bandgap polymers is the donor–acceptor approach, in which alternating electron-rich and electron-poor units define the polymer backbone.<sup>[34]</sup>

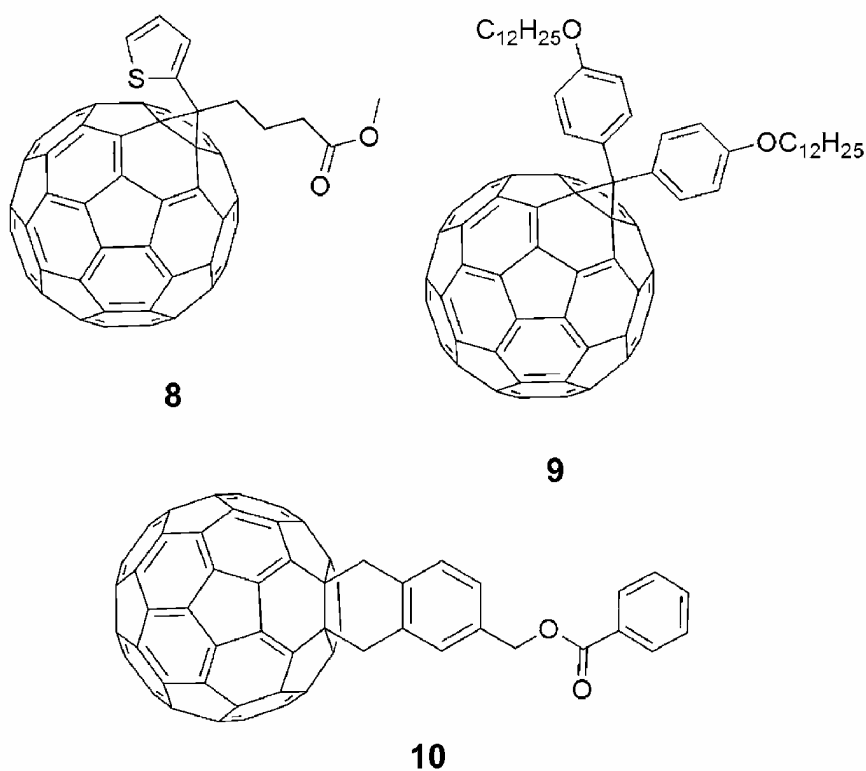
The best examples of this class reported thus far are based almost exclusively on benzothiadiazole (or analogues) as the acceptor in combination with several different donor groups. In addition, the APFO polymers (such as **3**) are reported to afford efficiencies as high as 2.8%<sup>[29]</sup> and EQE values greater than 50% in the 350–600 nm region in 1:3 or 1:4 blends with PCBM.<sup>[35]</sup>





The third approach is to synthesize a variety of soluble  $C_{60}$  derivatives have been synthesized (**8–10**)<sup>[36-38]</sup> and employed in BHJ solar cells with varying success. The focus in this case was not to increase the absorption of visible light, but rather to improve miscibility, the mobility of the charge carriers, and other aspects of performance that are influenced by the structure of the soluble fullerene employed. A further motivation for testing new soluble  $C_{60}$  derivatives is the development of a fundamental structure–property relationship and a guiding design principle for improving the performance of the solar cells through the use of the optimized

fullerene acceptors. For example, the simple benzoate derivative **10** gave the best performance with (un-optimized) efficiencies of 4.5% reported in P3HT solar cells at a polymer/fullerene ratio of 1:0.82, whereas P3HT/PCBM devices prepared in a parallel study showed 4.4% efficiency at an optimal ratio of 1:0.67.



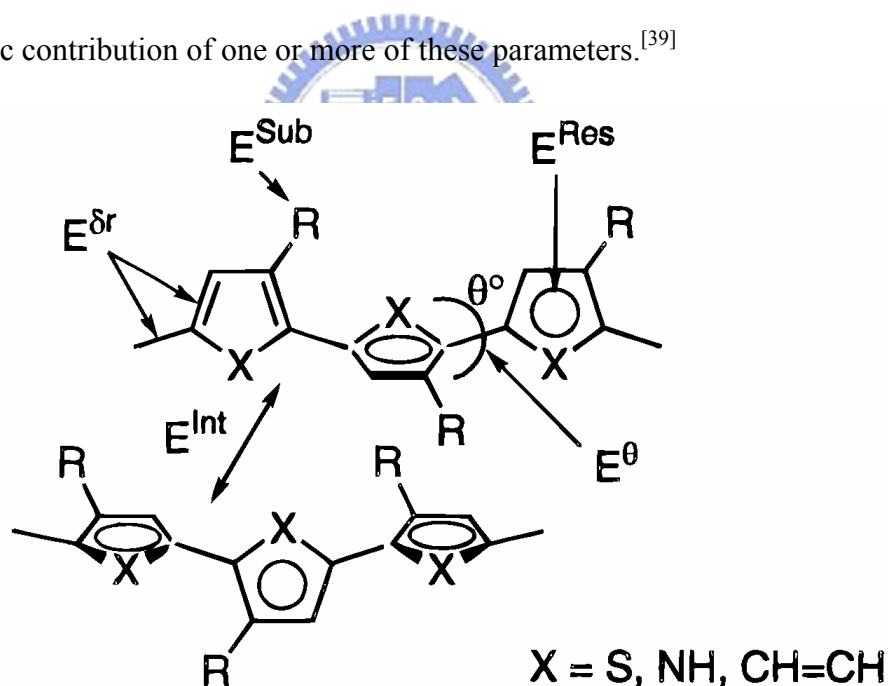
#### 1-4 Motivation

The bandgap of polyaromatic linear conjugated systems is determined by five contributions *i.e.* the energy related to bond length alternation,  $E^{\delta r}$  the mean deviation from planarity  $E^{\theta}$ , the aromatic resonance energy of the cycle  $E^{\text{Res}}$ , the inductive or mesomeric electronic effects of eventual substitution  $E^{\text{Sub}}$ , and the intermolecular or

interchain coupling in the solid state  $E^{\text{int}}$ . (as shown in Scheme 1-3)

$$E_g = E^{\delta r} + E^{\theta} + E^{\text{Res}} + E^{\text{Sub}} + E^{\text{int}}$$

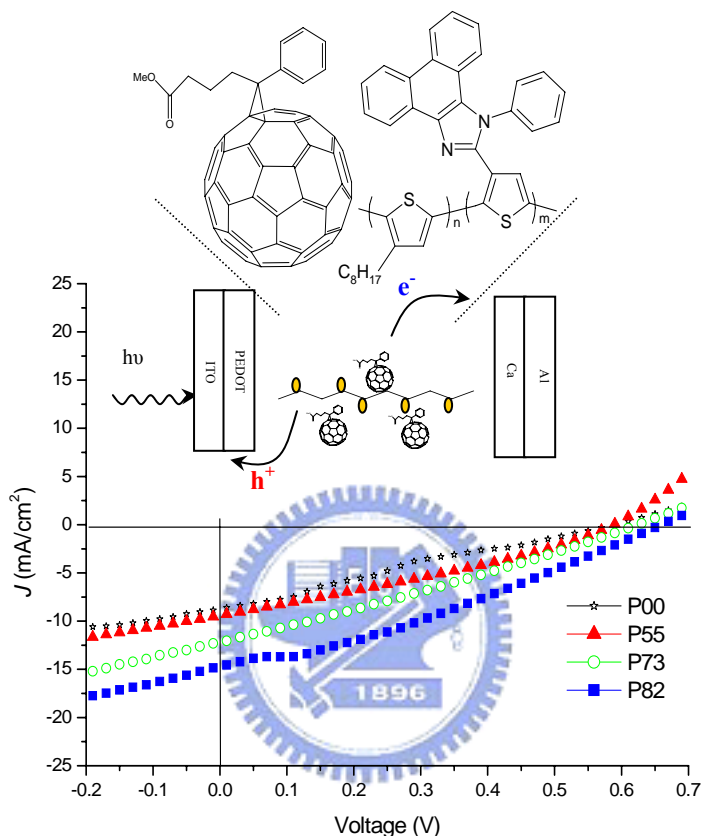
Probably the most important feature of this equation is that it makes clear the various structural variables that have to be mastered in order to control the gap of linear conjugated systems. Consequently, the main synthetic strategies adopted for the design of small bandgap linear conjugated systems will be focused on the reduction of the energetic contribution of one or more of these parameters.<sup>[39]</sup>



**Scheme 1-3.** The schematic draw of the five contributions of the bandgap of polyaromatic linear conjugated systems.

The side-chain effect and the regioregularity affect the absorption wavelength of the conjugation polymers. The side-chain effect has been studied for a period of time but they just used a spacer such as alkyl chain to link the bulky side chain to the polymer main chain, leading to photoluminescence quenching.<sup>[40]</sup> Therefore, to introduce an electron withdrawing group such as phenanthrenyl-imidazole as the side chain and to conjugated to the polymeric main chain would be a curious case for the synthesis of the conjugated polymers (donors) which can maintain the photoluminescence quenching effect and tune the bandgap of the polymers. For bulk heterojunction solar cell, the power conversion efficiency can be tuned by the differences of the regioregularity of alkyl polythiophene such as poly(3-hexylthiophene). This would destroy the crystallinity of the polymeric main chain resulting in the decrease of short-circuit current density. Therefore, to introduce a bulky coplanar moiety such as phenanthrenyl-imidazole as the side chain which is directly conjugated to the polymeric main chain might increase the intramolecular donor-acceptor effect between the polymeric main chain and side chain and the Grignard Metathesis was used to maintain the regioregularity.

## Chapter 2 : Soluble Phenanthrenyl-Imidazole-Presenting Regioregular Poly(3-octylthiophene) Copolymers having Tunable Bandgaps for Solar Cell Applications



A new family of regioregular copoly(3-octylthiophene) side chain tethered phenanthrenyl-imidazole that possess lowered bandgap and enhanced electron transfer property were synthesized for heterojunction polymer/PCBM solar cell applications. The short circuit current density and the power conversion efficiency of the copolymer having 80 mole% phenanthrenyl-imidazole group device improved to 14.2 mA/cm<sup>2</sup> and 2.8%, respectively, from 8.7 mA/cm<sup>2</sup> and 1.22% for pure poly(3-octylthiophene).

## 2-1. Introduction

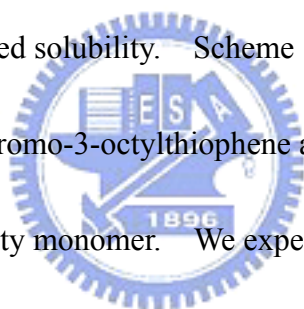
The development of conjugated polymers that possess extended delocalized  $\pi$ -electrons for use in organic optoelectronic devices has advanced dramatically in recent years. In particular, there have been extensive studies into solar cell devices based on bulk heterojunctions formed using conjugated polymers.<sup>[41–48]</sup> The structures of bulk heterojunction polymer solar cells have been prepared from a thin film of the electron-donating conjugated polymer and an electron-accepting species, which has been either another polymer or a set of nanoparticles. Polythiophene derivatives are recognized as being among the most promising materials for solar cell applications because of their excellent light absorption and electronic conductivity. Polymer solar cells containing blends of poly(3-hexylthiophene) and the buckminsterfullerene derivative [6,6]-phenyl-C<sub>61</sub>-butyric acid methyl ester (PCBM) have been studied in depth; recent reports<sup>[43]</sup> have indicated that power conversion efficiencies of around 1% ~ 2% under standard solar conditions (AM 1.5G, 100 mW/cm<sup>2</sup>, 25 °C ). There are a number of ways to proceed toward improving the power conversion efficiencies of these polymer solar cells. For example, varying the annealing temperature and time—to lower the electrical resistance of the devices—and introducing a lower-work-function electrode have been reported.<sup>[49–53]</sup> Alternatively, copolymerization with different conjugated monomers has also been

investigated, but with limited success in improving the power conversion efficiency.<sup>[50]</sup>

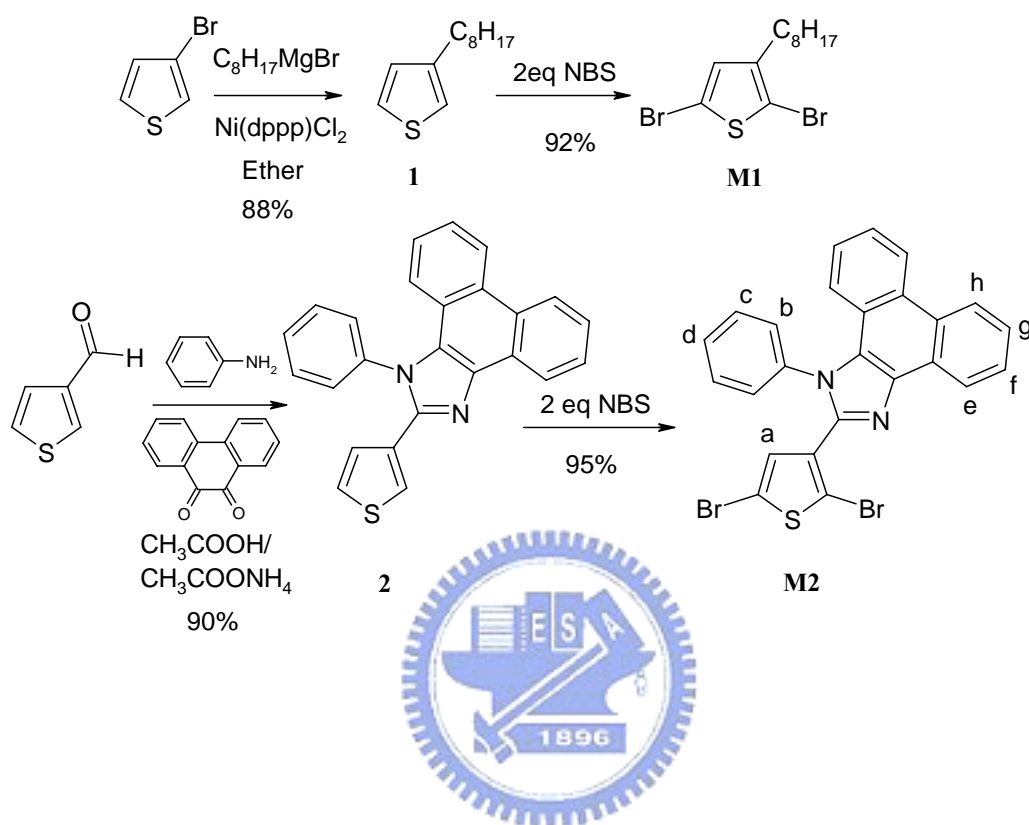
Semiconducting conjugated polymers that are used presently in light emitting diodes typically absorb in the range between 300 and 500 nm, which is only a small portion of the spectrum of sunlight. Thus, another approach toward higher-efficiency polymer solar cells is the use of conjugated polymers that absorb light more effectively. There are two main ways to tackle this problem. The first involves introducing chromophores that have different energy bandgaps into the conjugated polymers, thereby increasing the bandwidth of absorption. This method usually leads to some synthetic difficulties resulting from the typical bulkiness and low reactivity of functionalized chromophores or dyes. The second way is to incorporate electron-withdrawing moieties into side chains that are in conjugation with the main polymer chains. In this way, not only the electron transfer efficiency of the excitons of the side-chain-tethered phenanthrenyl-imidazole polymers can be improved but also their bandgaps can be lowered for matching the wavelength of the maximum photon flux of sunlight (700 nm), which is ca. 1.77 eV.<sup>[54]</sup> The extent of the reduction in the bandgap of the side-chain-tethered phenanthrenyl-imidazole polymers will depend on the effective conjugation length of the system, which are sometimes reduced by steric hindrance. Previously, oxadiazole-, triazole-,



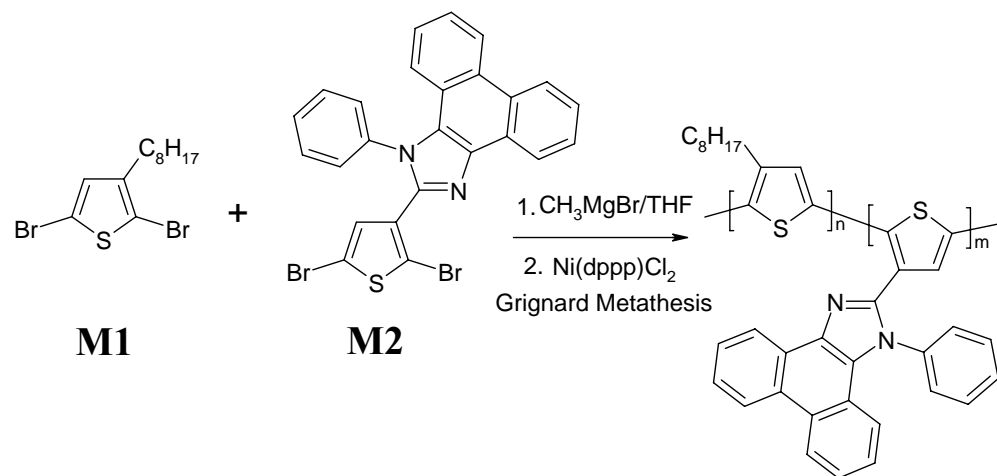
quinoxaline-, imidazole-, and triazine-containing moieties are used in semiconducting polymers for other applications.<sup>[55]</sup> In this present study, we designed an extended conjugated molecular structure in which phenanthrenyl-imidazole moieties were attached covalently to the side chain of thiophene units to form regioregular copolymers that had lowered bandgaps—which were tunable depending on the content of phenanthrenyl-imidazole moieties—and enhanced electron transferring abilities. Because of the poor solubility of the phenanthrenyl-imidazole moiety, we used a thiophene monomer (3-octylthiophene) presenting a long alkyl chain to form copolymers exhibiting improved solubility. Scheme 1 displays our synthetic approaches toward the 2,5-dibromo-3-octylthiophene and the planar phenanthrenyl-imidazole moiety monomer. We expected that the presence of phenanthrenyl-imidazole moieties conjugated to the thiophene units would enhance the electron transfer of polythiophene and alter the energy levels of the highest occupied molecular orbitals (HOMOs) and lowest unoccupied molecular orbitals (LUMOs) of our polymers, thereby decreasing the bandgap and enhancing their photovoltaic properties. Scheme 2-2 displays the copolymerization of the 2,5-dibromo-3-octylthiophene **M1** and 2-(2,5-dibromothiophen-3-yl)-1-phenyl-1*H*-phenanthro[9,10-d]imidazole monomer **M2**, performed using a Grignard metathesis method.



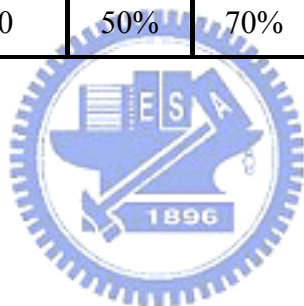
**Scheme 2-1.** The synthetic scheme of **M1** and **M2**; NBS: *N*-bromosuccinimide.



**Scheme 2-2.** The Grignard Metathesis polymerization of **M1** and **M2**; THF: tetrahydrofuran.



Polymer molar ratio	<b>P00</b>	<b>P55</b>	<b>P73</b>	<b>P82</b>
Molar fraction of <b>M1</b>	100%	50%	30%	20%
Molar fraction of <b>M2</b>	0	50%	70%	80%



## 2-2. Experimental

**Materials.** Chemicals were purchased from Aldrich, TCI, or Lancaster.

[6,6]-phenyl-C<sub>61</sub>-butyric acid methyl ester (PCBM) was purchased from Nano-C.

Polyethylenedioxythiophene/polystyrenesulphonate (PEDOT/PSS) was purchased from Baytron (P VP A1 4083).

**Preparation of Monomers:** Scheme 2-1 illustrates the synthetic route used for the preparation of the monomers 2,5-dibromo-3-octylthiophene (**M1**) and 2-(2,5-dibromothiophen-3-yl)-1-phenyl-1*H*-phenanthro[9,10-d]imidazole (**M2**).

1-Phenyl-2-(3-thienyl)-1*H*-phenanthro[9,10-d]imidazole (**2**), which was prepared from the reaction of 3-thiophenecarboxaldehyde, phenanthrenequinone, aniline, ammonium acetate, and acetic acid, was isolated in 92% yield. The structure of compound **2** was verified using <sup>1</sup>H and <sup>13</sup>C NMR spectroscopy and mass spectrometry.

**M2** was prepared from the reaction of compound **2** with NBS; it was isolated in 93% yield.<sup>[56]</sup> Detailed synthetic procedures and characterization data are provided below.

**3-Octylthiophene (1):** 3-Octylthiophene was synthesized as described previously in the literature.<sup>[57a]</sup>

**2,5-Dibromo-3-octylthiophene (M1):** 2,5-Dibromo-3-octylthiophene was synthesized as described previously in the literature.<sup>[58]</sup>

**1-Phenyl-2-(3-thioenyl)-1*H*-phenanthro[9,10-d]imidazole (2):** A mixture of aniline (7.95 g, 85.5 mmol), phenanthrenequinone (3.75 g, 17.1 mmol), 3-thiophenecarboxaldehyde (1.92 g, 17.1 mmol), ammonium acetate (5.28 g, 68.57 mmol), and acetic acid (100 mL) was heated under nitrogen in an oil bath to a bath temperature of 123 °C, maintained at this temperature for 2 h, and then cooled and filtered. The solid product was washed with an acetic acid/water mixture (1:1, 150 mL), washed with water, and then dried (5.94 g, 92% yield). <sup>1</sup>H NMR (300 MHz, CDCl<sub>3</sub>, ppm): 8.84–8.87 (m, 1H), 8.75 (d, *J* = 8.4 Hz, 1H), 8.69 (d, *J* = 8.4 Hz, 1H), 7.45–7.78 (m, 9H), 7.22–7.27 (m, 2H), 7.14 (m, 1H), 7.08 (m, 1H). <sup>13</sup>C NMR (75 MHz, CDCl<sub>3</sub>): 147.0, 138.7, 137.2, 131.5, 130.4, 130.2, 129.1, 1290, 128.3, 128.2, 127.7, 127.2, 127.1, 126.2, 125.5, 124.8, 124.8, 124.7, 124.0, 123.0, 122.9, 122.7, 120.6. HRMS-EI (*m/z*): [*M*<sup>+</sup>] calcd. for C<sub>25</sub>H<sub>16</sub>SN<sub>2</sub>, 376.1034; found, 376.1035.

**2-(2,5-Dibromothiophen-3-yl)-1-phenyl-1*H*-phenanthro[9,10-d]imidazole (M2).**

1-Phenyl-2-(3-thioenyl)-1*H*-phenanthro[9,10-d]imidazole (**3**, 4.14 g, 11.0 mmol) was dissolved in a mixture of THF (66 mL) and acetic acid (66 mL). NBS (4.73g, 26.0 mmol) was added portionwise and then the mixture was stirred for 20 min. The solution was washed with water (2 × 200 mL), saturated NaHCO<sub>3</sub> (1 × 200 mL), and then again with water (1 × 200mL). Follow by using ethyl acetate to extract. The organic layer was dried (MgSO<sub>4</sub>) and concentrated to recover **M2** (5.5g, 93% yield).

$^1\text{H}$  NMR (300 MHz,  $\text{CDCl}_3$ , ppm): 8.77–8.74 (m, 1H), 8.69 (d,  $J = 8.4$  Hz, 1H), 8.62 (d,  $J = 8.1$  Hz, 1H), 7.78–7.38 (m, 8H), 7.24–7.13 (m, 2H), 6.73 (m, 1H).  $^{13}\text{C}$  NMR (75 MHz,  $\text{CDCl}_3$ ): 146.1, 145.7, 137.4, 137.2, 131.5, 130.4, 130.2, 129.1, 1290, 128.3, 128.2, 127.7, 127.2, 127.1, 126.2, 125.5, 124.8, 124.8, 124.7, 124.0, 123.0, 122.9, 122.7, 120.6. HRMS-EI ( $m/z$ ):  $[\text{M}^+]$  calcd. for  $\text{C}_{25}\text{H}_{16}\text{Br}_2\text{SN}_2$ , 531.9244; found, 531.9250.

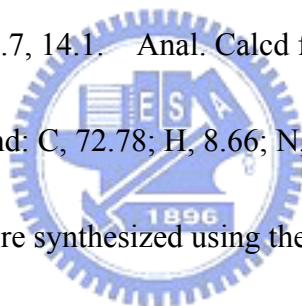
**Preparation of Polythiophene Derivatives:** All polymers were synthesized through Grignard metathesis polymerization in THF according to procedures similar to those described in the literature.<sup>[57]</sup> The Grignard metathesis polymerizations of 2,5-dibromo-3-octylthiophene (**M1**) and 2-(2,5-dibromothiophen-3-yl)-1-phenyl-1H-phenanthro[9,10-d]imidazole (**M2**) are illustrated in Scheme 2.

**Preparation of Polythiophene Derivatives:** All polymers were synthesized through Grignard metathesis polymerizations in THF, according to procedures similar to those described in the literature.<sup>[57b,57c]</sup> The Grignard metathesis polymerizations of 2,5-dibromo-3-octylthiophene (**M1**) and 2-(2,5-dibromothiophen-3-yl)-1-phenyl-1H-phenanthro[9,10-d]imidazole (**M2**) are illustrated in Scheme 2-2. Detailed synthetic procedures and characterization data are provided below.

**Poly(3-octylthiophene) (P00):** CH<sub>3</sub>MgBr (1.5mL, 4.5 mmol) was added via syringe to a stirred solution of 2,5-dibromo-3-octylthiophene (1.60g, 4.5 mmol) and freshly distilled THF (80 mL) in a three-necked 100-mL round-bottom flask. The solution was heated under reflux for 2 h and then Ni(dppp)Cl<sub>2</sub> (12 mg, 0.02 mmol) was added. The mixture was stirred for 1 h before the reaction was quenched through the addition of methanol. The solid polymer was washed with methanol within a Soxhlet extractor. The polymer then was dissolved through Soxhlet extraction with chloroform; the solvent was evaporated and the residue dried under vacuum to yield poly(3-octylthiophene) (0.54 g, 61%; 99% coupled head-to-tail). <sup>1</sup>H NMR (300 MHz, CDCl<sub>3</sub>): 6.98 (s, 1H), 2.78 (s, 2H), 0.86, 1.27, 1.68 (m, 15H). <sup>13</sup>C NMR (75 MHz, CDCl<sub>3</sub>): 139.9, 133.7, 130.5, 128.6, 31.9, 30.6, 29.6, 29.4, 29.3, 22.7, 14.1. Anal. Calcd for C<sub>12</sub>H<sub>18</sub>S: H, 9.34; C, 74.17; S, 16.50. Found: H, 11.14; C, 73.58; S, 15.28.

**P19:** CH<sub>3</sub>MgBr (1.5mL, 4.5 mmol) was added via syringe to a stirred solution of 2,5-dibromo-3-octylthiophene (1.44 g, 4.05 mmol), 2-(2,5-dibromothiophen-3-yl)-1-phenyl-1*H*-phenanthro[9,10-*d*]imidazole (0.24 g, 0.45 mmol), and freshly distilled THF (80 mL) in a three-necked 100-mL round-bottom flask. The solution was heated under reflux for 2 h and then Ni(dppp)Cl<sub>2</sub> (12 mg, 0.02 mmol) was added. The mixture was stirred for 1 h and

then the reaction was quenched through the addition of methanol. The solid polymer was washed with methanol within a Soxhlet extractor. The polymer then was dissolved through Soxhlet extraction with chloroform; the chloroform was evaporated and the residue dried under vacuum to yield **P19** (0.54 g, 61%; 99% coupled head-to-tail).  $^1\text{H}$  NMR (300 MHz,  $\text{CDCl}_3$ ): 8.4–8.9 (br, 3H), 7.3–7.9 (br, 13H), 6.98 (s, 1H), 2.75 (s, 3H), 0.85, 1.26, 1.64 (m, 14H).  $^{13}\text{C}$  NMR (75 MHz,  $\text{CDCl}_3$ ): 146.2, 145.7, 139.9, 137.4, 137.1, 133.2, 131.1, 130.4, 130.1, 129.6, 129.0, 128.4, 128.2, 127.5, 127.0, 126.5, 126.2, 125.5, 124.6, 123.4, 122.6, 122.0, 121.1, 120.0, 119.7, 31.9, 30.6, 29.6, 29.4, 29.3, 22.7, 14.1. Anal. Calcd for  $\text{C}_{13.3}\text{H}_{17.8}\text{SN}_{0.2}$ : C, 74.73; H, 8.83; N, 0.74; S, 15.72. Found: C, 72.78; H, 8.66; N, 0.77; S, 14.90.



Other polymer samples were synthesized using the method described for the preparation of **P19**, but with different amounts of 2-(2,5-dibromothiophen-3-yl)-1-phenyl-1*H*-phenanthro[9,10-*d*]imidazole (**M2**).

**P28**:  $^1\text{H}$  NMR (300 MHz,  $\text{CDCl}_3$ ): 8.4–8.9 (br, 3H), 7.3–7.9 (br, 13H), 6.98 (s, 1H), 2.75 (s, 3H), 0.85, 1.26, 1.64 (m, 14H).  $^{13}\text{C}$  NMR (75 MHz,  $\text{CDCl}_3$ ): 146.2, 145.7, 139.9, 137.4, 137.1, 133.2, 131.1, 130.4, 130.1, 129.6, 129.0, 128.4, 128.2, 127.5, 127.0, 126.5, 126.2, 125.5, 124.6, 123.4, 122.6, 122.0, 121.1, 120.0, 119.7, 31.9, 30.6, 29.6, 29.4, 29.3, 22.7, 14.1. Anal. Calcd for  $\text{C}_{13.6}\text{H}_{17.6}\text{SN}_{0.4}$ : C, 75.29; H, 8.33; N, 1.49; S, 14.92. Found: C, 74.78; H, 7.66; N, 1.39; S, 14.80.



**P37:**  $^1\text{H}$  NMR (300 MHz,  $\text{CDCl}_3$ ): 8.4–8.9 (br, 3H), 7.3–7.9 (br, 13H), 6.98 (s, 1H), 2.75 (s, 3H), 0.85, 1.26, 1.64 (m, 14H).  $^{13}\text{C}$  NMR (75 MHz,  $\text{CDCl}_3$ ): 146.2, 145.7, 139.9, 137.4, 137.1, 133.2, 131.1, 130.4, 130.1, 129.6, 129.0, 128.4, 128.2, 127.5, 127.0, 126.5, 126.2, 125.5, 124.6, 123.4, 122.6, 122.0, 121.1, 120.0, 119.7, 31.9, 30.6, 29.6, 29.4, 29.3, 22.7, 14.1. Anal. Calcd for  $\text{C}_{15.9}\text{H}_{17.4}\text{SN}_{0.6}$ : C, 75.85; H, 7.82; N, 2.23; S, 14.12. Found: C, 74.30; H, 7.20; N, 2.41; S, 13.9.

**P55:**  $^1\text{H}$  NMR (300 MHz,  $\text{CDCl}_3$ ): 8.4–8.9 (br, 3H), 7.3–7.9 (br, 13H), 6.98 (s, 1H), 2.75 (s, 3H), 0.85, 1.26, 1.64 (m, 14H).  $^{13}\text{C}$  NMR (75 MHz,  $\text{CDCl}_3$ ): 146.2, 145.7, 139.9, 137.4, 137.1, 133.2, 131.1, 130.4, 130.1, 129.6, 129.0, 128.4, 128.2, 127.5, 127.0, 126.5, 126.2, 125.5, 124.6, 123.4, 122.6, 122.0, 121.1, 120.0, 119.7, 31.9, 30.6, 29.6, 29.4, 29.3, 22.7, 14.1. Anal. Calcd for  $\text{C}_{18.5}\text{H}_{17}\text{SN}$ : C, 76.97; H, 6.81; N, 3.72; S, 12.52. Found: C, 74.22; H, 6.72; N, 3.93; S, 11.83.

**P73:**  $^1\text{H}$  NMR (300 MHz,  $\text{CDCl}_3$ ): 8.4–8.9 (br, 3H), 7.3–7.9 (br, 13H), 6.98 (s, 1H), 2.75 (s, 3H), 0.85, 1.26, 1.64 (m, 14H).  $^{13}\text{C}$  NMR (75 MHz,  $\text{CDCl}_3$ ): 146.2, 145.7, 139.9, 137.4, 137.1, 133.2, 131.1, 130.4, 130.1, 129.6, 129.0, 128.4, 128.2, 127.5, 127.0, 126.5, 126.2, 125.5, 124.6, 123.4, 122.6, 122.0, 121.1, 120.0, 119.7, 31.9, 30.6, 29.6, 29.4, 29.3, 22.7, 14.1. Anal. Calcd for  $\text{C}_{20.1}\text{H}_{16.6}\text{SN}_{1.4}$ : C, 78.08; H, 5.80; N, 5.21; S, 10.92. Found: C, 77.22; H, 5.72; N, 4.93; S, 10.51.

**P82:**  $^1\text{H}$  NMR (300 MHz,  $\text{CDCl}_3$ ): 8.4–8.9 (br, 3H), 7.3–7.9 (br, 13H), 6.98 (s,

1H), 2.75 (s, 3H), 0.85, 1.26, 1.64 (m, 14H).  $^{13}\text{C}$  NMR (75 MHz,  $\text{CDCl}_3$ ): 146.2, 145.7, 139.9, 137.4, 137.1, 133.2, 131.1, 130.4, 130.1, 129.6, 129.0, 128.4, 128.2, 127.5, 127.0, 126.5, 126.2, 125.5, 124.6, 123.4, 122.6, 122.0, 121.1, 120.0, 119.7, 31.9, 30.6, 29.6, 29.4, 29.3, 22.7, 14.1. Anal. Calcd for  $\text{C}_{22.4}\text{H}_{16.4}\text{SN}_{1.6}$ : C, 78.64; H, 5.29; N, 5.95; S, 10.12. Found: C, 77.22; H, 5.20; N, 5.03; S, 10.21.

$^1\text{H}$  and  $^{13}\text{C}$  NMR spectra were recorded on a Varian Unity-300 NMR spectrometer.

Infrared spectra were recorded from KBr disks on a Nicolet Protégé-460 FTIR

spectrophotometer. Elemental analyses (EA) of our polymers were performed using

a Heraeus CHN-OS Rapid instrument. Thermal gravimetric analyses of the

polythiophene derivatives were performed using a Du Pont TGA 2950 instrument

operated at a heating rate of  $10\text{ }^\circ\text{C}/\text{min}$  under a nitrogen purge. Differential scanning

calorimetry (DSC) was performed on a Du Pont DSC 2010 instrument operated at a

heating rate of  $10\text{ }^\circ\text{C}/\text{min}$  under a nitrogen purge. Samples were heated from 30 to

$200\text{ }^\circ\text{C}$ , cooled to  $20\text{ }^\circ\text{C}$ , and then heated again from 30 to  $200\text{ }^\circ\text{C}$ ; the glass transition

temperatures ( $T_g$ ) were determined from the second heating scans. The redox

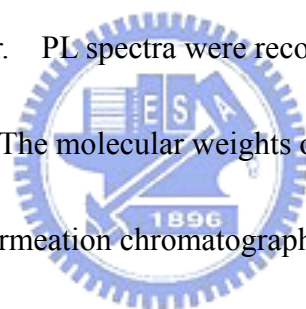
behavior of each polymer was investigated through cyclic voltammetry using an

electrolyte of 0.1 M tetrabutylammonium hexafluorophosphate ( $n\text{-Bu}_4\text{NPF}_6$ ) in

acetonitrile. Cyclic voltammetry was performed using a BAS 100 electrochemical

analyzer operated at a potential scan rate of  $40\text{ mV}/\text{s}$ . In each case, a glassy disk

carbon electrode coated with a thin layer of the polymer was used as the working electrode. A platinum wire was used as the counter electrode and a silver wire was used as the quasi-reference electrode. All of the potentials quoted herein are referenced to the Ag wire as the quasi-reference electrode; the electrochemical potential of Ag is  $-0.02$  V vs SCE.  $E_{\text{HOMO}} = -E_{\text{ox}} - 4.4$  eV and  $E_{\text{LUMO}} = -E_{\text{red}} - 4.4$  eV, where  $E_{\text{ox}}$  and  $E_{\text{red}}$  are the onset potentials of the oxidation and reduction peaks (vs saturated calomel electrode, SCE), respectively, and the value of 4.4 eV relates the SCE reference to a vacuum.<sup>[59]</sup> UV-Vis spectra were measured using an HP 8453 diode array spectrophotometer. PL spectra were recorded using a Hitachi F-4500 luminescence spectrometer. The molecular weights of the polythiophene derivatives were measured through gel permeation chromatography (GPC) using a Waters chromatography unit interfaced to a Waters 2414 differential refractometer. Three  $5\text{-}\mu\text{m}$  Waters styragel columns were connected in series in decreasing order of pore size ( $10^4$ ,  $10^3$ , and  $10^2$  Å); THF was the eluent and standard polystyrene samples were used for calibration.

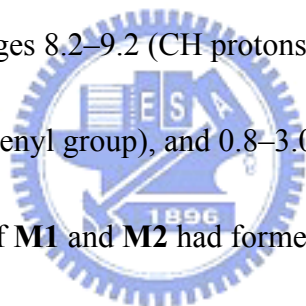


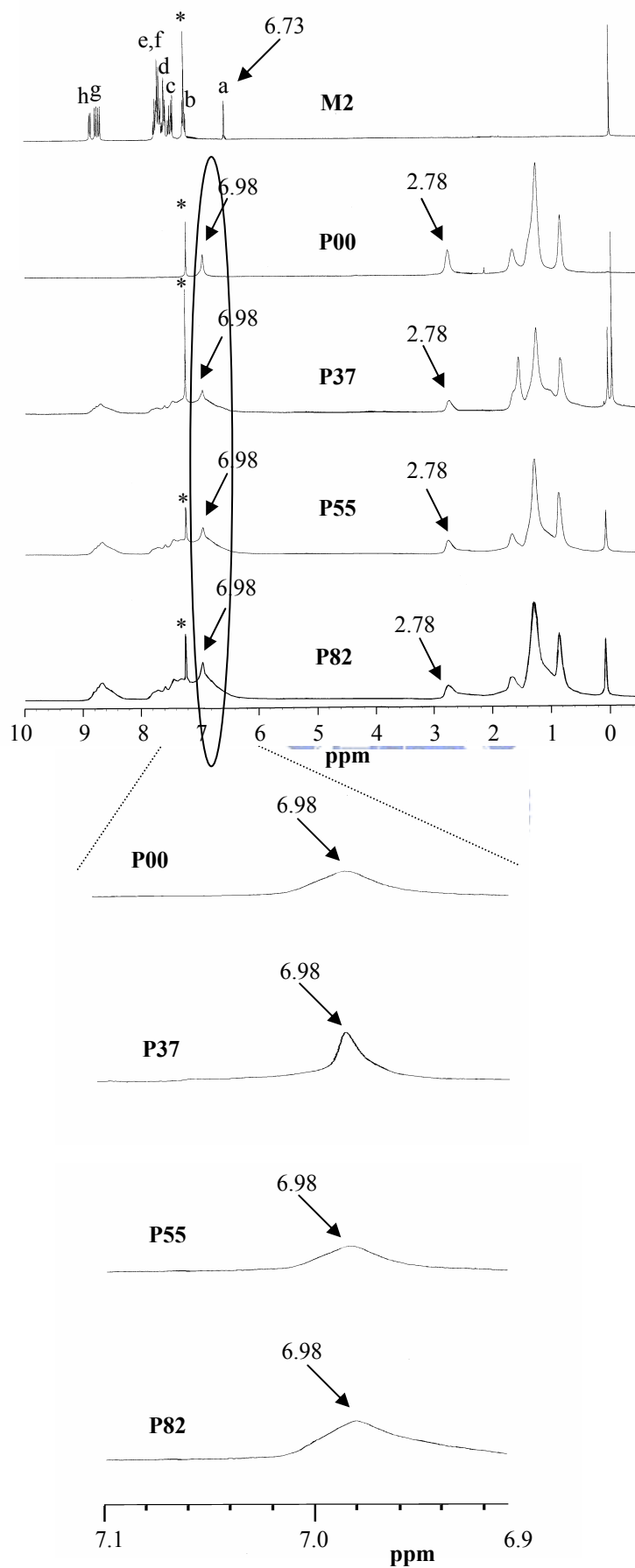
**Device Fabrication:** The current density–voltage (J–V) measurements of our polymers were performed using devices having a sandwich structure (ITO/PEDOT:PSS/polymer:PCBM (1:2, w/w)/Ca/Al). An ITO-coated glass substrate was pre-cleaned and treated with oxygen plasma prior to use. The

polymer/PCBM layer was spin-coated at 1500 rpm from the corresponding dichlorobenzene solution (15 mg/mL). The nominal thickness of the polymer/PCBM layer was ca. 80 nm. Using a base pressure below  $1 \times 10^{-6}$  torr, a layer of Ca (30 nm) was vacuum-deposited as the cathode and then a thick layer of Al (100 nm) was deposited as the protecting layer and the effective area of one cell is  $0.04 \text{ cm}^2$ . Testing of the devices was performed under simulated AM1.5 irradiation ( $100 \text{ mW/cm}^2$ ) using a xenon lamp-based Newport 66902 150W solar simulator. A Xenon lamp with AM1.5 filter was used as the white light source, and the optical power at the sample was  $100 \text{ mW/cm}^2$  detected by OPHIR thermopie 71964. The J–V characteristics were measured using a Keithley 236 electrometer. The spectrum of our solar simulator had a mismatch of less than 25 %. Reported efficiencies are the averages obtained from four devices prepared on each substrate. The external quantum efficiency (EQE) was measured using a Keithley 236 coupled with Oriel Cornerstone 130 monochromator. The light intensity at each wavelength was calibrated with OPHIR 71580 (diode).

### 2-3. Results and Discussion

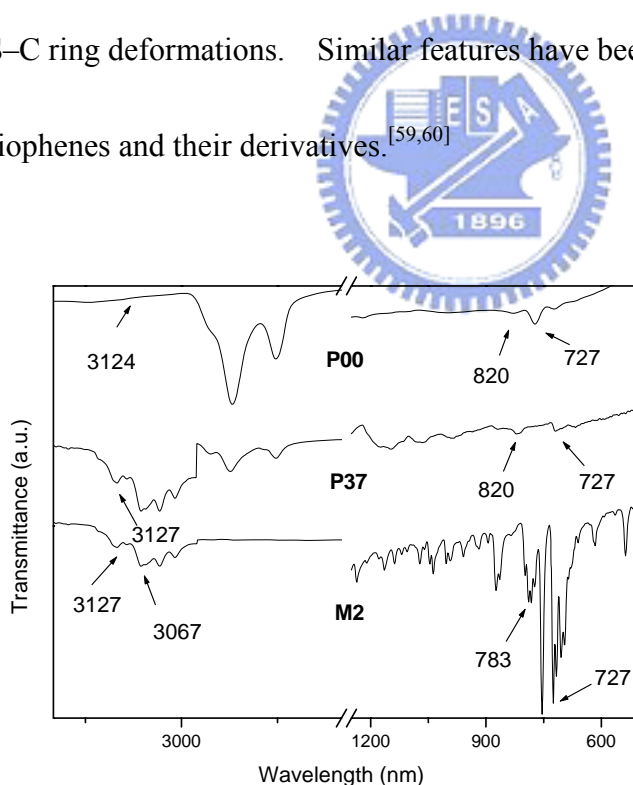
Figure 2-1 presents the  $^1\text{H}$  NMR spectra of **M2** and some of the synthesized polymers. The regioregularity of the polymers can be determined from the ratio of the area under the peak at 6.98 ppm to the area under all of the peaks ranging from 6.98 to 7.04 ppm. Because only a signal at 6.98 ppm is present in the spectrum of **P00**, with no other peaks nearby, we believe that this polymer possesses an almost complete head-to-tail configuration (i.e., the regioregularity close to 100%).<sup>[57a]</sup> In the spectrum of **P37**, the peak at 6.73 ppm (CH proton of the thiophene ring) is absent, and the broad peaks in the ranges 8.2–9.2 (CH protons of the phenathrenyl group), 7.2–8.2 (CH protons on the phenyl group), and 0.8–3.0 ppm (octyl chain protons) confirm that the copolymers of **M1** and **M2** had formed.





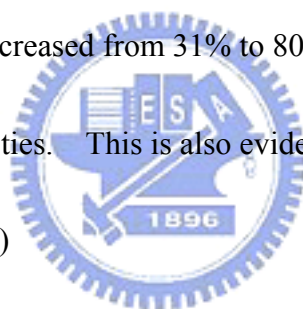
**Figure 2-1.** The  $^1\text{H}$  NMR spectra of **M2**, **P00**, **P37**, **P55**, and **P82**.

Figure 2-2 displays the FTIR spectra of **M2** and the synthesized polymers. In the spectrum of **M2**, we observe distinct and sharp absorption bands at 3067 and 3127  $\text{cm}^{-1}$  that correspond to the stretching of the  $\beta$ -CH units on the thiophene ring. We assign the band at 820  $\text{cm}^{-1}$  to the C–H out-of-plane deformation of the thiophene ring. The absence of any signals at 783  $\text{cm}^{-1}$  (for bending of  $\alpha$ -CH units on the thiophene ring) in the spectra of **P00** and **P37** indicates that the polymerization occurred through reactions of the thiophene ring. The  $\text{CH}_3$  and  $\text{CH}_2$  stretching vibrations appear as the band at 2800–3000  $\text{cm}^{-1}$  in the spectra of **P00** and **P37**. The peak at 727  $\text{cm}^{-1}$  is due to C–S–C ring deformations. Similar features have been reported for other polythiophenes and their derivatives.<sup>[59,60]</sup>



**Figure 2-2.** FTIR spectra of **M2**, **P00**, and **P37**.

Table 2-1. displays the molecular weight, the degradation temperature and the glass transition temperatures of synthesized copolymers, **P00** to **P82**. The number molecular weight ( $M_n$ ) of our polymers range from 7.2 kg/mole to 11.6 kg/mole and the polydispersity index (PDI) shows at the range of 1.28 and 1.61. The thermal degradation temperatures of these copolymers increased upon increasing the content of phenanthrenyl-imidazole moieties. For instance, the degradation temperature of **P82** improved to 432.2°C from 370.1°C for **P00**, an increase of 62°C. Whereas, the glass transition temperature of **P82** was not detectable as compared to 40°C for **P00**. The residual parts at 600 °C increased from 31% to 80% with the relative amount of phenanthrenyl-imidazole moieties. This is also evidence that the copolymerization had occurred. (See Figure 2-3.)



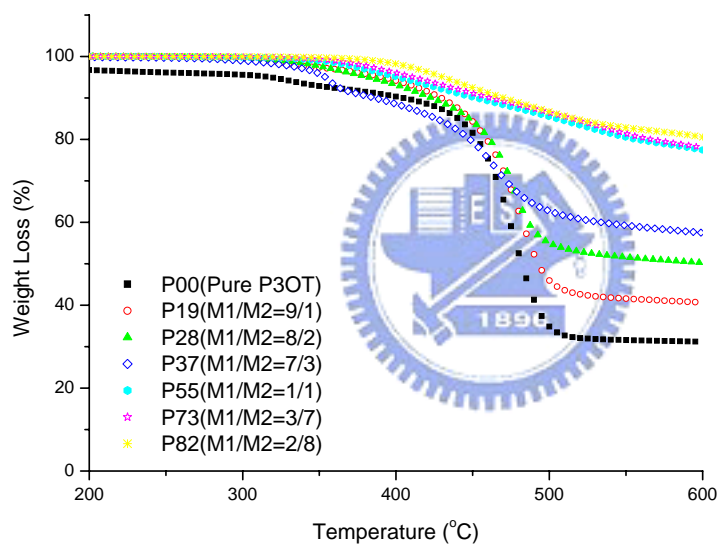


**Table 2-1.** Molecular weights and thermal properties of synthesized polymers.

	Mn(x10 <sup>3</sup> )	Mw(x10 <sup>3</sup> )	PDI	T <sub>d</sub> <sup>a</sup> (°C)	T <sub>g</sub> (°C)
<b>P00</b>	11.6	15.6	1.34	370.1	40.0
<b>P55</b>	11.2	17.8	1.61	404.5	*
<b>P73</b>	7.2	12.2	1.58	430.2	*
<b>P82</b>	7.7	9.9	1.28	432.2	*

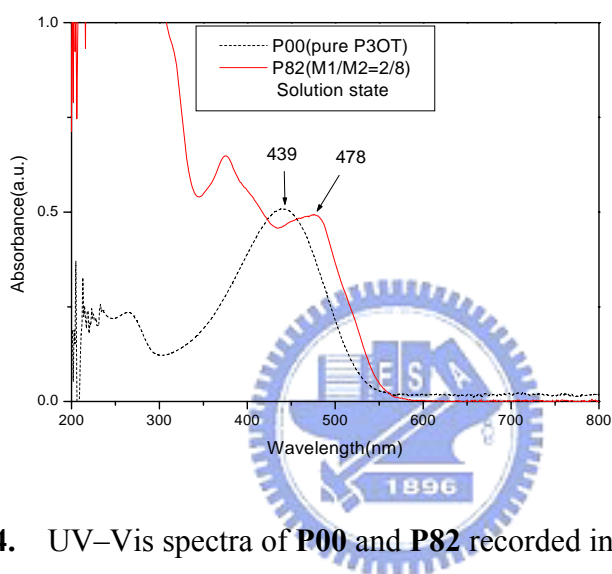
a: The temperature at which 5% weight loss occurred based on the initial weight.

\*: The glass transition temperature can not be observed.



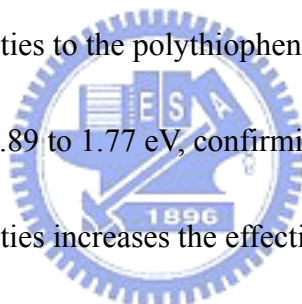
**Figure 2-3.** The thermal degradation temperature of synthesized polymers

Figure 2-4 displays UV–Vis spectra of the polymers both in solution. The  $\pi$ – $\pi^*$  transitions are responsible for the maximum absorptions ( $\lambda_{\text{max}}$ ) that occur at ca. 439 and 478 nm for the solutions of **P00** and **P82**, respectively. These data indicate that the bandgap of the copolymer is lower than that of pure **P3OT**.<sup>[58]</sup>



**Figure 2-4.** UV–Vis spectra of **P00** and **P82** recorded in THF solution.

Figure 2-5 displays UV–Vis spectra of the polymers in the solid state. The small peak at 270 nm is caused by the presence of conjugated phenanthrenyl-imidazole moieties that are not fully coplanar to the polythiophene chain owing to steric hindrance. The  $\pi$ – $\pi^*$  transitions are responsible for the maximum absorptions ( $\lambda_{\text{max}}$ ) that occur at ca. 520 nm for **P00** and 556 nm for **P82** thin films.<sup>[55]</sup> These data indicate that the optical bandgap of the **P82** copolymer is lower than that of pure **P3OT**. Table 2-2. lists the absorption maxima, and the optical bandgaps of the synthesized polymers. Optimally, conjugating 80 mol% of phenanthrenyl-imidazole moieties to the polythiophene chains led to the optical bandgap being reduced from 1.89 to 1.77 eV, confirming that the presence of the phenanthrenyl-imidazole moieties increases the effective conjugation length of the polythiophene main chain to some extent.<sup>[55]</sup> The cyclic voltammogram data also shows the same trend, despite absolute values being different ( see Table 2-3).



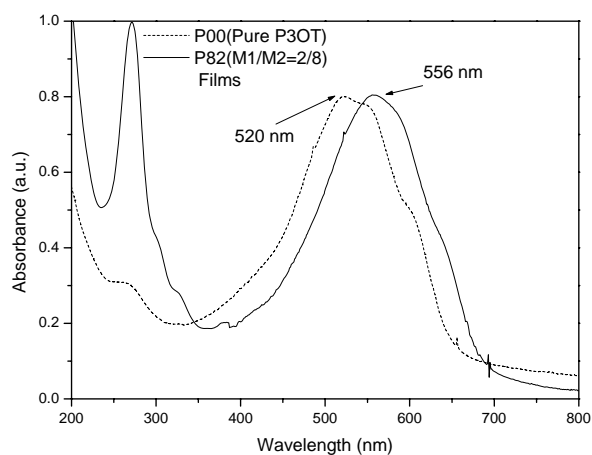


**Figure 2-5.** The UV–Vis spectra of **P00** and **P82** recorded in the solid state.

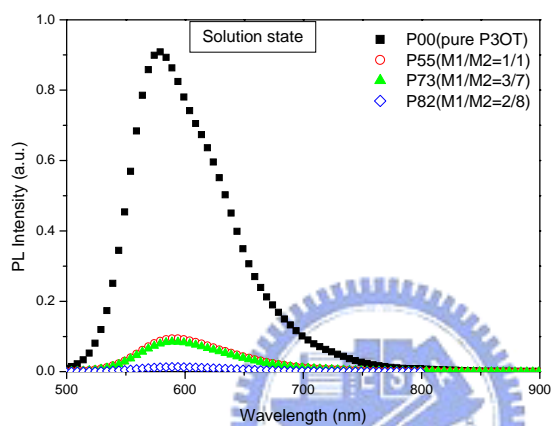
**Table 2-2.** UV-Visible absorption peaks and optical bandgaps of synthesized polymers.

Polymer	Absorption $\lambda_{\max}$		Optical bandgap (eV)
	Solution (nm)	Film (nm)	
<b>P00</b>	439	520(549, 603)	1.89
<b>P55</b>	470	540(628)	1.82
<b>P73</b>	476	548(631)	1.81
<b>P82</b>	478	556(638)	1.77

**Table 2-3.** Redox data, HOMO, LUMO energy levels, and band gap energies of our synthesized polymers.

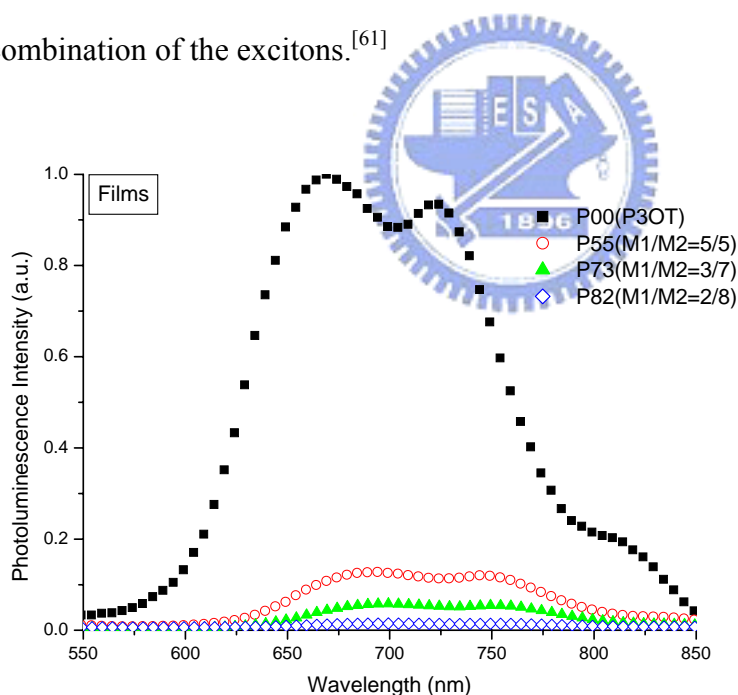
Polymer	Oxidation onset potential (eV)	Reduction onset potential (eV)	HOMO (eV)	LUMO (eV)	$E_g$ (eV)
<b>P00</b>	1.00	-0.85	-5.4	-3.55	1.85
<b>P19</b>	0.95	-0.83	-5.35	-3.57	1.78
<b>P28</b>	0.90	-0.80	-5.30	-3.60	1.70
<b>P37</b>	0.85	-0.76	-5.25	-3.64	1.61
<b>P55</b>	0.81	-0.74	-5.21	-3.66	1.55
<b>P73</b>	0.80	-0.70	-5.20	-3.70	1.50
<b>P82</b>	0.75	-0.65	-5.15	-3.75	1.40

Figure 2-6 displays PL spectra of polymer solutions and films recorded at excitation wavelengths of 400 and 450 nm, respectively. The PL of the phenanthrenyl-imidazole-containing copolymers solutions was quenched relative to that of pure **P3OT**, with the degree of quenching increasing upon increasing the content of phenanthrenyl-imidazole units in the copolymer.



**Figure 2-6.** Photoluminescence (PL) spectra, normalized to the number of absorbed photons, of all seven polymers in solution state.

Figure 2-7 displays photoluminescence (PL) spectra of polymer films recorded at excitation wavelengths of 450 nm, respectively. The PL of the phenanthrenyl-imidazole-containing copolymers films was dramatically quenched relative to that of pure **P3OT**, with the degree of quenching increasing upon increasing the content of phenanthrenyl-imidazole units in the copolymer. This finding suggests that photoinduced charge transfer occurred from the photoexcited polythiophene backbone to the electron-withdrawing phenanthrenyl-imidazole side chains, and that this charge transfer was sufficiently rapid to compete with radiative recombination of the excitons.<sup>[61]</sup>



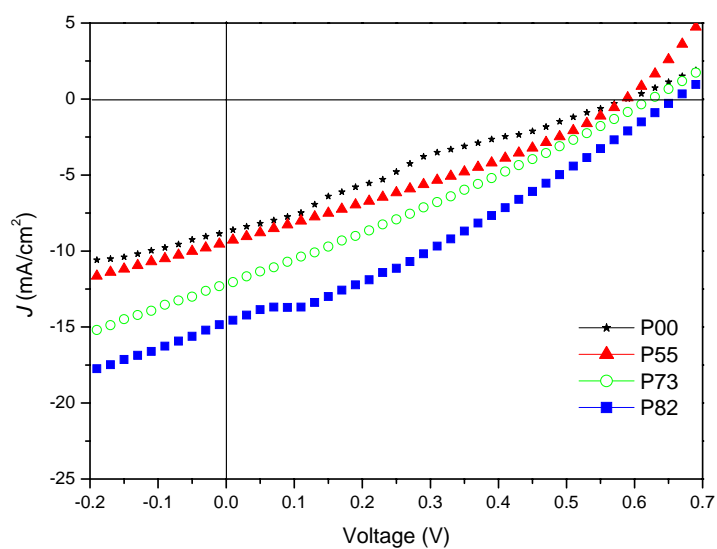
**Figure 2-7.** Photoluminescence (PL) spectra, normalized to the number of absorbed photons, of synthesized polymers in the solid state.

Figure 2-8 displays the photocurrents of diodes having the structure ITO/PEDOT:PSS/polymer: [6,6]-phenyl-C<sub>61</sub>-butyric acid methyl ester (PCBM) (1:2, w/w)/Ca/Al that were illuminated at AM 1.5 G and 100 mW/cm<sup>2</sup>. In Figure 8, the short circuit current density (*J<sub>sc</sub>*) increased upon increasing the content of the phenanthrenyl-imidazole moieties, probably as a consequence of enhanced light absorption at longer wavelength due to the extended conjugation and the fast charge transfer of the copolymers.<sup>[62]</sup> For all efficiency values reported in this paper we used a spectral mismatch factor of 0.8 to account for deviations in the spectral output of the solar simulator with respect to the standard AM 1.5 spectrum and deviations in the spectral response of the device with respect to that of the reference cell. Table 2-4. lists the detailed photovoltaic properties of these polymer solar cells. In particular, the short circuit current densities of the device containing the copolymer having 80 mol % phenanthrenyl-imidazole, **P82**, improved to 14.2 mA/cm<sup>2</sup> from 8.7 mA/cm<sup>2</sup> for the device of pure poly(3-octylthiophene), **P00**, an increase of 62%. Because of the increased degree of the short circuit current density that occurred when the phenanthrenyl-imidazole content increased, the current density–voltage characteristics of our solar cell devices suggest that charge transfer occurred from the photoexcited polythiophene backbone through the phenanthrenyl-imidazole moieties and PCBM to the electrode. The open circuit voltages (*V<sub>oc</sub>*) of the **P82**

heterojunction device increased to 0.69 V from 0.59 V for the **P00** device. The open circuit voltages of polymer heterojunction cell is usually proportional to the difference between the lowest unoccupied molecular orbital (LUMO) of the electron acceptor and the highest occupied molecular orbital (HOMO) of the electron donor<sup>[63]</sup> but are influenced by many other factors, for example, solvent effects.<sup>[64]</sup> In the **P82** device case, it appears that the fact that the copolymers became less soluble and less miscible with PCBM at higher phenanthrenyl-imidazole moieties contents<sup>[64]</sup> dominates over the decrease between the LUMO of the electron acceptor and the HOMO of the electron donor, resulting in a slightly higher  $V_{oc}$  than that of the **P00** device.

Nevertheless, the filled factors remained low as a result of the devices maintaining large series resistances and low shunt resistances.<sup>[65]</sup> Even with the disadvantage of low filled factors, the power conversion efficiency increased dramatically to 2.8% for **P82** from 1.22% for **P00**, presumably due to the lowered bandgap and the enhanced electron transfer for the former polymer.





**Figure 2-8.** Current density–voltage characteristics of illuminated (AM 1.5G, 100 mW/cm<sup>2</sup>) polymer solar cells incorporating **P00**, **P55**, **P73**, and **P82** and PCBM.

**Table 2-4.** Photovoltaic properties of the polymer solar cells.

Weight ratio of polymer to PCBM	$V_{oc}$ (V)	$J_{sc}$ (mA/cm <sup>2</sup> )	FF (%)	PCE (%)
<b>P00</b> :PCBM = 1:2	0.59	8.7	23.6	1.22
<b>P55</b> :PCBM = 1:2	0.64	9.4	30.2	1.68
<b>P73</b> :PCBM = 1:2	0.62	12.4	28.0	2.15
<b>P82</b> :PCBM = 1:2	0.69	14.2	31.1	2.80

The photophysics of the devices using the synthesized copolymers can be manifested by examining their external quantum efficiency and light absorption data. Figure 2-9(a) and (b) show the external quantum efficiency (EQE) of the polythiophene side-chain-tethered phenanthrenyl-imidazole/PCBM devices and the UV-Vis absorption of the copolymer/PCBM blends experienced the same annealing condition as that of the device, respectively. The EQE values of **P82** device is at least 19% larger than that of the **P00** device at wavelength from 400 to 600 nm. In a detailed comparison, the EQE value of the **P82** device improved to 50% from 29% for the **P00** device at 450 nm incident light, almost 100% increase. The maximum EQE value of the **P82** and **P00** devices reaches 69% and 29%, respectively, at 480 nm, with a 1.5 times increase. Even at a much longer wavelength of 600 nm, the EQE of **P82** device improved to 33% from 11% for **P00** device, a two-fold increase. The relative light absorption intensity of **P82**/PCBM blend is about 20% higher than that of **P00**/PCBM blend at 400 nm and 600 nm, respectively. The similarity between the shape of the EQE curves of these copolymers and their corresponding UV-Vis absorption spectra indicated that the enhanced photocurrent current densities,  $J_{sc}$ , are mainly generated by the rapid electron transfer of the dissociated excitons in polythiophene backbone to the conjugated phenanthrenyl-imidazole side chain and lowered bandgap of the copolymers. The large increase in the short-circuit current

density of the polythiophene-side-chain tethered phenanthrenyl-imidazole device in turn accounts for the large increase in the power conversion efficiency of **P82** device as compared to that of **P00** device. These results demonstrate that the introduction of electron-withdrawing and conjugated phenanthrenyl-imidazole onto polythiophene side chains can quite effectively improve the photon conversion efficiency of poly(3-octylthiophene).

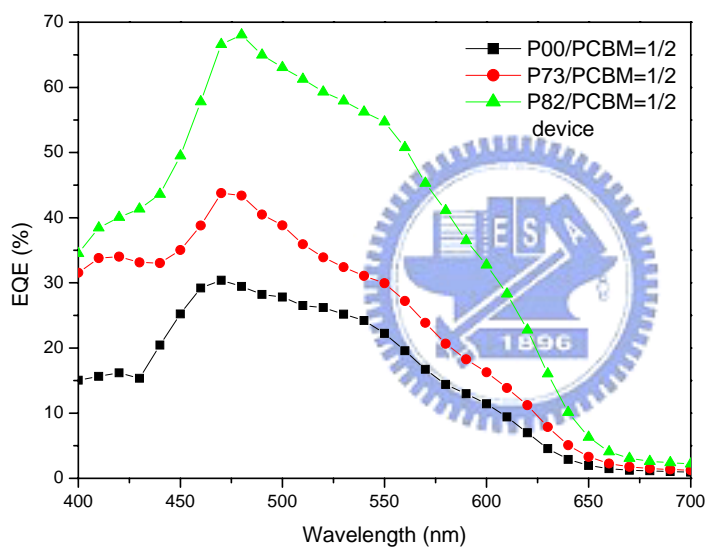


**Figure 2-9.** (a) The external quantum efficiency of **P00**, **P73** and **P82/PCBM** solar cells

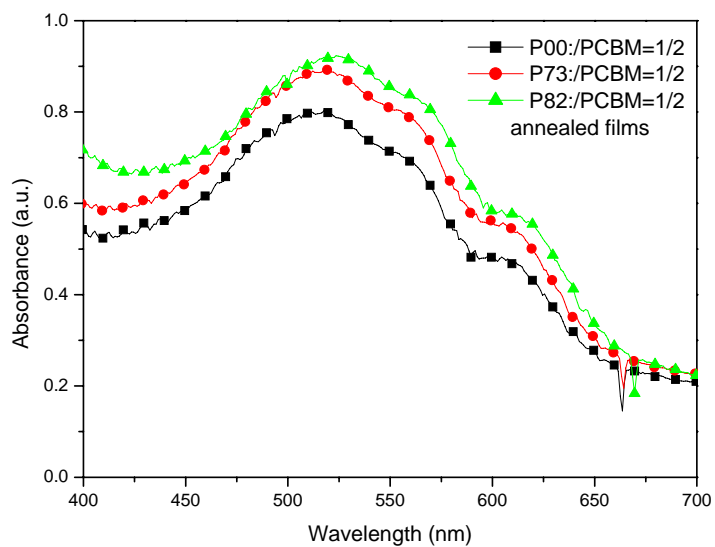
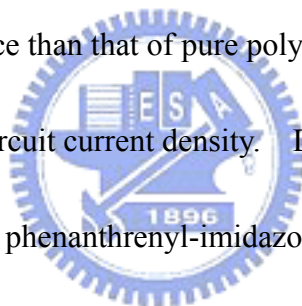


**Figure 2-9.** (b) The UV-Vis absorption of the copolymer/PCBM blends experience the same annealing condition as that of the device.



## ***2-4. Conclusions***

In summary, we have prepared a new family of regioregular thiophene copolymers presenting phenanthrenyl-imidazole side chains in conjugation with the main polymeric chain, leading to lowered bandgaps. The reduction in the bandgap energy in conjunction with the observed photoluminescence quenching indicates that rapid charge transfer occurred from the photoexcited polythiophene backbone through the phenanthrenyl-imidazole moieties to PCBM in the device. The much higher external quantum efficiency of the polythiophene-side-chain-tethered phenanthrenyl-imidazole device than that of pure poly(3-octylthiophene) device results in much higher short circuit current density. Due to the high short circuit current density obtained in the phenanthrenyl-imidazole presenting regioregular poly(3-octylthiophene), the power conversion efficiency improved dramatically to 2.80% for the copolymer containing 80 mol % phenanthrenyl-imidazole from 1.22% for pure poly(3-octylthiophene).

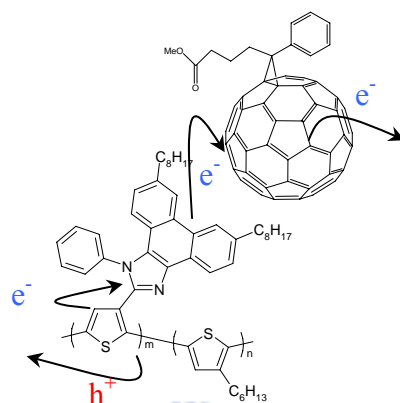


## Chapter 3: Intramolecular Donor–Acceptor Regioregular

### Poly(3-hexylthiophene)s Presenting Octylphenanthrenyl-Imidazole

### Moieties Exhibit Enhanced Charge Transfer for Heterojunction Solar

### Cell Applications



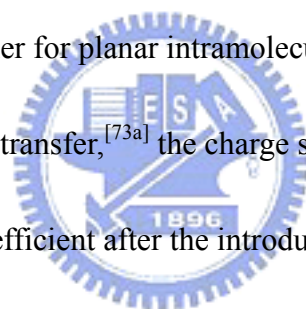
A new family of regioregular copolymers of poly(3-hexylthiophene) side chain-tethered with octylphenanthrenyl-imidazole moieties possess lowered bandgaps and enhanced charge transfer properties that make them suited for use in heterojunction polymer/**PCBM** solar cell applications. The short circuit current density and the power conversion efficiency of the copolymer having 90 mole% octylphenanthrenyl-imidazole group device improved to 13.7 mA/cm<sup>2</sup> and 3.45%, respectively.

### **3-1. Introduction**

The development of conjugated polymers that possess extended delocalized  $\pi$ -electrons for use in organic optoelectronic devices has been an area of extensive investigation, with some studies having focused on solar cell devices based on bulk heterojunctions using conjugated polymers.<sup>[66–72]</sup> Recently, research into conjugated polymers containing electron donor–acceptor pairs has become quite active<sup>[73]</sup> because such materials exhibit unusual optical, electrical, and electronic properties. There are two kinds of donor–acceptor systems: intermolecular donor–acceptor systems, which are usually encountered in such devices as bulk heterojunction solar cells, and intramolecular donor–acceptor systems, which enhance the rate of charge transfer within molecules or polymers.<sup>[73,74]</sup> With intermolecular donor–acceptor systems, bulk heterojunction polymer solar cells have been prepared using a thin film of an electron-donating conjugated polymer and an electron-accepting species that has been either another polymer or a set of nanoparticles.<sup>[73]</sup> The intramolecular donor–acceptor systems typically consist of electron donating groups (such as conjugated polymers or small conjugated molecules), a bridge (such as another conjugated group or a long alkyl chain), and electron acceptors.<sup>[74]</sup> The photochemical and photophysical properties of molecules or polymers depend upon the kinetics of excited-state processes that occur after the absorption of a photon.

After being photoexcited, the generated excitons can be stabilized for further separation because of the extended conjugation length, and the electrons then can be transferred from donors to acceptors rapidly.<sup>[73]</sup> Understanding how excited states behave as a function of time is a critical challenge toward designing new molecules for solar cell applications. Typically, femtosecond time-resolved photoluminescence spectroscopy is used to obtain such information.<sup>[74]</sup> Two models of the intramolecular charge transfer process have been proposed: the twisted intramolecular charge transfer model and the planar intramolecular charge transfer model. Because the charge transfer rate is higher for planar intramolecular charge transfer than it is for twisted intramolecular charge transfer,<sup>[73a]</sup> the charge separation process after photoexcitation will be more efficient after the introduction of electron-acceptor groups onto the polymer side chains in a coplanar manner. Moreover, the introduction of an electron-acceptor unit, which is usually a conjugated species that can absorb a different wavelength of sunlight, onto the side chain of a conjugated polymer can increase the breadth of wavelengths of light absorbed. Therefore, conjugated polymers that contain side chain-tethered conjugated acceptor moieties not only absorb light more effectively (multiple absorption) but also exhibit enhanced charge transfer ability—two desirable properties for photovoltaics applications.<sup>[75]</sup>

There are three methods for introducing electron acceptors onto polymers. The first

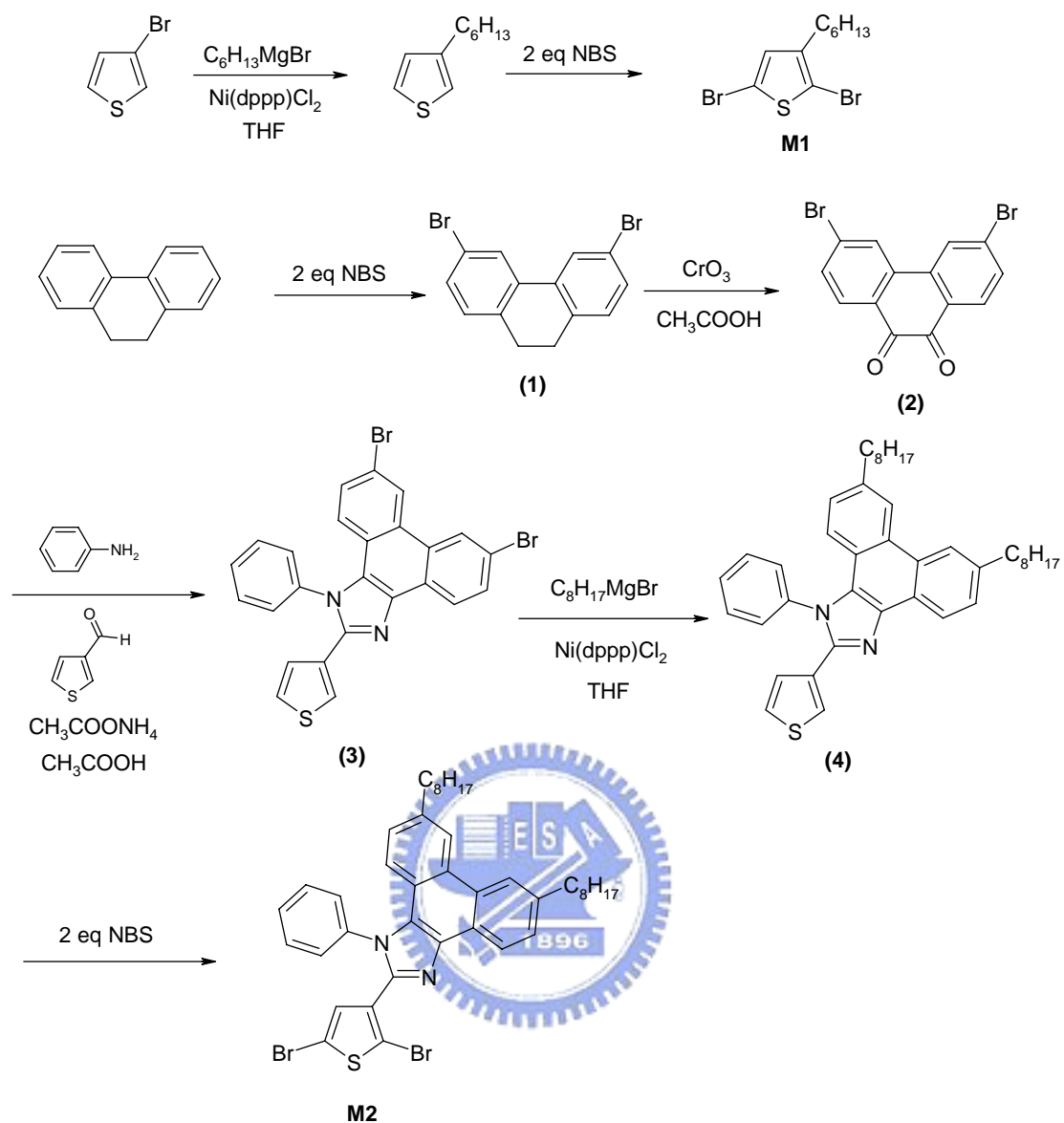




method is the introduction of  $C_{60}$  pendent groups onto the polymers as side chains that enhance charge transfer; unfortunately, such  $C_{60}$  groups absorb very little light and tend to destroy the crystalline ability of the polymeric chain, leading lower power conversion efficiency.<sup>[76]</sup> The second method involves synthesizing panchromatic conjugated polymers containing alternating donor–acceptor units in the main chains;<sup>[76]</sup> with this approach, the preparation of the monomers becomes a critical issue because it is very difficult to purify them. The third method is the incorporation of electron-withdrawing moieties as side chains that exist in conjugation with and coplanar to the polymeric main chains, which are the electron donors. This method has the additional advantages of allowing charge separation through sequential transfer of electrons from the main chains to the side chains and then to [6,6]-phenyl- $C_{61}$ -butyric acid methyl ester (**PCBM**).

Polythiophene derivatives are among the most promising materials for solar cell applications because of their excellent light absorption and electronic conductivity properties. Polymer solar cells containing blends of poly(3-hexylthiophene) and **PCBM** have been studied in depth; recent reports have described power conversion efficiencies of ca. 4% under standard solar conditions (AM 1.5G, 100 mW/cm<sup>2</sup>, 25 °C).<sup>[78–83]</sup> To further improve the power conversion efficiencies of these heterojunction polymer solar cells, we designed a conjugated donor–acceptor polymer

comprising poly(3-hexylthiophene) (**P3HT**) as the donor and side chain-tethered octylphenanthrenyl-imidazole groups as acceptors. In such systems, the charge transfer rate of the side chain-tethered octylphenanthrenyl-imidazole polymers can be improved and their bandgaps can be lowered as a result of the increase in the effective conjugation length. The extent of the reduction in the bandgap of these polymers, however, will depend on the effective conjugation length of the system, which is sometimes reduced through steric hindrance.<sup>[74c, 74d]</sup> Previously, we synthesized poly(3-octylthiophene)s (**P3OT**) containing phenanthrenyl-imidazole moieties that did not exhibit good solubility because of their rigid chemical structures.<sup>[84]</sup> In this present study, we chose **P3HT** because the power conversion efficiency of a device incorporating **P3HT** and **PCBM** was higher than that of a device containing **P3OT** and **PCBM**. The two octyl chains onto the phenanthrenyl-imidazole moiety were introduced to improve the solubility of the polymers. Scheme 3-1 displays our synthetic approaches toward 2,5-dibromo-3-hexylthiophene and the planar phenanthrenyl-imidazole moiety-tethered thiophene monomer. We expected that the presence of the octylphenanthrenyl-imidazole moieties conjugated to the thiophene units would enhance the charge transfer rate of the polythiophene, with the octyl substituents improving the solubility of the polymer derivatives.



**Scheme 3-1.** Synthesis of **M1** and **M2**; NBS: *N*-bromosuccinimide.

Scheme 3-2 illustrates the copolymerization of 2,5-dibromo-3-hexylthiophene

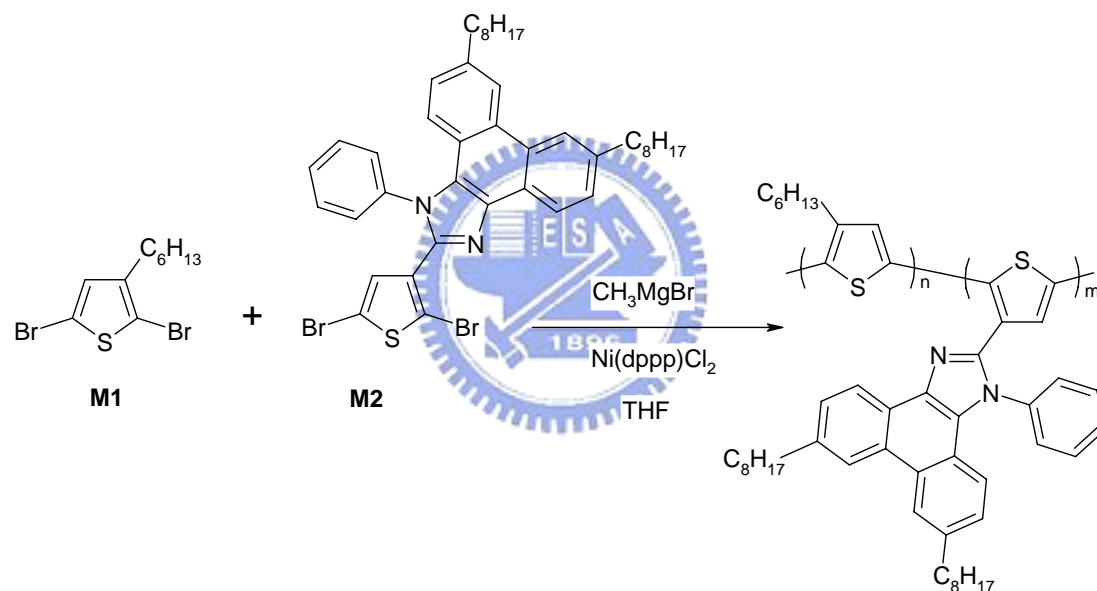
**M1** and

2-(2,5-dibromothiophen-3-yl)-6,9-dioctyl-1-phenyl-1*H*-phenanthro[9,10-*d*]imida

-zole monomer **M2**, performed using a Grignard metathesis approach. We also used

a Grignard metathesis method to prepare **P3HT** for control experiments on comparing

the device performance by **P3HT** with that of our synthesized copolymers.



Polymer molar ratio	<b>P3HT</b>	<b>P46</b>	<b>P64</b>	<b>P82</b>	<b>P91</b>
Molar fraction of <b>M1</b>	100%	60%	40%	20%	10%
Molar fraction of <b>M2</b>	0	40%	60%	80%	90%

**Scheme 3-2.** Grignard metathesis polymerization of **M1** and **M2**; THF: tetrahydrofuran.

### 3-2. Experimental

**Materials.** Chemicals were purchased from Aldrich, TCI, or Lancaster.

[6,6]-Phenyl-C<sub>61</sub>-butyric acid methyl ester (**PCBM**) was purchased from Nano-C.

Polyethylenedioxythiophene/polystyrenesulphonate (PEDOT/PSS) was purchased from Baytron (P VP A1 4083).

**Preparation of Monomers.** Scheme 3-1 illustrates the synthetic route followed for the preparation of the monomers 2,5-dibromo-3-hexylthiophene (**M1**) and

2-(2,5-dibromothiophen-3-yl)-6,9-dioctyl-1-phenyl-1*H*-phenanthro[9,10-d]imidazole

(**M2**). 6,9-Dibromo-1-phenyl-2-(thiophen-3-yl)-1*H*-phenanthro[9,10-d]imidazole (**3**)

was isolated in 92% yield after the reaction of 3-thiophenecarboxaldehyde, phenanthrenequinone, aniline, ammonium acetate, and acetic acid.

6,9-Dioctyl-1-phenyl-2-(thiophen-3-yl)-1*H*-phenanthro[9,10-d]imidazole (**4**) was

isolated in 80% yield from the reaction of compound **3** with octyl magnesium

bromide and Ni(dppp)Cl<sub>2</sub> under reflux.

2-(2,5-Dibromothiophen-3-yl)-6,9-dioctyl-1-phenyl-1*H*-phenanthro[9,10-d]imidazole

(**M2**) was isolated in 93% yield from the reaction between compound **2** and NBS.<sup>[84]</sup>

Detailed synthetic procedures and characterization data are provided below.

**3,6-Dibromo-9,10-dihydrophenanthrene (1).** NBS (9.88 g, 55.48 mmol) was

added portionwise to a solution of 9,10-dihydrophenanthrene (5.0 g, 27.74 mmol) in

THF (66 mL) and acetic acid (66 mL) and then the mixture was stirred for 20 min.

The solution was washed with water (2 × 200 mL), saturated NaHCO<sub>3</sub> (1 × 200 mL), and then again with water (1 × 200 mL). Follow extraction with ethyl acetate, the organic layer was dried (MgSO<sub>4</sub>) and concentrated to yield **1** (8.0 g, 85%). <sup>1</sup>H NMR (300 MHz, CDCl<sub>3</sub>, ppm): 7.60 (s, 2H), 7.34 (d, *J* = 8.1 Hz, 2H), 7.08 (s, 2H), 2.88 (s, 2H). <sup>13</sup>C NMR (75 MHz, CDCl<sub>3</sub>): 136.3, 134.0, 132.5, 131.5, 130.2, 120.4, 29.7.

HRMS-EI (*m/z*): [*M*<sup>+</sup>] calcd. for C<sub>14</sub>H<sub>10</sub>Br<sub>2</sub>, 335.9149; found, 335.9147.

### **3,6-Dibromophenanthrene-9,10-dione (2).**

3,6-Dibromo-9,10-dihydrophenanthrene (7.0 g, 20.7 mmol) and chromic trioxide (4.84 g, 46.6 mmol) were dissolved in acetic anhydride (100 mL) and reacted for 3 h at room temperature. The solution was poured into 1 N HCl solution (300 mL) and extracted with ethyl acetate. The organic layer was dried (MgSO<sub>4</sub>) and concentrated to yield **2** (6.8 g, 89%). <sup>1</sup>H NMR (300 MHz, CDCl<sub>3</sub>, ppm): 7.88 (s, 2H), 7.74 (d, *J* = 8.4 Hz, 2H), 7.51 (s, 2H). <sup>13</sup>C NMR (75 MHz, CDCl<sub>3</sub>): 180.2, 136.3, 134.0, 132.5, 131.5, 130.2, 129.4. HRMS-EI (*m/z*): [*M*<sup>+</sup>] calcd. for C<sub>14</sub>H<sub>6</sub>Br<sub>2</sub>O<sub>2</sub>, 363.8734; found, 363.8732.

### **6,9-Dibromo-1-phenyl-2-(thiophen-3-yl)-1*H*-phenanthro[9,10-*d*]imidazole (3).**

A mixture of aniline (7.95 g, 85.5 mmol), 3,6-dibromophenanthrene-9,10-dione (**2**, 6.63 g, 17.1 mmol), 3-thiophenecarboxaldehyde (1.92 g, 17.1 mmol), ammonium

acetate (5.28 g, 68.57 mmol), and acetic acid (100 mL) was heated for 2 h under nitrogen in an oil bath maintained at a bath temperature of 120 °C. After cooling and filtering, the solid product was washed sequentially with an acetic acid/water mixture (1:1, 150 mL) and water, and then dried to yield **3** (8.22 g, 90%). <sup>1</sup>H NMR (300 MHz, CDCl<sub>3</sub>, ppm): 8.84–8.87 (m, 1H), 8.75 (d, *J* = 8.4 Hz, 1H), 8.69 (d, *J* = 8.4 Hz, 1H), 7.45–7.78 (m, 7H), 7.22–7.27 (m, 2H), 7.14 (m, 1H), 7.08 (m, 1H). <sup>13</sup>C NMR (75 MHz, CDCl<sub>3</sub>): 149.2, 137.3, 134.0, 132.5, 131.5, 130.2, 128.4, 126.4, 125.7, 120.4. HRMS-EI (*m/z*): [*M*<sup>+</sup>] calcd. for C<sub>25</sub>H<sub>14</sub>Br<sub>2</sub>SN<sub>2</sub>, 531.9244; found, 531.9250.

**6,9-Dioctyl-1-phenyl-2-(thiophen-3-yl)-1*H*-phenanthro[9,10-*d*]imidazole (4).** A 100-mL round-bottom three-neck flask equipped with a stirrer bar, condenser, addition funnel, and N<sub>2</sub> inlet/outlet was charged with Mg (0.79 g, 32.7 mmol) and dry ether (10 mL). Bromooctane (2.89 g, 14.8 mmol) in dry ether (20 mL) was added dropwise to maintain a mild reflux. The mixture was heated under reflux for an additional 2.5 h. The Grignard reagent solution was then added dropwise to an ice-cooled 250-mL three-neck round-bottom flask containing 6,9-dibromo-1-phenyl-2-(thiophen-3-yl)-1*H*-phenanthro[9,10-*d*]imidazole (**3**, 4.00 g, 7.4 mmol), Ni(dppp)Cl<sub>2</sub> (0.04 g, 0.08 mmol), and dry ether (30 mL). The solution was then heated under reflux overnight. The cooled reaction mixture was quenched carefully with HCl (5%, 75 mL); the ether layer was separated, washed with H<sub>2</sub>O (2 ×

75 mL), and dried (MgSO<sub>4</sub>). The crude product was purified by column chromatography (silica gel, 8% EtOAc/hexane) to yield **4** (4.0 g, 88%). <sup>1</sup>H NMR (300 MHz, CDCl<sub>3</sub>, ppm): 8.84–8.87 (m, 1H), 8.75 (d, *J* = 8.4 Hz, 1H), 8.69 (d, *J* = 8.4 Hz, 1H), 7.45–7.78 (m, 7H), 7.22–7.27 (m, 2H), 7.14 (m, 1H), 7.08 (m, 1H), 1.00–1.80 (m, 30H), 2.66 (t, *J* = 7.2 Hz, 4H). <sup>13</sup>C NMR (75 MHz, CDCl<sub>3</sub>): 149.2, 137.3, 134.0, 132.5, 131.5, 130.2, 128.4, 126.4, 125.7, 124.7, 31.9, 30.6, 29.6, 29.4, 29.3, 22.7, 14.1. HRMS-EI (*m/z*): [*M*<sup>+</sup>] calcd. for C<sub>41</sub>H<sub>48</sub>SN<sub>2</sub>, 600.3538; found, 600.3533.

**2-(2,5-Dibromothiophen-3-yl)-6,9-dioctyl-1-phenyl-1*H*-phenanthro[9,10-d]imidaz**

**-ole (M2).** NBS (2.07 g, 11.6 mmol) was added portionwise to a solution of 6,9-dioctyl-1-phenyl-2-(thiophen-3-yl)-1*H*-phenanthro[9,10-d]imidazole (**4**, 3.5 g, 5.82 mmol) in THF (33 mL) and acetic acid (33 mL) and then the mixture was stirred for 20 min. The solution was washed with water (2 × 200 mL), saturated NaHCO<sub>3</sub> (1 × 200 mL), and then again with water (1 × 200mL). Following extraction with ethyl acetate, the organic layer was dried (MgSO<sub>4</sub>) and concentrated to yield **M2** (4.0 g, 90%). <sup>1</sup>H NMR (300 MHz, CDCl<sub>3</sub>, ppm): 8.84–8.87 (m, 1H), 8.75 (d, *J* = 8.4 Hz, 1H), 8.69 (d, *J* = 8.4 Hz, 1H), 7.45–7.78 (m, 7H), 7.22–7.27 (m, 1H), 6.73 (s, 1H), 1.00–1.80 (m, 30H), 2.66 (t, *J* = 7.5 Hz, 4H). <sup>13</sup>C NMR (75 MHz, CDCl<sub>3</sub>): 149.2, 137.3, 134.0, 132.5, 131.5, 130.2, 128.4, 126.4, 125.7, 124.7, 117.3, 99.2, 31.9, 30.6,



29.6, 29.4, 29.3, 22.7, 14.1. HRMS-FAB ( $m/z$ ):  $[M^+ - H]$  calcd. for  $C_{41}H_{47}SN_2Br_2$ , 757.1826; found, 757.1817.

**Preparation of Polythiophene Derivatives.** All polymers were synthesized through Grignard metathesis polymerizations in THF, according to procedures similar to those described in the literature.<sup>[85]</sup> The Grignard metathesis polymerizations of 2,5-dibromo-3-hexylthiophene (**M1**) and 2-(2,5-dibromothiophen-3-yl)-1-phenyl-1*H*-phenanthro[9,10-*d*]imidazole (**M2**) are illustrated in Scheme 3-2. Detailed synthetic procedures and characterization data are provided below.

**Poly(3-hexylthiophene) (P3HT).**  $CH_3MgBr$  (1.5 mL, 4.5 mmol) was added via syringe to a stirred solution of 2,5-dibromo-3-hexylthiophene (1.60 g, 4.5 mmol) and freshly distilled THF (80 mL) in a three-necked 100-mL round-bottom flask. The solution was heated under reflux for 2 h and then  $Ni(dppp)Cl_2$  (12 mg, 0.02 mmol) was added. The mixture was stirred for 1 h before the reaction was quenched through the addition of methanol. The solid polymer was washed with methanol within a Soxhlet extractor. The polymer then was dissolved through Soxhlet extraction with chloroform; the solvent was evaporated and the residue dried under vacuum to yield poly(3-octylthiophene) (0.54 g, 61%; 99% coupled head-to-tail).  $^1H$  NMR (300 MHz,  $CDCl_3$ ): 6.98 (s, 1H), 2.78 (s, 2H); 0.86, 1.27, and 1.68 (m, 15H).

$^{13}\text{C}$  NMR (75 MHz,  $\text{CDCl}_3$ ): 139.9, 133.7, 130.5, 128.6, 31.9, 30.6, 29.6, 29.4, 22.7,

14.1. Anal. Calcd for  $\text{C}_{10}\text{H}_{14}\text{S}$ : H, 8.49; C, 72.27; S, 19.28. Found: H, 8.28; C,

72.58; S, 19.0.

**P28.**  $\text{CH}_3\text{MgBr}$  (1.5 mL, 4.5 mmol) was added via syringe to a stirred solution of 2,5-dibromo-3-octylthiophene (1.44 g, 4.05 mmol),

2-(2,5-dibromothiophen-3-yl)-1-phenyl-1*H*-phenanthro[9,10-d]imidazole (0.24 g,

0.45 mmol), and freshly distilled THF (80 mL) in a three-necked 100-mL

round-bottom flask. The solution was heated under reflux for 2 h and then

$\text{Ni}(\text{dppp})\text{Cl}_2$  (12 mg, 0.02 mmol) was added. The mixture was stirred for 1 h and

then the reaction was quenched through the addition of methanol. The solid polymer

was washed with methanol within a Soxhlet extractor. The polymer then was

dissolved through Soxhlet extraction with chloroform; the chloroform was evaporated

and the residue dried under vacuum to yield **P28** (0.51 g, 60%; 99% coupled

head-to-tail).  $^1\text{H}$  NMR (300 MHz,  $\text{CDCl}_3$ ): 8.4–8.9 (br, 2H), 7.3–7.9 (br, 13H), 6.98

(s, 1H), 2.75 (s, 9H); 0.85, 1.26, and 1.64 (m, 38H).  $^{13}\text{C}$  NMR (75 MHz,  $\text{CDCl}_3$ ):

149.2, 139.9, 137.4, 137.1, 133.2, 131.1, 130.4, 130.1, 129.6, 129.0, 128.4, 128.2,

127.5, 127.0, 126.5, 126.2, 125.5, 124.6, 123.4, 122.6, 122.0, 121.1, 120.0, 119.7,

31.9, 30.6, 29.6, 29.4, 29.3, 22.7, 14.1. Anal. Calcd for  $\text{C}_{16.2}\text{H}_{21}\text{SN}_{0.4}$ : C, 74.1; H,

8.4; N, 0.93; S, 16.57. Found: C, 72.78; H, 8.66; N, 0.87; S, 15.90.

Other polymer samples were synthesized using the method described for the preparation of **P28**, but with different amounts of

2-(2,5-dibromothiophen-3-yl)-1-phenyl-1*H*-phenanthro[9,10-*d*]imidazole (**M2**).

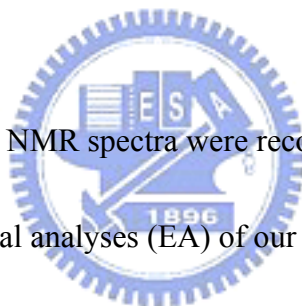
**P46.**  $^1\text{H}$  NMR (300 MHz,  $\text{CDCl}_3$ ): 8.4–8.9 (br, 2H), 7.3–7.9 (br, 13H), 6.98 (s, 1H), 2.75 (s, 9H); 0.85, 1.26, and 1.64 (m, 38H).  $^{13}\text{C}$  NMR (75 MHz,  $\text{CDCl}_3$ ): 149.2, 139.9, 137.4, 137.1, 133.2, 131.1, 130.4, 130.1, 129.6, 129.0, 128.4, 128.2, 127.5, 127.0, 126.5, 126.2, 125.5, 124.6, 123.4, 122.6, 122.0, 121.1, 120.0, 119.7, 31.9, 30.6, 29.6, 29.4, 29.3, 22.7, 14.1. Anal. Calcd for  $\text{C}_{22.4}\text{H}_{28}\text{SN}_{0.8}$ : C, 76.1; H, 8.38; N, 1.86; S, 13.66. Found: C, 74.78; H, 7.66; N, 1.69; S, 14.80.

**P64.**  $^1\text{H}$  NMR (300 MHz,  $\text{CDCl}_3$ ): 8.4–8.9 (br, 2H), 7.3–7.9 (br, 13H), 6.98 (s, 1H), 2.75 (s, 9H); 0.85, 1.26, and 1.64 (m, 38H).  $^{13}\text{C}$  NMR (75 MHz,  $\text{CDCl}_3$ ): 149.2, 139.9, 137.4, 137.1, 133.2, 131.1, 130.4, 130.1, 129.6, 129.0, 128.4, 128.2, 127.5, 127.0, 126.5, 126.2, 125.5, 124.6, 123.4, 122.6, 122.0, 121.1, 120.0, 119.7, 31.9, 30.6, 29.6, 29.4, 29.3, 22.7, 14.1. Anal. Calcd for  $\text{C}_{28.6}\text{H}_{35}\text{SN}_{1.2}$ : C, 77.98; H, 8.32; N, 2.79; S, 10.91. Found: C, 74.78; H, 7.66; N, 2.59; S, 10.80.

**P82.**  $^1\text{H}$  NMR (300 MHz,  $\text{CDCl}_3$ ): 8.4–8.9 (br, 2H), 7.3–7.9 (br, 13H), 6.98 (s, 1H), 2.75 (s, 9H); 0.85, 1.26, and 1.64 (m, 38H).  $^{13}\text{C}$  NMR (75 MHz,  $\text{CDCl}_3$ ): 149.2, , 139.9, 137.4, 137.1, 133.2, 131.1, 130.4, 130.1, 129.6, 129.0, 128.4, 128.2, 127.5, 127.0, 126.5, 126.2, 125.5, 124.6, 123.4, 122.6, 122.0, 121.1, 120.0, 119.7,

31.9, 30.6, 29.6, 29.4, 29.3, 22.7, 14.1. Anal. Calcd for  $C_{33.2}H_{42}SN_{1.6}$ : C, 79.9; H, 8.27; N, 3.72; S, 8.11. Found: C, 78.22; H, 8.72; N, 3.93; S, 7.83.

**P91.**  $^1H$  NMR (300 MHz,  $CDCl_3$ ): 8.4–8.9 (br, 2H), 7.3–7.9 (br, 13H), 6.98 (s, 1H), 2.75 (s, 9H); 0.85, 1.26, and 1.64 (m, 38H).  $^{13}C$  NMR (75 MHz,  $CDCl_3$ ): 149.2, 139.9, 137.4, 137.1, 133.2, 131.1, 130.4, 130.1, 129.6, 129.0, 128.4, 128.2, 127.5, 127.0, 126.5, 126.2, 125.5, 124.6, 123.4, 122.6, 122.0, 121.1, 120.0, 119.7, 31.9, 30.6, 29.6, 29.4, 29.3, 22.7, 14.1. Anal. Calcd for  $C_{37.9}H_{45.5}SN_{1.8}$ : C, 80.85; H, 8.24; N, 4.12; S, 6.79. Found: C, 81.22; H, 7.72; N, 3.93; S, 6.51.



**Characterization:**  $^1H$  and  $^{13}C$  NMR spectra were recorded on a Varian Unity-300 NMR spectrometer. Elemental analyses (EA) of our polymers were performed using a Heraeus CHN-OS Rapid instrument. Thermal gravimetric analyses of the polythiophene derivatives were performed using a Du Pont TGA 2950 instrument operated at a heating rate of 10 °C/min under a nitrogen purge. Differential scanning calorimetry (DSC) was performed on a Du Pont DSC 2010 instrument operated at a heating rate of 10 °C/min under a nitrogen purge. Samples were heated from 30 to 200 °C, cooled to 20 °C, and then heated again from 30 to 200 °C; the glass transition temperatures ( $T_g$ ) were determined from the second heating scans. UV–Vis spectra were measured using an HP 8453 diode array spectrophotometer. PL spectra were

recorded using a Hitachi F-4500 luminescence spectrometer. The molecular weights of the polythiophene derivatives were measured through gel permeation chromatography (GPC) using a Waters chromatography unit interfaced to a Waters 2414 differential refractometer. Three 5- $\mu\text{m}$  Waters styragel columns were connected in series in decreasing order of pore size ( $10^4$ ,  $10^3$ , and  $10^2$  Å); THF was the eluent and standard polystyrene samples were used for calibration. The redox behavior of each polymer was investigated by cyclic voltammetry using an electrolyte of 0.1 M tetrabutylammonium hexafluorophosphate ( $n\text{-Bu}_4\text{NPF}_6$ ) in acetonitrile.

Cyclic voltammetry measurements on our synthesized polymers were performed using a BAS 100 electrochemical analyzer, operated at a potential scan rate of 40 mV/s. In each case, a glassy disk carbon electrode coated with a thin layer of a polymer was used as the working electrode; a platinum wire was used as the counter electrode, and a silver wire was used as the quasi-reference electrode. All of the potentials quoted herein used Ag wire as the quasi-reference electrode; the electrochemical potential of Ag is  $-0.02$  V vs. saturated calomel electrode (SCE).

$E_{\text{HOMO}} = -E_{\text{ox}} - 4.4$  eV and  $E_{\text{LUMO}} = -E_{\text{red}} - 4.4$  eV, where  $E_{\text{ox}}$  and  $E_{\text{red}}$  are the onset potentials of the oxidation and reduction peaks (vs. SCE), respectively, and the value of 4.4 eV relates the SCE reference to a vacuum. The topography of **P3HT/PCBM** and **P91/PCBM** films was obtained by using atomic force microscope (AFM) with a

Digital Instruments Nanoscope IIIa, analyzed at a scan rate 1.0 Hz with the tapping mode. The AFM samples were prepared by spin-coating the solutions of polymer and **PCBM** blends in dichlorobenzene on silica wafer substrates, followed by annealing them at 120°C for two hours in an oven.

**Time-Resolved Photoluminescence Spectra.** The relaxation dynamics of the thin-film samples were studied using the femtosecond fluorescence up-conversion technique; the experimental details are available elsewhere.<sup>[86]</sup> In brief, a fluorescence optically gated system (FOG100, CDP) was used in conjunction with a mode-locked Ti-sapphire laser (Mira900D, Coherent) pumped with a 10-W Nd:YVO4 laser (Verdi-V10, Coherent) where femtosecond pulses were produced having a pulse width of 160 fs, a wavelength centered at 880 nm, and a repetition rate of 76 MHz. The frequency of the laser pulse was doubled using a non-linear crystal to obtain a pulse of 440 nm, which was used as an excitation pulse, while the residual fundamental pulse was used as an optical gate. A dichroic beam splitter separated the excitation and gate beams. The intensity of the excitation beam was attenuated appropriately using various neutral density filters and the plane of polarization was altered to maintain the magic angle conditions at 54.7°. The excitation beam was then focused onto a 1-mm rotating cell containing the solid thin-film samples. The emission was directed toward another non-linear crystal with the aid of a pair of

parabolic mirrors. The gated pulse and the emission were focused on the BBO crystal to obtain maximum spatial overlap when the sum-frequency was generated. This sum-frequency signal was passed through an iris and band-pass filter to eliminate stray light, focused on a double-monochromator (DH10, Jobin Yvon) with a lens, and then detected with a photomultiplier (R1527P, Hamamatsu) connected to a computer-controlled photon-counting system. A temporal profile could be obtained by varying the delay between the gate and the excitation pulses via a stepping-motor translational stage.

**Device Fabrication.** The current density–voltage ( $J$ – $V$ ) measurements of our polymers were performed using devices having a sandwich structure [ITO/PEDOT:PSS/polymer:**PCBM** (1:1, w/w)/Ca/Al]. The ITO-coated glass substrate was pre-cleaned and treated with oxygen plasma prior to use. The polymer/**PCBM** layer was spin-coated at 1500 rpm from the corresponding dichlorobenzene solution (20 mg/mL). Dichlorobenzene is the best solvent to dissolve our polymers, after having tried several other solvents such as toluene, chloroform, and tetrahydrofuran. The nominal thickness of the polymer/**PCBM** layer was ca. 80 nm. The active layers of our devices were thermal annealed at 120°C for 30 minutes prior to electrode depositions. Different thermal treatment conditions for the samples were performed- samples were subject to thermal

annealing at 110 °C, 120 °C and 150 °C for 30 minutes, respectively. The thermal treatment of 120 °C for 30 minutes on the samples is the one that was found to give the optimal power conversion efficiency for the eventual devices. Using a base pressure below  $1 \times 10^{-6}$  torr, a layer of Ca (30 nm) was vacuum-deposited as the cathode and then a thick layer of Al (100 nm) was deposited as the protecting layer; the effective area of one cell is 0.04 cm<sup>2</sup>. Testing of the devices was performed under simulated AM 1.5G irradiation (100 mW/cm<sup>2</sup>) using a xenon lamp-based Newport 66902 150W solar simulator. A xenon lamp with an AM1.5 filter was used as the white light source; the optical power at the sample was 100 mW/cm<sup>2</sup>, detected by an OPHIR thermopie 71964. The  $J-V$  characteristics were measured using a Keithley 236 electrometer. The spectrum of our solar simulator had a mismatch of less than 25%. The spectrum of the solar simulator was calibrated by a PV-measurement (PVM-154) mono-Si solar cell (NREL calibrated), and Si photo diode (Hamamatsu S1133) was used to check the uniformity of the exposed area. AM 1.5G (ASTM G173)<sup>[87]</sup> light intensity was calibrated by thermopie and PV-measurement. The mismatch factor (M) was 1.34, which was obtained by taking the PVM-154 as the reference cell and devices of **P3HT/PCBM** and **P91/PCBM** as the test cells and calculating the spectrum from 300 nm to 900 nm with interval of 10 nm (see Eq. (1)). The PVM-154 combined with KG-5 filter (350 nm~ 700 nm



passed, Newport) was to simulate a reference solar cell with spectral responsivity from 350 nm to 700 nm. Reported efficiencies are the averages obtained from four devices prepared on each substrate. The external quantum efficiency (EQE) was measured using a Keithley 236 coupled with Oriel Cornerstone 130 monochromator. The light intensity at each wavelength was calibrated using an OPHIR 71580 diode.



### 3-3. Results and Discussion

The regioregularity of the polymers was determined from  $^1\text{H}$  NMR spectra, analyzing the ratio of the area under the peak at 6.98 ppm to the area under all of the peaks ranging from 6.98 to 7.04 ppm. Because only a signal at 6.98 ppm is present in the spectra of **P3HT** and **P91**, with no other peaks nearby, we believe that these polymers possess an almost complete head-to-tail configuration (i.e., regioregularity close to 100%).<sup>[85]</sup> Due to the bulky octylphenanthrenyl-imidazole on the side of thiophene monomers, the selectivity of these monomers during their Grignard reaction becomes very high—the reaction first took place on the bromide on the 5-position then on the bromide on the 2-position of the thiophene monomers. Hence, the regioregularity of **P91** obtained was very high after polymerization. In the NMR spectra of **P91**, the peak at 6.73 ppm (CH proton of the thiophene ring) is absent; the broad peaks in the ranges 8.4–8.9 (CH protons of the phenanthrenyl group), 7.2–8.2 (CH protons on the phenyl group), and 0.8–3.0 ppm (octyl and hexyl chain protons) confirm that the copolymers of **M1** and **M2** had formed. The details of the  $^1\text{H}$  NMR spectra of the synthesized polymers are presented in Figure 3-1.

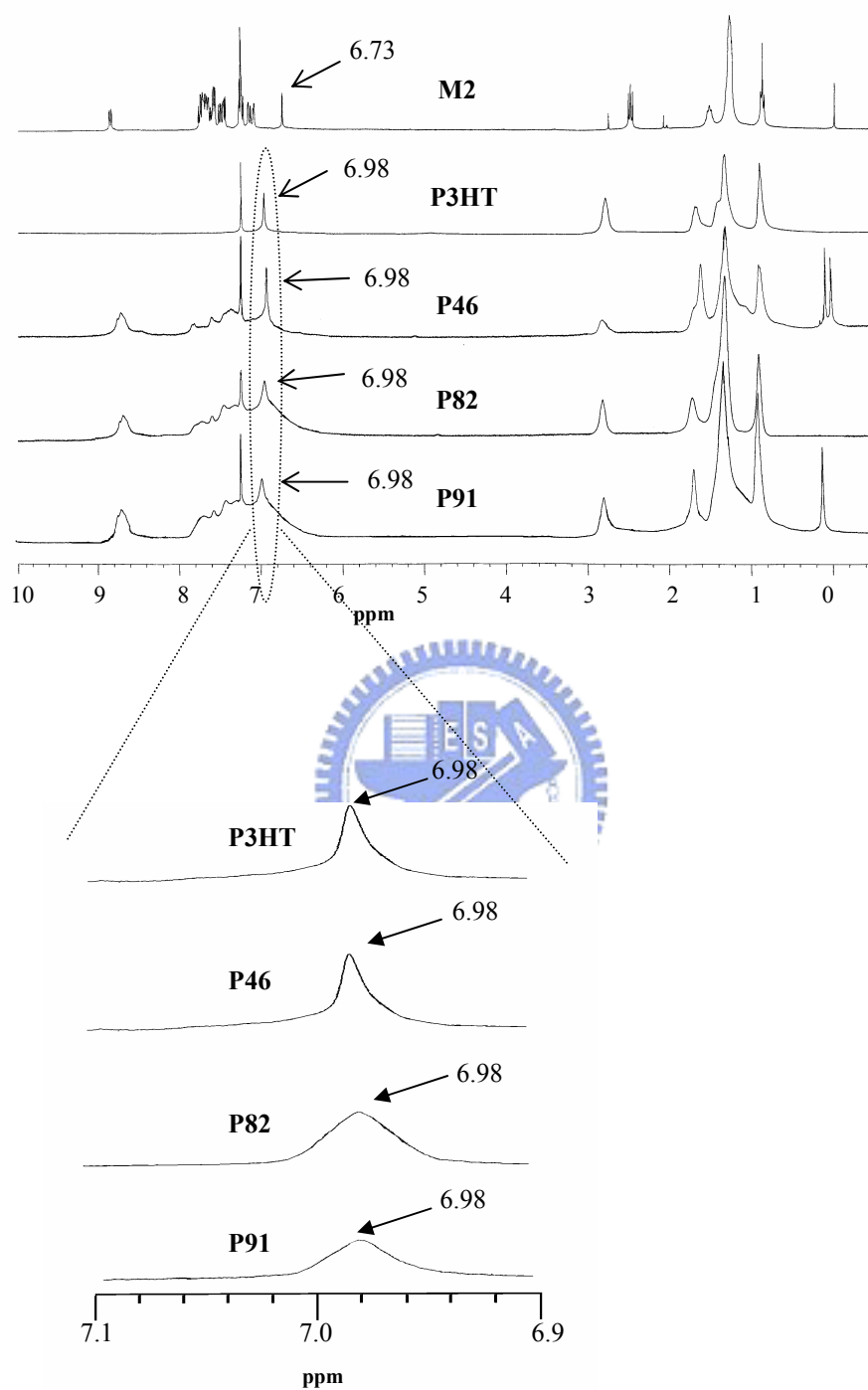


**Figure 3-1.** The  $^1\text{H}$  NMR spectra of **M2**, **P3HT**, **P46**, **P82**, and **P91**.

Table 3-1 displays the molecular weights, the degradation temperatures, and the glass transition temperatures of copolymers synthesized from **P3HT** to **P91**. The number molecular weights ( $M_n$ ) of our polymers range from 8.9 to 13.5 kg/mol, with polydispersity index (PDI) in the range from 1.20 to 1.56. The thermal degradation temperatures of these copolymers decreased upon increasing the content of octylphenanthrenyl-imidazole moieties because of the introduction of the octyl chains. The glass transition temperature of **P91** was not detectable, whereas it was 54.8 °C for **P3HT**.

**Table 3-1.** Molecular Weights and Thermal Properties of Synthesized Polymers.

	$M_n (\times 10^4)$	$M_w (\times 10^4)$	PDI	Tg (°C)	Td (°C) <sup>a</sup>
<b>P3HT</b>	1.35	1.57	1.20	54.8	387.9
<b>P46</b>	1.05	1.44	1.47	**	367.1
<b>P64</b>	0.98	1.46	1.48	**	332.4
<b>P82</b>	0.90	1.39	1.54	**	321.2
<b>P91</b>	0.89	1.38	1.56	**	313.3

<sup>a</sup> Temperature at which 5% weight loss occurred, based on the initial weight.

\*\* Glass transition temperature could not be observed.

Figure 3-2 displays UV–Vis spectra of the polymers in the solid state. The dihedral angle between the plane of octyl-phenanthrenyl-imidazole and that of thiophene determined by molecular modeling (Chem. 3D) was 82.13° (see Figure 3-3.). Therefore, the small peak at 270 nm is caused by the presence of conjugated phenanthrenyl-imidazole moieties that are not fully coplanar to the polythiophene chain owing to steric hindrance. The  $\pi$ – $\pi^*$  transitions are responsible for the maximum absorptions ( $\lambda_{\text{max}}$ ) that occur at ca. 510 nm for **P3HT** and 550 nm for the **P91** thin films.<sup>[88]</sup> These data indicate that the optical bandgap of the **P91** copolymer is lower than that of pure **P3HT**. Table 3-2 lists the absorption maxima and optical bandgaps of the synthesized polymers. Optimally, conjugating 90 mol% of octylphenanthrenyl-imidazole moieties to the polythiophene chains led to the optical bandgap being reduced from 1.91 to 1.80 eV, confirming that the presence of the octylphenanthrenyl-imidazole moieties increased the effective conjugation length of the polythiophene main chain to some extent.<sup>[89]</sup> The cyclic voltammogram data of these polymers also indicates the same phenomenon that the bandgap of the copolymer reduced with the increasing mole fraction of octylphenanthrenyl-imidazole moieties, despite absolute values being different ( see Table 3-3).

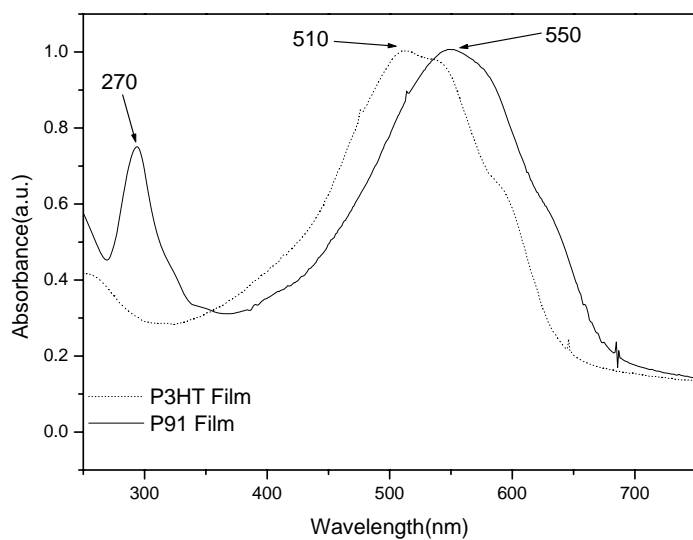


**Figure 3-2.** UV-Vis spectra of **P3HT** and **P91** in the solid state.

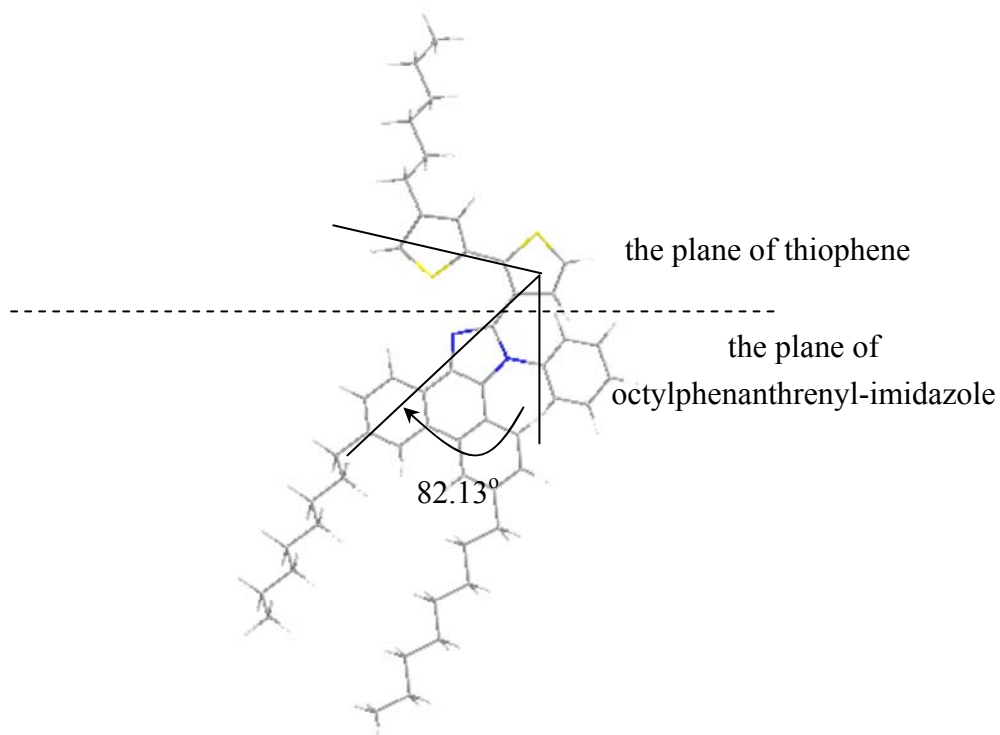


**Figure 3-3.** The chemical structure diagram of HT and octylphenanthrenyl-imidazole moiety.

**Table 3-2.** UV–Vis Absorption Peaks and Optical Bandgaps of Synthesized Polymers.

Polymer	Absorption $\lambda_{\max}$		Optical bandgap (eV)
	Solution (nm)	Film (nm)	
<b>P3HT</b>	439	510 (544, 595)	1.91
<b>P46</b>	451	530 (611)	1.86
<b>P64</b>	460	538 (628)	1.85
<b>P82</b>	466	546 (630)	1.83
<b>P91</b>	470	550 (634)	1.80

**Table 3-3.** Redox data, HOMO, LUMO energy levels, and band gap energies of our synthesized polymers.

	Reduction Onset Potential (eV)	Oxidation Onset Potential (eV)	HOMO (eV)	LUMO (eV)	Bandgap (eV)
<b>P3HT</b>	-1.75	0.35	-4.75	-2.75	2.0
<b>P46</b>	-1.63	0.30	-4.70	-2.87	1.83
<b>P64</b>	-1.55	0.25	-4.65	-2.95	1.70
<b>P82</b>	-1.48	0.25	-4.65	-3.02	1.63
<b>P91</b>	-1.35	0.25	-4.65	-3.05	1.60

Figure 3-4 displays photoluminescence (PL) spectra of the polymer films, recorded at an excitation wavelength of 440 nm. The PL of the octylphenanthrenyl-imidazole-containing copolymers films was quenched dramatically relative to that of pure **P3HT**, with the degree of quenching increasing upon increasing the content of phenanthrenyl-imidazole units in the copolymer. This finding suggests that photoinduced charge transfer occurred when the polymers were photoexcited. The charge transfer from the photoexcited polythiophene backbone to the electron-withdrawing phenanthrenyl-imidazole side chains was sufficiently rapid to compete with radiative recombination of the excitons.<sup>[90]</sup>

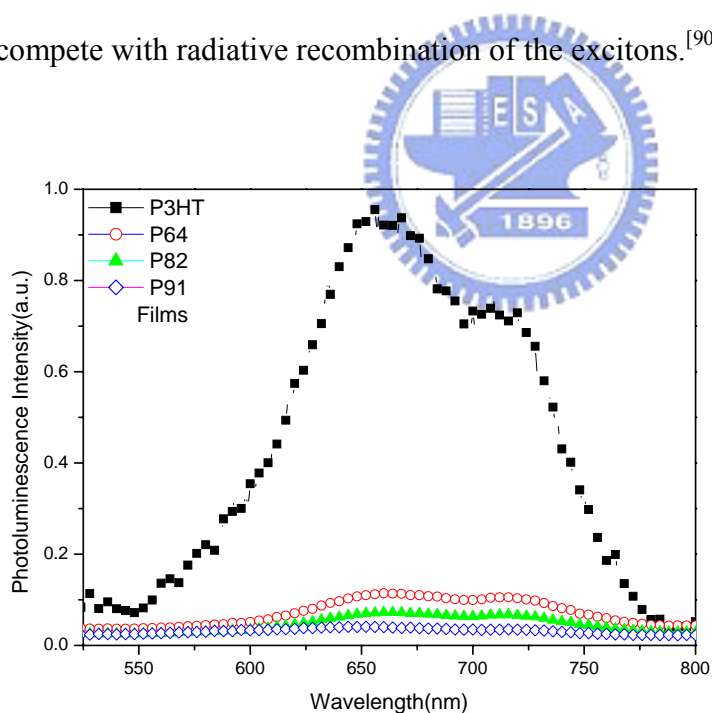


**Figure 3-4.** Photoluminescence (PL) spectra, normalized to the number of absorbed photons, of the synthesized polymers in the solid state.

The transients of the pure polymers and the blends with **PCBM** were found to be



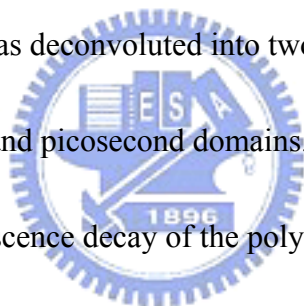
comprised of two time constants. For the sake of easy comparison, an amplitude-averaged rate constant of each transient was calculated. The averaged rate constants were calculated using the following equation:<sup>[91]</sup>

$$\langle \tau \rangle_a = \sum_{i=1}^n a_i \tau_i \quad (3)$$

where  $a_i$  are the fractional amplitudes where  $\sum_{i=1}^n a_i = 1$  and  $\tau_i$  are the individual rate constants, which are the reciprocals of the time constants.

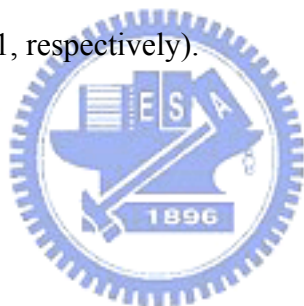
Figure 3-5 displays the normalized fluorescence up-conversion transients of **PCBM**, the polymers, and blends of the polymers with **PCBM**, with excitation ( $\lambda_{ex}$ ) at 440 nm and emission ( $\lambda_{em}$ ) at 600 nm. The transient of **PCBM** alone exhibits only the background signal, whereas the transients of the polymer alone feature a biphasic relaxation feature. The excited-state relaxation of the polymer is due mainly to de-excitation of the quasi-thermal self-trapping exciton (STE).<sup>[92]</sup> The fluorescence decay of pure **P91** was slower than that of pure **P3HT**, possibly due to less aggregation of **P91** molecules than that of **P3HT** molecules in the film, as a result of the steric effect of the bulky and conjugated octylphenanthrenyl-imidazole side groups. The fluorescence decay of the blend of the polymers with **PCBM** was faster than that of individual polymers in both cases. When the polymers were blended

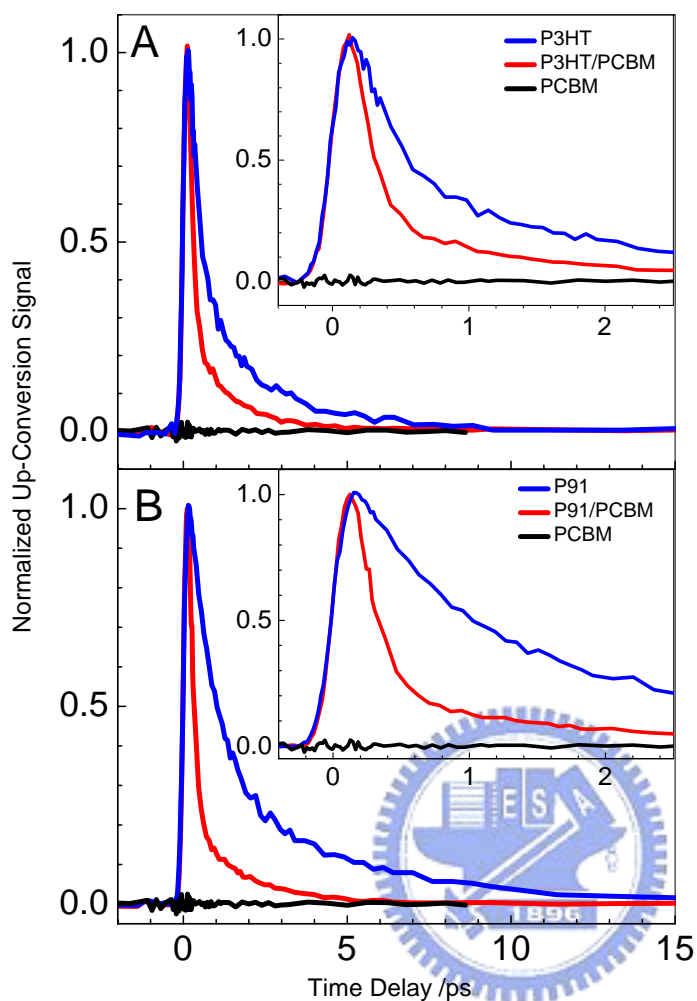
with **PCBM**, the transients were quenched substantially, but the biphasic feature was retained. These phenomena can be observed in the case of MEHPPV and **PCBM**,<sup>[93]</sup> the shortening of the lifetime is rationalized in terms of a rapid electron transfer resulting from the dissociation of the  $S_1$  exciton of the polymer when there is a **PCBM** molecule in the vicinity of the polymer exciton. The fluorescence transients were thus fitted with two decay components according to a parallel kinetic model.<sup>[86]</sup> In Figures 3-6–3-8, we provide the fluorescence decay data and kinetic fits of both polymers and their blends with **PCBM** at values of  $\lambda_{em}$  of 600, 620, and 660 nm ( $\lambda_{ex}$  = 440 nm). Each transient was deconvoluted into two components with time constants in the femtosecond and picosecond domains.



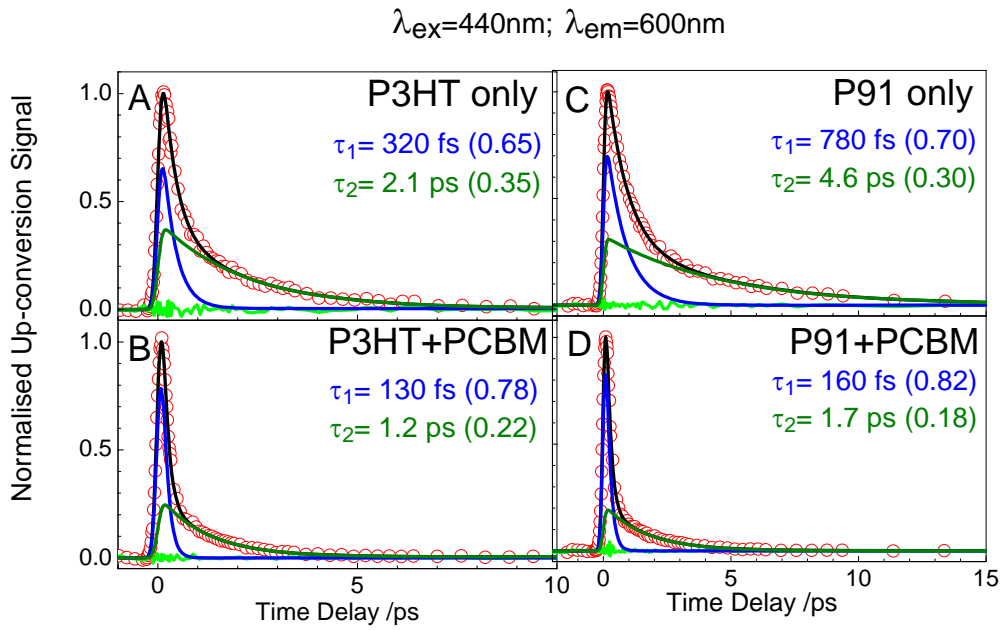
In the study of the fluorescence decay of the polymer, the only mode responsible for de-excitation was quenching; in the case of the blends of polymers with **PCBM**, there was an additional de-excitation pathway due to electron transfer between the donor (polymer) and an acceptor (**PCBM**). Thus, the averaged rate constant of the pure polymer can be considered to be  $k_q$  (the quenching rate constant), while that of the blend of polymers with **PCBM** was the total rate constant,  $k_T$ , which includes both the quenching rate and electron transfer rate constants. Therefore, it is feasible to evaluate the rate constant of the electron transfer process from the averaged rate constants of the polymer and the blend of the polymers with **PCBM** ( $k_{ET} = k_T - k_q$ ).

Table 3-4 lists the averaged rate constants of the polymers ( $k_q$ ) and the blends of polymers and **PCBM** ( $k_T$ ), and the net electron transfer rate constants ( $k_{ET} = k_T - k_q$ ). The ratio of  $k_{ET}$  to  $k_q$  provides a comparison between the two different pathways of de-excitation: electron transfer vs. quenching. The  $k_{ET}/k_q$  ratios at 600 nm were 1.45 and 3.46 for **P3HT/PCBM** and **P91/PCBM**, respectively; i.e., a relatively higher electron transfer probability existed for the case of **P91** than that for the case of **P3HT**, when blended with **PCBM**. Even at the emission wavelengths of 620 and 660 nm, the electron transfer was still much more favored for **P91** than for **P3HT** (ratios of (1.67 vs. 0.31 and 1.04 vs. 0.31, respectively).





**Figure 3-5.** Normalized fluorescence transients of (A) **P3HT** and (B) **P91** coated on quartz, recorded at values of  $\lambda_{\text{ex}}$  and  $\lambda_{\text{em}}$  at 440 and 600 nm, respectively. The blue curves represent the normalized transients of the polymer; the red and the black curves correspond to those of the blend of polymer and **PCBM** and **PCBM**, respectively. The insets display the same transients at a shorter time range.



**Figure 3-6.** Time-resolved transients of (A) **P3HT**, (B) the blend of **P3HT** and **PCBM**, (C) **P91**, and (D) the blend of **P91** and **PCBM** coated on quartz at values of  $\lambda_{\text{ex}}$  and  $\lambda_{\text{em}}$  of 440 and 600 nm, respectively.

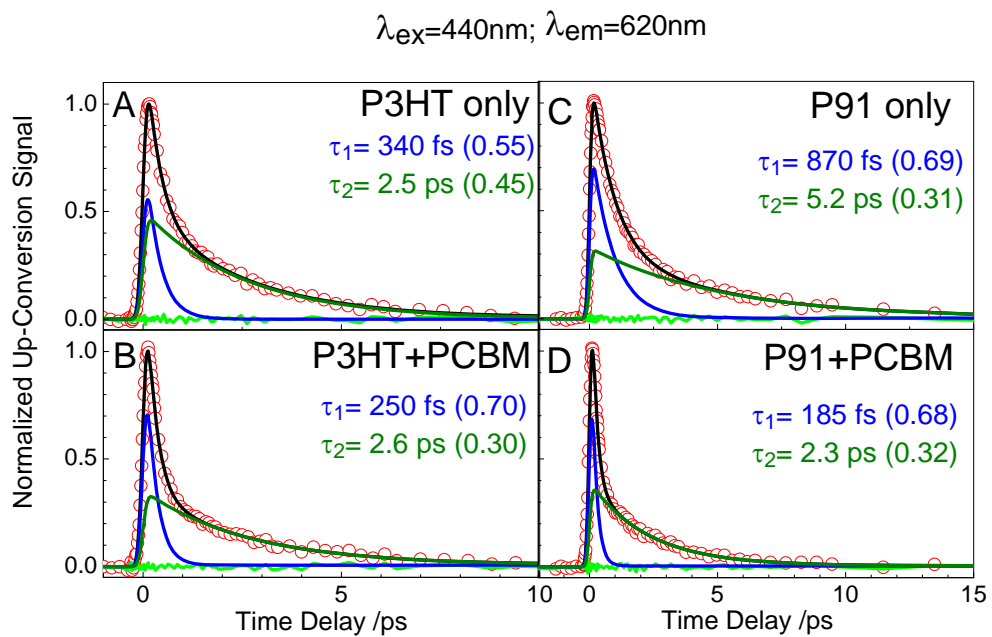


**Figure 3-7.** Time-resolved transients of (A) **P3HT**, (B) the blend of **P3HT** and **PCBM**, (C) **P91**, and (D) the blend of **P91** and **PCBM** coated on quartz at values of  $\lambda_{\text{ex}}$  and  $\lambda_{\text{em}}$  of 440 and 620 nm, respectively.

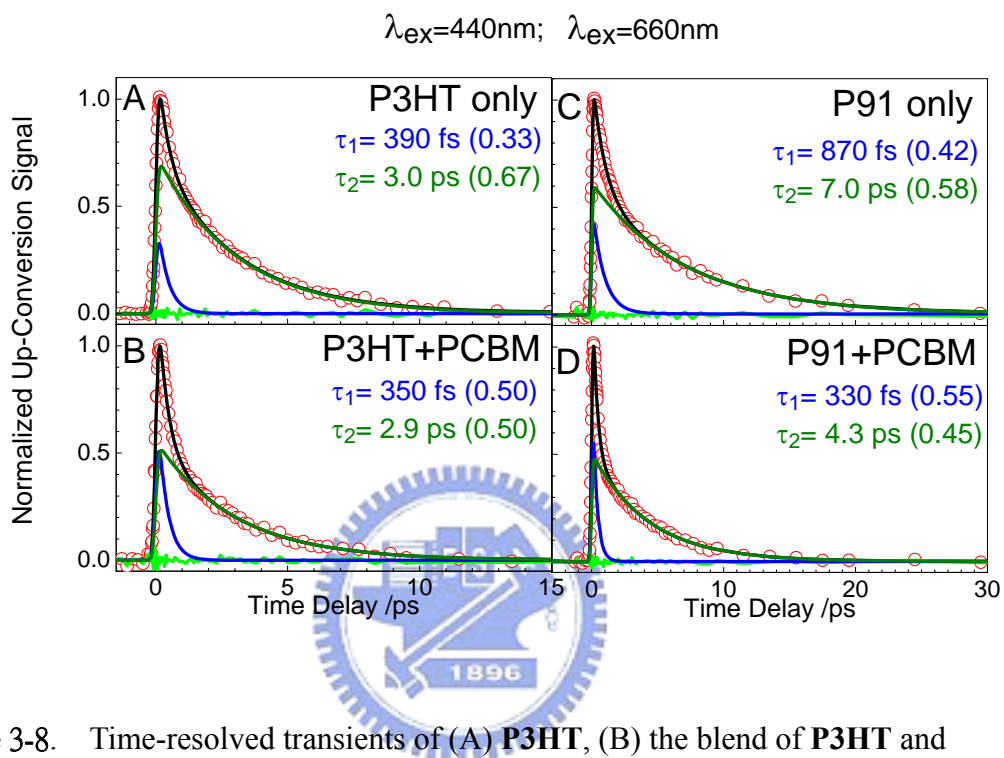
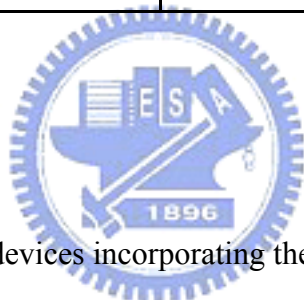


**Figure 3-8.** Time-resolved transients of (A) **P3HT**, (B) the blend of **P3HT** and **PCBM**, (C) **P91**, and (D) the blend of **P91** and **PCBM** coated on quartz at values of  $\lambda_{\text{ex}}$  and  $\lambda_{\text{em}}$  of 440 and 660 nm, respectively.

**Table 3-4.** Rate Constants for the Polymer, its Blend with **PCBM**, and Electron Transfer for **P3HT** and **P91** at Different Wavelengths.

Species $\lambda/\text{nm}$		<b>P3HT</b>			
		$k_q/\text{s}^{-1}$	$k_T/\text{s}^{-1}$	$k_{ET}/\text{s}^{-1}$	$k_{ET}/k_q$
600		$1.1 \times 10^{12}$	$2.7 \times 10^{12}$	$1.6 \times 10^{12}$	1.45
620		$7.6 \times 10^{11}$	$1.0 \times 10^{12}$	$2.4 \times 10^{11}$	0.31
660		$4.7 \times 10^{11}$	$6.2 \times 10^{11}$	$1.5 \times 10^{11}$	0.31
Species $\lambda/\text{nm}$		<b>P91</b>			
		$k_q/\text{s}^{-1}$	$k_T/\text{s}^{-1}$	$k_{ET}/\text{s}^{-1}$	$k_{ET}/k_q$
600		$5.2 \times 10^{11}$	$2.3 \times 10^{12}$	$1.8 \times 10^{12}$	3.46
620		$4.5 \times 10^{11}$	$1.2 \times 10^{12}$	$7.5 \times 10^{11}$	1.67
660		$2.3 \times 10^{11}$	$4.7 \times 10^{11}$	$2.4 \times 10^{11}$	1.04



The photophysics of the devices incorporating the synthesized copolymers can be determined by examining their external quantum efficiencies. Figure 3-9 displays the external quantum efficiencies (EQE) of the polythiophene side chain-tethered octylphenanthrenyl-imidazole/**PCBM** devices. The EQE values of the devices these active layers had been calibrated by using a reference cell and were divided by a mismatch factor of 1.34. The absolute EQE values of **P91** were at least about 20% higher than that of self-made **P3HT** ( $M_n \cong 13,500$ ) at wavelengths from 400 to 650 nm. In a detailed comparison, the EQE value of the **P91** device at an incident wavelength of 460 nm improved to 73% from 52% for the **P3HT** device—an increase of over

40%. The maximum EQE values of the **P91** and **P3HT** devices at 400 nm reached 83% and 56%, respectively—a 48% increase for the former over the latter. Even at a much longer wavelength of 640 nm, the EQE of the **P91**-containing device improved to 47% from 14% for the **P3HT**-based device—a twofold increase. This result indicates that introduction of octylphenanthrenyl-imidazole moieties onto a polythiophene backbone can improve the light absorption of the heterojunction copolymer/**PCBM** devices.

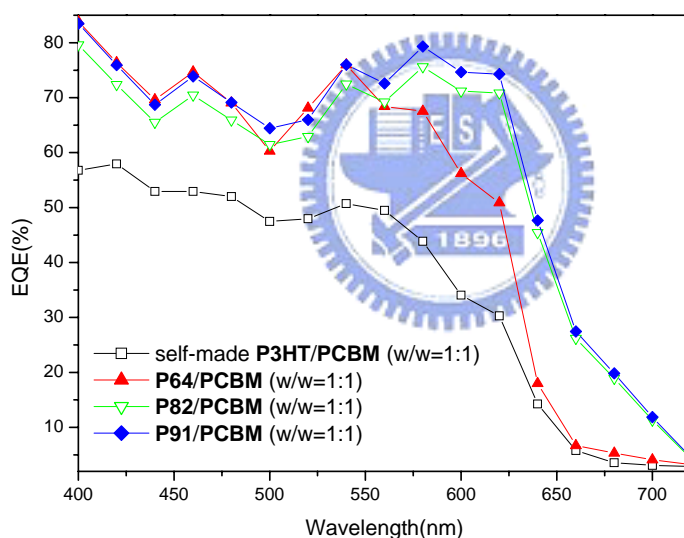


**Figure 3-9.** External quantum efficiencies of the copolymer/**PCBM** solar cells.



Figure 3-10 displays photocurrents of the diodes having the structure ITO/PEDOT:PSS/polymer:PCBM (1:1, w/w)/Ca/Al that were illuminated at AM 1.5G and 100 mW/cm<sup>2</sup> as well as the dark current of self-made P3HT/PCBM and P91/PCBM blends. In Figure 3-10, the short-circuit current density ( $J_{sc}$ ) increased upon increasing the content of the octylphenanthrenyl-imidazole moieties, probably as a consequence of enhanced light absorption at longer wavelength due to the extended conjugation and fast rate of charge transfer of the copolymers.<sup>[94]</sup> Table 3-5 lists the detailed short-circuit current density, open-circuit voltage and power conversion efficiencies of these heterojunction polymer solar cells, where the short-circuit current density values was obtained after dividing the measured  $J_{sc}$  by a mismatch factor of 1.34. In particular, the short-circuit current densities of the device containing the copolymer having 90 mol% octylphenanthrenyl-imidazole, P91, improved to 13.7 mA/cm<sup>2</sup> from 8.3 mA/cm<sup>2</sup> for the device containing pure poly(3-hexylthiophene)—an increase of 65%. The calibrated short-circuit current density for P91 device, 13.7 mA/cm<sup>2</sup>, is reasonably close to its empirical value of 13.4 mA/cm<sup>2</sup> that was obtained by integrating the current density-wavelength curves (see Figure 3-11).

Equation (1) is used to calculate the mismatch factor of our light source illuminating at a standard AM 1.5G global spectrum (ASTM G173).

$$M = \frac{\int_{\lambda_1}^{\lambda_2} E_{\text{Ref}}(\lambda) S_{\text{R}}(\lambda) d\lambda}{\int_{\lambda_1}^{\lambda_2} E_{\text{Ref}}(\lambda) S_{\text{T}}(\lambda) d\lambda} \frac{\int_{\lambda_1}^{\lambda_2} E_{\text{S}}(\lambda) S_{\text{T}}(\lambda) d\lambda}{\int_{\lambda_1}^{\lambda_2} E_{\text{S}}(\lambda) S_{\text{R}}(\lambda) d\lambda} \quad (1)$$

where  $E_{\text{Ref}}(\lambda)$  is the reference spectral irradiance,  $E_{\text{S}}(\lambda)$  is the source spectral irradiance,  $S_{\text{R}}(\lambda)$  is the spectral responsivity of the reference cell, and  $S_{\text{T}}(\lambda)$  is the spectral responsivity of the test cell, each as a function of wavelength ( $\lambda$ ). The limits of integration  $\lambda_1$  and  $\lambda_2$  in the above equation should encompass the range of the reference cell and the test-device spectral responses, and the simulator and reference spectra should encompass  $\lambda_1$  and  $\lambda_2$  to avoid errors.

Figure 3-11 presents the current density at the wavelength from 400 nm to 720 nm converted from the output signal of the external quantum efficiencies. The calibrated current densities were calculated using the following equation:

$$I^{\text{T,R}} = \frac{I^{\text{R,R}} I^{\text{T,S}}}{I^{\text{R,S}} M} \quad (2)$$

where  $I^{\text{R,R}}$  is the calibrated short-circuit current of the reference cell under the reference spectrum and total irradiance,  $I^{\text{T,S}}$  is the short-circuit current of a test cell measured under the source spectrum, and  $I^{\text{R,S}}$  is the short-circuit current of the reference cell under the source spectrum.<sup>[95, 96]</sup> The current densities of our polymers/**PCBM** devices calculated from the integration of the area from 400 nm to 720 nm are 8.1, 11.4, 12.7 and 13.4 mA/cm<sup>2</sup>, respectively.

Therefore, the reported short-circuit current density value of our devices are quite reasonable. We performed two control experiments for device comparison: self-made **P3HT** having similar molecular weight ( $M_n \approx 13,500$ ) to that of **P91** ( $M_n \approx 8,900$ )<sup>[97]</sup> and commercially available high molecular weight **P3HT** ( $M_n \approx 33,000$ ) for making devices that were subjected to the same processing conditions as that of **P91**. When experienced the same thermal treatment, the power conversion efficiency of the device by self-made low molecular weight **P3HT** and **PCBM** was 2.26% , similar to that reported in the literature,<sup>[97a]</sup> and the power conversion efficiency of the device by commercially available **P3HT** and **PCBM** was 2.9%, which is lower than the nominal value  $\sim 4\%$ , as shown in Figure 3-10. The device performance of self-made **P3HT/PCBM**, commercial **P3HT/PCBM** and **P91/PCBM** experienced the same thermal treatment condition were compared. The thermal treatment at 120°C for 30 minutes is the optimal one for **P91** blend but is not the case for self-made **P3HT** and commercial **P3HT** blend. Consequently, the **P91/PCBM** device has higher power conversion efficiency than that of self-made **P3HT/PCBM** or commercial **P3HT/PCBM** devices under this particular thermal treatment, but this comparison result will not hold for other thermal treatment conditions. The main point in this comparison is that despite the much lower molecular weight of polythiophene-imidazole copolymers than that of the



commercial **P3HT**, the power conversion efficiency of the **P91/PCBM** device is close to that (~4%) of an optimal commercial **P3HT/PCBM** device, indicating the advantages of using this particular molecular architecture.

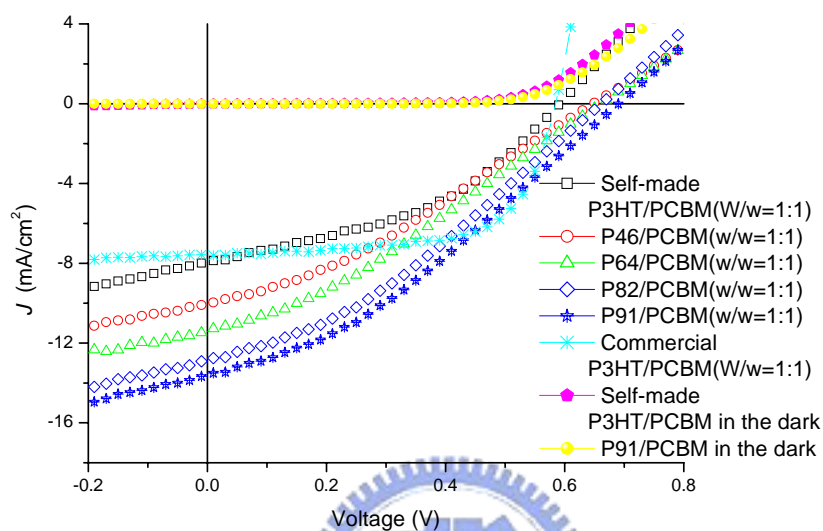


**Figure 3-10.** Current density–voltage characteristics of illuminated (AM 1.5G, 100 mW/cm<sup>2</sup>) polymer solar cells incorporating self-made **P3HT**, **P64**, **P82**, and **P91** and **PCBM**.

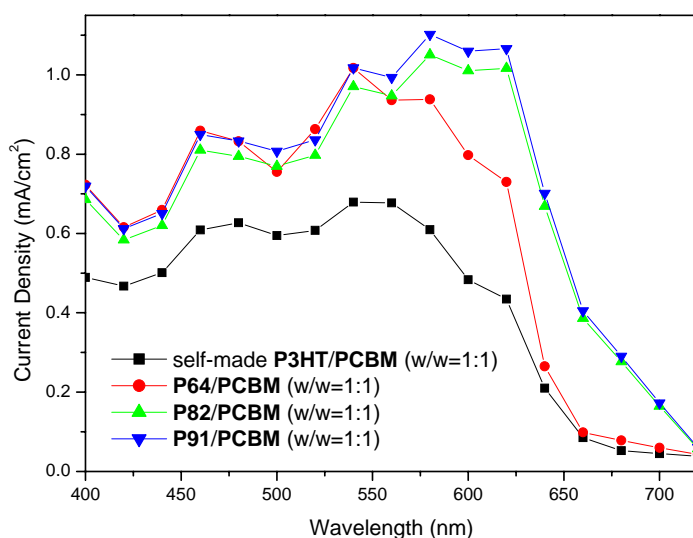
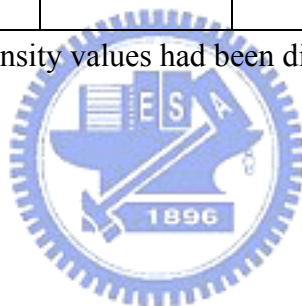


**Figure 3-11.** The current density vs. wavelength diagram of self-made **P3HT/PCBM**, **P64/PCBM**, **P82/PCBM**, and **P91/PCBM** devices.

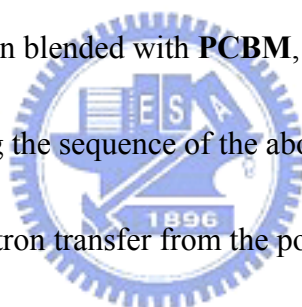
**Table 3-5.** Photovoltaic Properties of the Polymer Solar Cells.

	short-circuit current density, $J_{sc}$ (mA/cm <sup>2</sup> )*	open-circuit voltage, $V_{oc}$ (V)	fill factor, FF (%)	power conversion efficiency, PCE (%)
Self-made <b>P3HT</b>	8.3	0.6	42.0	2.26
<b>P46</b>	10.1	0.64	37.4	2.42
<b>P64</b>	11.7	0.66	34.2	2.63
<b>P82</b>	13.0	0.67	33.1	2.85
<b>P91</b>	13.7	0.68	37.2	3.45
Commercial <b>P3HT</b>	7.6	0.58	65.9	2.90

\* : The short-circuit current density values had been divided by a mismatch factor of 1.34.



Because of the increased short-circuit current density that occurred when the octylphenanthrenyl-imidazole content increased, the current density–voltage characteristics of our solar cell devices suggest that charge transport occurred from the photoexcited polythiophene backbone, through the octylphenanthrenyl-imidazole moieties and **PCBM**, to the electrode.<sup>[78, 99]</sup> The evidence that charge transfer from the photoexcited polythiophene backbone to the electron-withdrawing phenanthrenyl-imidazole was provided from the photoluminescence quenching data in Figure 3-4. While the conclusion from the data in Table 3-4 by the fluorescence decay study indicates that when blended with **PCBM**, electron transfer from **P91** to **PCBM** occurs. By analyzing the sequence of the above two events, it is quite possible that the stepwise electron transfer from the polythiophene main chain to the imidazole and then to **PCBM** occurs. The possible mechanism of charge transport can be explained by the following sequential event—that initially the electrons can be withdrawn to the octylphenanthrenyl-imidazole moieties from photoexcited polythiophene backbone while the holes are being retained on polythiophene. Then, these electrons were transferred to the nearby **PCBM**, followed by transferring to another **PCBM** by tunneling through **P91**, and eventually reached the Ca/Al electrode. The holes can be transported along the photoexcited polythiophene backbone and then reached another **P91** molecules by tunneling through **PCBM**. Eventually, these



holes pass through the PEDOT to reach the ITO electrode. The open circuit voltage ( $V_{oc}$ ) of the **P91/PCBM** heterojunction device increased to 0.68 V from 0.60 V for the **P3HT/PCBM** device. The open circuit voltage of a polymer heterojunction cell is usually proportional to the difference between the lowest unoccupied molecular orbital (LUMO) of the electron acceptor and the highest occupied molecular orbital (HOMO) of the electron donor,<sup>[100]</sup> but it is also influenced by many other factors—e.g., solvent effects.<sup>[101]</sup> From the cyclic voltammogram data (see Table 3-6), the HOMO of **P91**,  $-4.65$  eV, is slightly higher than that of **P3HT** ( $-4.75$  eV), a difference of 0.1 eV. The solubility of **P91**, however, is still much less than that of **P3HT** in dichlorobenzene despite the fact that two octyl chains were added to the phenanthrenyl-imidazole for improving its solubility.<sup>[102]</sup> In the case of the **P91/PCBM** device, it appears that the effect of the copolymers becoming less miscible with **PCBM** at high content of octylphenanthrenyl-imidazole moieties<sup>[101]</sup> dominated over the effect of the decrease, 0.1 eV, between the LUMO of the electron acceptor (**PCBM**) and the HOMO of the electron donor (**P91**), resulting in a slightly higher value of  $V_{oc}$  than that of the **P3HT/PCBM** device. This is because the octylphenanthrenyl-imidazole moiety can form  $\pi$ - $\pi$  stacking among themselves and therefore is not quite miscible with **PCBM**. The two octyl chains on imidazole groups also increase the spatial distance between the

octylphenanthrenyl-imidazole moiety and **PCBM**. Hence, the  $V_{oc}$  of **P91/PCBM** device was higher than that of the **P3HT/PCBM** device. Nevertheless, the fill factors remained low as a result of the devices maintaining large series resistances and low shunt resistances.<sup>[103]</sup> Compared with our findings of a previous study, however, the fill factors were improved when the dioctyl groups were incorporated onto the phenanthrenyl-imidazole moieties because of the improved solubility.

**Table 3-6.** Redox data, HOMO, LUMO energy levels, and band gap energies of our synthesized polymers.

	Reduction Onset Potential (eV)	Oxidation Onset Potential(eV)	HOMO (eV)	LUMO (eV)	Bandgap (eV)
<b>P3HT</b>	-1.75	0.35	-4.75	-2.75	2.0
<b>P46</b>	-1.63	0.30	-4.70	-2.87	1.83
<b>P64</b>	-1.55	0.25	-4.65	-2.95	1.70
<b>P82</b>	-1.48	0.25	-4.65	-3.02	1.63
<b>P91</b>	-1.35	0.25	-4.65	-3.05	1.60



Figure 3-12 displays the atomic force microscopy images of self-made **P3HT/PCBM** and **P91/PCBM** (1:1, w/w) films. The root-mean-square roughness of the **P91/PCBM** film, 2.26 nm, was twice of that, 1.13 nm, of **P3HT/PCBM** film, and the structure of **P91/PCBM** appears better organized than that of **P3HT/PCBM**. Hence, we suspected that the rough surface may effectively reduce the charge-transport distance while providing nanoscaled texture that further enhances internal light absorption.<sup>[81b, 103]</sup> Consequently, the power conversion efficiency for **P91** increased dramatically to 3.45% for **P91**, presumably as a result of the lowered bandgap and enhanced electron transfer as well as more organized structures in the active layer of the device.

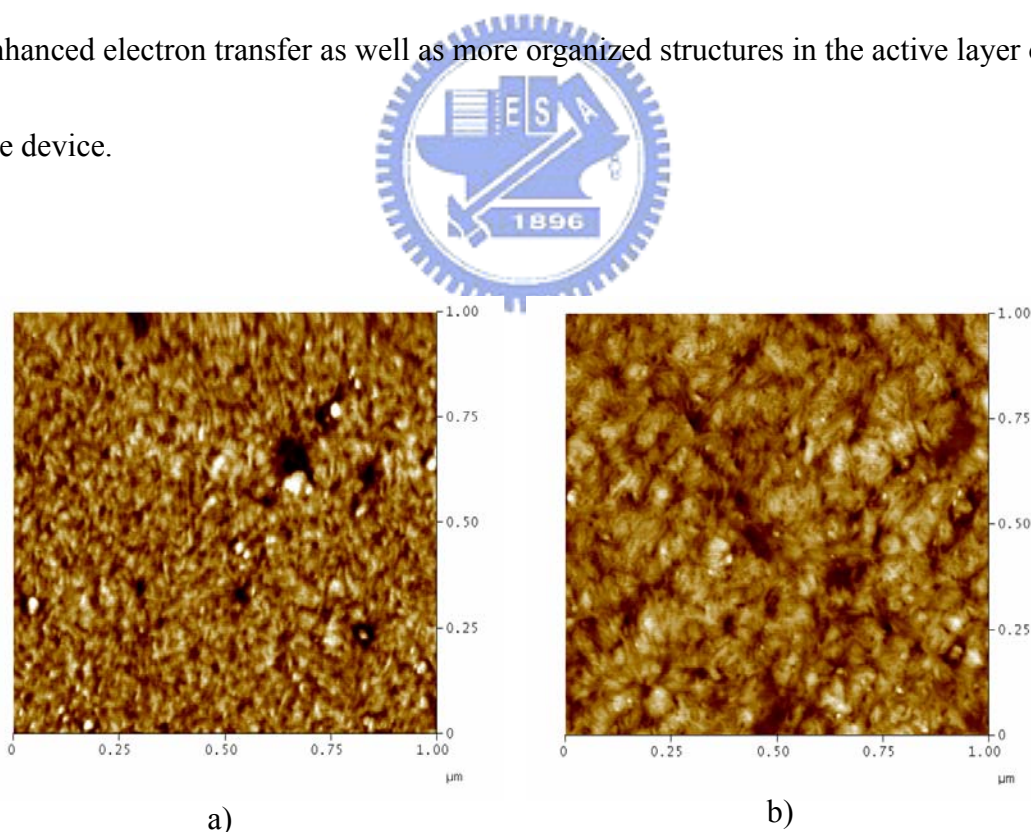


**Figure 3-12.** The atomic force microscopy images of a) self-made **P3HT/PCBM** and b) **P91/PCBM** films.

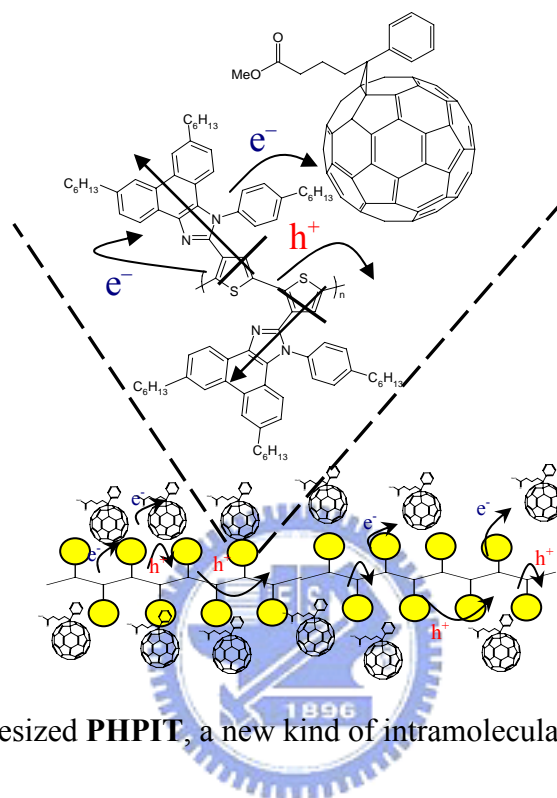
### **3-4. Conclusions**

We have prepared a new family of regioregular poly(3-hexyl-thiophene) copolymers—presenting octylphenanthrenyl-imidazole side chains in conjugation with the main polymeric chain—that exhibit lowered bandgaps. The reduction in the bandgap energy in conjunction with photoluminescence quenching indicates that rapid charge transfer occurred in the device from the photoexcited polythiophene backbone, through the octylphenanthrenyl-imidazole moieties, to the **PCBM** units. The ratios of the net electron transfer rate constant to the quenching rate constant at different wavelengths were much higher for the copolymer incorporating 90 mol% octylphenanthrenyl-imidazole moieties/**PCBM** than for **P3HT/PCBM**, indicating that electron transfer probability in the former case was greatly favored over that of the latter. The high external quantum efficiency of the device that incorporates the polythiophene-side-chain-tethered octylphenanthrenyl-imidazole results in its high short-circuit current density. Because of the high short-circuit current density as well as more organized active layer structures obtained for the octylphenanthrenyl-imidazole presenting regioregular poly(3-hexylthiophene), the power conversion efficiency improved dramatically to 3.45% for the copolymer containing 90 mol% octylphenanthrenyl-imidazole.

## Chapter 4: Intramolecular Donor–Acceptor Regioregular

### Poly(hexylphenanthrenyl-imidazole thiophene) Exhibits Enhanced

### Hole Mobility for Heterojunction Solar Cell Applications



We have synthesized **PHPIT**, a new kind of intramolecular D–A side-chain-tethered hexylphenanthrenyl-imidazole polythiophene. The more-balanced electron and hole mobilities and the enhanced visible and internal light absorptions in the devices consisting of annealed **PHPIT/PCBM** blends both contributed to a much higher short-circuit current density, which in turn led to a power conversion efficiency as high as 4.1%, despite the fact that **PHPIT** is only comprised of ca. 20 repeating units.

#### 4-1. Introduction

Conjugated polymers possessing extended arrays of delocalized  $\pi$  electrons are being investigated intensively for their potential use in organic optoelectronic devices, with some studies focused on solar cell devices incorporating bulk heterojunctions using conjugated polymers.<sup>[104–110]</sup> Polythiophene derivatives are at present among the most promising materials for solar cell applications because of their high light absorption and electronic conductivity. For example, polymer solar cells containing blends of poly(3-hexylthiophene) (**P3HT**) and [6,6]-phenyl-C<sub>61</sub>-butyric acid methyl ester (**PCBM**) have recently reached power conversion efficiencies of ca. 4–5% under standard solar conditions (AM 1.5G, 100 mW/cm<sup>2</sup>, 25 °C).<sup>[111–116]</sup> If the power conversion efficiency of these devices is to be improved further, the light absorption of the active polymer must be improved because **P3HT** absorbed only ca. 20% of sunlight, i.e., the bandgap of **P3HT** must be reduced to meet the maximum photon flux of sunlight. Research into conjugated polymers containing electron donor–acceptor (D–A) pairs in the polymeric main chain has become quite active recently<sup>[117]</sup> because such materials exhibit narrow bandgaps. Alternatively, the introduction of an electron-acceptor unit—usually a conjugated species that can absorb a different wavelength of sunlight—onto the side chain of a conjugated polymer can increase the breadth of wavelengths of light absorbed and also can lower the bandgap to some extent.<sup>[118]</sup> Additionally, the generated excitons can be readily

dissociated into electrons and holes in this type of conjugated polymer because of the internal field produced by the dipole moment built on its D–A molecular structure and subsequent charge transfer to nearby n-type nanoparticles (e.g., **PCBM**). Therefore, conjugated polymers that contain side chain-tethered conjugated acceptor moieties not only absorb light more effectively (multiple absorption) but also exhibit enhanced charge transfer ability—two desirable properties for photovoltaics applications.<sup>[119]</sup>

In a heterojunction polymer solar cell, however, the photocurrent depends not only on the rate of photogeneration of free electrons and holes but also on the transport

properties of the electrons and holes in the acceptor and donor, respectively. In fact, the overall performance of bulk heterojunction solar cells is directly limited by the ambipolar carrier transport.<sup>[120,121]</sup>

In the **P3HT/PCBM** system, the slower rate of hole transport governs the recombination process,<sup>[122]</sup> increasing the carrier mobilities results in both increased extraction of the charge carriers and increased bimolecular recombination.<sup>[123]</sup> Therefore, the incorporation of electron-withdrawing moieties as

side chains that are conjugated with the polymeric main chains should also alleviate the recombination problem, because such a molecular architecture has the advantage in a heterojunction device of allowing charge separation through sequential transfer of electrons from the main chains to the side chains and then to **PCBM**. Hence, in this present study, we synthesized a new kind of intramolecular D–A thiophene-type

homopolymer presenting phenanthrenyl-imidazole moieties. Scheme 1 displays our synthetic approach toward the planar phenanthrenyl-imidazole moiety-tethered thiophene monomer and its polymerization. We expected that the presence of the hexylphenanthrenyl-imidazole moieties conjugated to the thiophene units would reduce the bandgap of the polythiophene and that the hexyl substituents would improve the solubility of the polymer. The extent of reduction of the bandgap of our synthesized polymer would, however, depend on the effective conjugation length of the system, which is sometimes reduced by steric hindrance.<sup>[124]</sup> We polymerized

the

2-(2,5-dibromothiophen-3-yl)-6,9-dihexyl-1-(4-hexylphenyl)-1*H*-phenanthro-[9,10-d]-imidazole (**HPIT**) monomer using a Grignard metathesis approach. The presence

of the bulky hexylphenanthrenyl-imidazole unit appended to the thiophene monomer

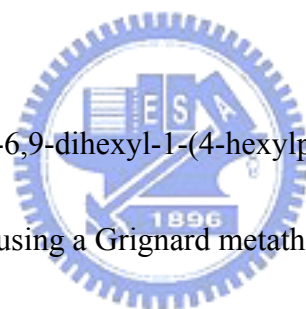
led to very high selectivity during the Grignard reaction, resulting a highly

regioregular poly(hexylphenanthrenyl-imidazole thiophene) (**PHPIT**). The number

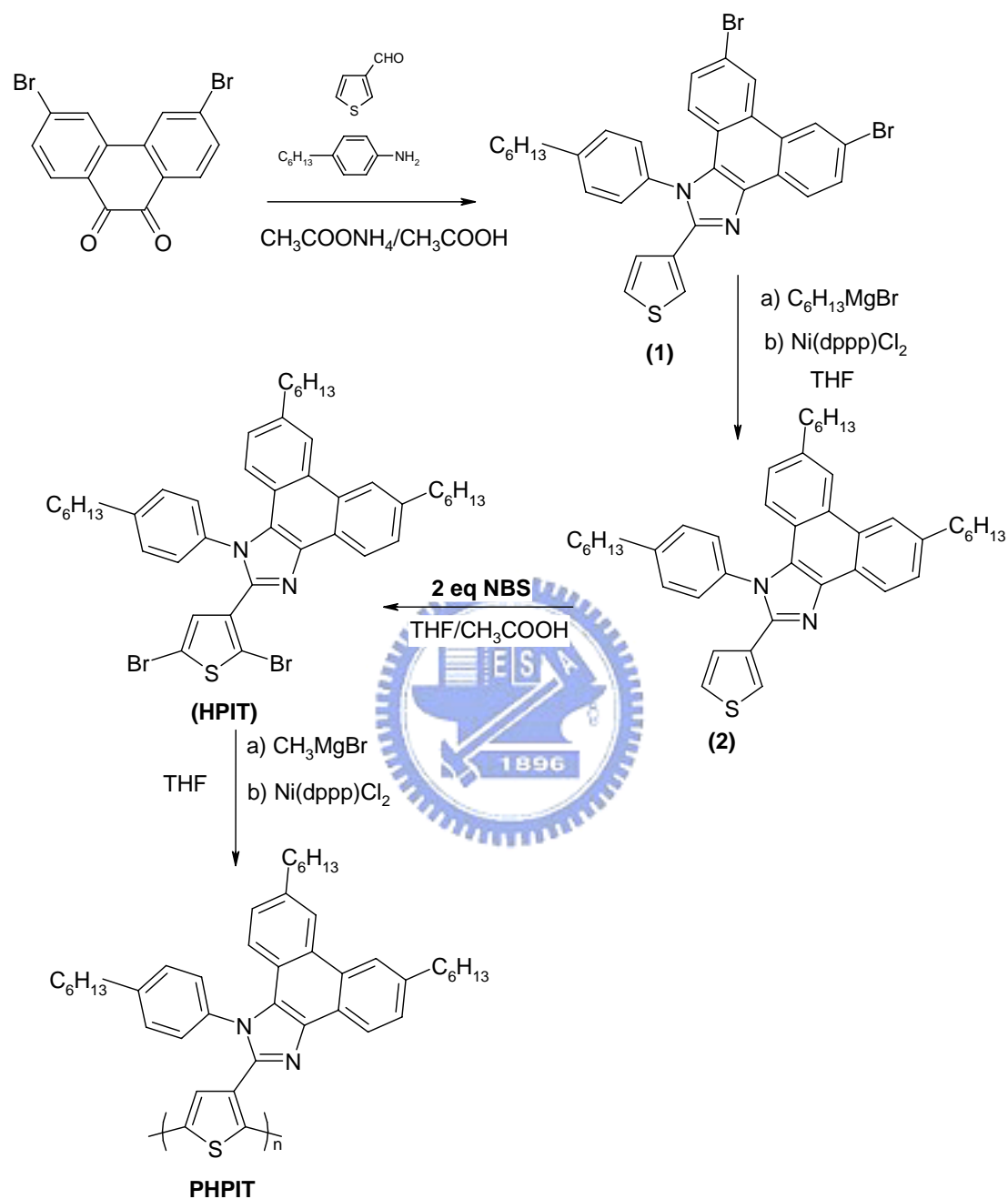
molecular weight ( $M_n$ ) of **PHPIT** was 15.3 kg/mol and the polydispersity index (PDI)

was 1.35, indicating that **PHPIT** possessed ca. 20 repeating units. The 5% thermal

degradation temperature of this polymer was 355 °C.



**Scheme 4-1.** Synthesis of the monomer and polymer; NBS: *N*-bromosuccinimide; THF: tetrahydrofuran; dppp: 1,3-bis(diphenylphosphino)propane.



## 4-2. Experimental

**Materials.** Chemicals were purchased from Aldrich, TCI, or Lancaster.

[6,6]-Phenyl-C<sub>61</sub>-butyric acid methyl ester (**PCBM**) was purchased from Nano-C.

**Preparation of Monomers.** Scheme 4-1 illustrates the synthetic route followed for the preparation of the monomer

2-(2,5-dibromothiophen-3-yl)-6,9-dihexyl-1-(4-hexylphenyl)-1*H*-phenanthro[9,10-d]-imidazole. (**HPIT**).

6,9-Dihexyl-1-(4-hexylphenyl)-3a,11b-dihydro-2-(thiophen-3-yl)-1*H*-phenanthro[9,10-d]imidazole (**2**) was isolated in 80% yield from the reaction of compound (**1**) with hexylmagnesium bromide and Ni(dppp)Cl<sub>2</sub> under reflux.

2-(2,5-Dibromothiophen-3-yl)-6,9-dihexyl-1-(4-hexylphenyl)-1*H*-phenanthro[9,10-d]-imidazole (**HPIT**) was isolated in 93% yield from the reaction between **2** and NBS.

Detailed synthetic procedures and characterization data are provided below.

**Preparation of Polythiophene Derivatives.**<sup>[125]</sup> The Grignard metathesis polymerization of

2-(2,5-dibromothiophen-3-yl)-1-phenyl-1*H*-phenanthro[9,10-d]-imidazole is

illustrated in Scheme 4-1. Detailed synthetic procedures and characterization data are provided below.



**6,9-Dibromo-1-phenyl-2-(thiophen-3-yl)-1*H*-phenanthro[9,10-*d*]imidazole (1).**

A mixture of 3-hexylaniline (15.7 g, 85.5 mmol), 3,6-dibromophenanthrene-9,10-dione (6.63 g, 17.1 mmol), 3-thiophenecarboxaldehyde (1.92 g, 17.1 mmol), ammonium acetate (5.28 g, 68.6 mmol), and acetic acid (100 mL) was heated for 2 h under nitrogen in an oil bath maintained at 123 °C. After cooling and filtering, the solid product was washed sequentially with an acetic acid/water mixture (1:1, 150 mL) and water and then dried to yield **1** (9.52 g, 90%). <sup>1</sup>H NMR (300 MHz, CDCl<sub>3</sub>, ppm): 8.84–8.87 (m, 1H), 8.75 (d, *J* = 8.4 Hz, 1H), 8.69 (d, *J* = 8.4 Hz, 1H), 7.45–7.78 (m, 2H), 7.22–7.27 (m, 2H), 7.14–7.18 (m, 1H), 6.90–7.08 (m, 3H), 6.40 (d, *J* = 8.4 Hz, 2H), 2.66 (t, *J* = 7.2 Hz, 2H), 1.00–1.80 (m, 8H), 0.97 (t, *J* = 7.2 Hz, 3H). <sup>13</sup>C NMR (75 MHz, CDCl<sub>3</sub>): 149.2, 137.3, 134.0, 132.5, 131.5, 130.2, 128.4, 126.4, 125.7, 120.4, 31.9, 30.6, 29.4, 29.3, 22.7, 14.1. HRMS-EI (*m/z*): [*M*<sup>+</sup>] calcd. for C<sub>31</sub>H<sub>26</sub>Br<sub>2</sub>SN<sub>2</sub>, 616.0183; found, 616.0179.

**6,9-Dihexyl-1-(4-hexylphenyl)-3*a*,11*b*-dihydro-2-(thiophen-3-yl)-1*H*-phenanthro[9,10-*d*]imidazole. (2).** A 250-mL round-bottom three-neck flask equipped with a stirrer bar, condenser, addition funnel, and N<sub>2</sub> inlet/outlet was charged with Mg (1.43 g, 63.4 mmol) and dry ether (30 mL). Bromooctane (9.62 g, 58.4 mmol) in dry ether (20 mL) was added dropwise to maintain a mild reflux. The mixture was heated

under reflux for an additional 2.5 h. This solution of Grignard reagent was then added dropwise to an ice-cooled 250-mL three-neck round-bottom flask containing 6,9-dibromo-1-phenyl-2-(thiophen-3-yl)-1*H*-phenanthro[9,10-*d*]imidazole (**1**, 18.0 g, 29.2 mmol), Ni(dppp)Cl<sub>2</sub> (0.16 g, 0.30 mmol), and dry ether (80 mL). The solution was then heated under reflux overnight. The cooled reaction mixture was quenched carefully with HCl (5%, 75 mL); the ether layer was separated, washed with H<sub>2</sub>O (2 × 75 mL), and dried (MgSO<sub>4</sub>). The crude product was purified through column chromatography (SiO<sub>2</sub>; 8% EtOAc/hexane) to yield **2** (16.2 g, 88%). <sup>1</sup>H NMR (300 MHz, CDCl<sub>3</sub>, ppm): 8.84–8.87 (m, 1H), 8.75 (d, *J* = 8.4 Hz, 1H), 8.69 (d, *J* = 8.4 Hz, 1H), 7.45–7.78 (m, 2H), 7.22–7.27 (m, 2H), 7.14–7.18 (m, 1H), 6.90–7.08 (m, 3H), 6.40 (d, *J* = 8.4 Hz, 2H), 2.50–2.66 (m, 6H) 1.00–1.80 (m, 24H), 0.97 (t, *J* = 7.2 Hz, 9H). <sup>13</sup>C NMR (75 MHz, CDCl<sub>3</sub>): 148.2, 137.3, 134.0, 132.5, 131.5, 130.2, 128.4, 126.4, 125.7, 124.7, 31.9, 30.6, 29.4, 29.3, 22.7, 14.1. HRMS-EI (*m/z*): [M<sup>+</sup>] calcd. for C<sub>43</sub>H<sub>52</sub>SN<sub>2</sub>, 628.3812; found, 628.3810.

**2-(2,5-Dibromothiophen-3-yl)-6,9-dihexyl-1-(4-hexylphenyl)-1*H*-phenanthro[9,10-*d*]imidazole (HPIT).** NBS (6.21 g, 34.1 mmol) was added portionwise to a solution of 6,9-dioctyl-1-phenyl-2-(thiophen-3-yl)-1*H*-phenanthro[9,10-*d*]imidazole (**2**, 10.0 g, 15.9 mmol) in THF (66 mL) and acetic acid (66 mL) and then the mixture was stirred for 20 min. The solution was washed with water (2 × 200 mL), saturated

NaHCO<sub>3</sub> (1 × 200 mL), and then again with water (1 × 200 mL). Following extraction with ethyl acetate, the organic layer was dried (MgSO<sub>4</sub>) and concentrated to yield the monomer (11.3 g, 90%). <sup>1</sup>H NMR (300 MHz, CDCl<sub>3</sub>, ppm): 8.75 (s, 2H), 8.07 (d, *J* = 8.4 Hz, 2H), 7.45–7.78 (m, 2H), 7.12–7.27 (m, 4H), 6.73 (s, 1H), 2.55–2.66 (m, 6H), 1.00–1.80 (m, 24H), 0.97 (t, *J* = 7.2 Hz, 9H). <sup>13</sup>C NMR (75 MHz, CDCl<sub>3</sub>): 149.2, 137.0, 134.0, 132.5, 131.5, 130.2, 128.4, 126.4, 125.7, 124.7, 117.3, 99.2, 30.6, 29.6, 29.4, 29.3, 22.7, 14.1. HRMS-FAB (*m/z*): [M – H]<sup>+</sup> calcd. for C<sub>43</sub>H<sub>50</sub>SN<sub>2</sub>Br<sub>2</sub>, 784.2061; found, 783.2059.

**Preparation of Polythiophene Derivatives.**<sup>[125]</sup> CH<sub>3</sub>MgBr (1.5 mL, 4.5 mmol) was added via syringe to a stirred solution of 2-(2,5-dibromothiophen-3-yl)-6,9-dihexyl-1-(4-hexylphenyl)-1*H*-phenanthro[9,10-*d*]-imidazole (2.07 g, 2.03 mmol), and freshly distilled THF (80 mL) in a three-necked 100-mL round-bottom flask. The solution was heated under reflux for 2 h and then Ni(dppp)Cl<sub>2</sub> (12 mg, 0.02 mmol) was added. The mixture was stirred for 1 h and then the reaction was quenched through the addition of methanol. The solid polymer was washed with methanol within a Soxhlet extractor. The polymer then was dissolved through Soxhlet extraction with chloroform; the chloroform was evaporated and the residue dried under vacuum to yield **PHPIT** (0.51 g, 20%; 99% coupled head-to-tail). <sup>1</sup>H NMR (300 MHz, CDCl<sub>3</sub>): 8.40–8.90 (br, 2H), 7.30–7.90 (br, 8H),

6.98 (s, 1H), 2.75 (s, 6H), 0.85–1.64 (m, 33H).  $^{13}\text{C}$  NMR (75 MHz,  $\text{CDCl}_3$ ): 149.2, 139.9, 137.4, 137.1, 133.2, 131.1, 130.4, 130.1, 129.6, 129.0, 128.4, 128.2, 127.5, 127.0, 126.5, 126.2, 125.5, 124.6, 123.4, 122.6, 122.0, 121.1, 120.0, 119.7, 31.9, 30.6, 29.4, 29.3, 22.7, 14.1. Anal. Calcd for  $\text{C}_{43}\text{H}_{50}\text{SN}_2$ : C, 82.38; H, 8.04; N, 4.47; S, 5.10. Found: C, 82.78; H, 7.66; N, 4.37; S, 5.19.

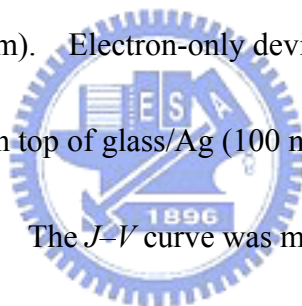
**Characterization.**  $^1\text{H}$  and  $^{13}\text{C}$  NMR spectra were recorded on a Varian Unity-300 NMR spectrometer. Elemental analyses (EA) of the polymers were performed using a Heraeus CHN-OS Rapid instrument. Thermal gravimetric analyses of the polythiophene derivatives were performed using a Du Pont TGA 2950 instrument operated at a heating rate of  $10\text{ }^\circ\text{C}/\text{min}$  under a nitrogen purge. Differential scanning calorimetry (DSC) was performed using a DuPont DSC 2010 instrument operated at a heating rate of  $10\text{ }^\circ\text{C}/\text{min}$  under a nitrogen purge. Samples were heated from  $30$  to  $200\text{ }^\circ\text{C}$ , cooled to  $20\text{ }^\circ\text{C}$ , and then heated again from  $30$  to  $200\text{ }^\circ\text{C}$ ; the glass transition temperatures ( $T_g$ ) were determined from the second heating scans. The redox behavior of each polymer was investigated through cyclic voltammetry using a BAS 100 electrochemical analyzer operated at a potential scan rate of  $40\text{ mV}/\text{s}$  and an electrolyte of  $0.1\text{ M}$  tetrabutylammonium hexafluorophosphate ( $n\text{-Bu}_4\text{NPF}_6$ ) in acetonitrile. In each case, a glassy disk carbon electrode coated with a thin layer of the polymer was used as the working electrode; a platinum wire was

used as the counter electrode; a silver wire was used as the quasi-reference electrode. All of the potentials quoted herein are referenced to the Ag wire as the quasi-reference electrode; the electrochemical potential of Ag is  $-0.02$  V vs SCE. The HOMO and LUMO energy levels were determined using the equations  $E_{\text{HOMO}} = -E_{\text{ox}} - 4.4$  eV and  $E_{\text{LUMO}} = -E_{\text{red}} - 4.4$  eV, where  $E_{\text{ox}}$  and  $E_{\text{red}}$  are the onset potentials of the oxidation and reduction peaks [vs saturated calomel electrode (SCE)], respectively, and the value of 4.4 eV relates the SCE reference to a vacuum.<sup>[118a,122a]</sup> UV-Vis spectra were measured using an HP 8453 diode array spectrophotometer. The molecular weights of the polythiophene derivatives were measured through gel permeation chromatography (GPC) using a Waters chromatography unit interfaced to a Waters 2414 differential refractometer. Three  $5\text{-}\mu\text{m}$  Waters styragel columns were connected in series in decreasing order of pore size ( $10^4$ ,  $10^3$ , and  $10^2$  Å); THF was the eluent and standard polystyrene samples were used for calibration. The AFM samples were prepared by spin-coating solutions of polymer/**PCBM** blends in dichlorobenzene onto ITO glass substrates, followed by annealing in an oven at 120 °C for 20, 30, or 45 min.

**Device Fabrication.** The current density–voltage ( $J$ – $V$ ) characteristics of the polymers were measured using devices having a sandwich structure [ITO/PEDOT:PSS/polymer:**PCBM** (1:1, w/w)/Ca/Al]. The ITO-coated glass

substrate was pre-cleaned and treated with oxygen plasma prior to use. The polymer/**PCBM** layer was spin-coated at 700 rpm from a dichlorobenzene solution (20 mg/mL). Dichlorobenzene was a better solvent for these polymers than were toluene, chloroform, and tetrahydrofuran. The thickness of the polymer/**PCBM** layer was ca. 100 nm. The active layers of our devices were thermally annealed at 120 °C for 30 min prior to electrode deposition. Using a base pressure below  $1 \times 10^{-6}$  torr, a layer of Ca (30 nm) was vacuum-deposited as the cathode and then a thick layer of Al (100 nm) was deposited as the protecting layer; the effective area of one cell was 0.04 cm<sup>2</sup>. Testing of the devices was performed under simulated AM 1.5G irradiation (100 mW/cm<sup>2</sup>) using a xenon lamp-based Newport 66902 150W solar simulator. A xenon lamp equipped with an AM1.5 filter was used as the white light source; the optical power at the sample was 100 mW/cm<sup>2</sup>, detected by an OPHIR thermopile 71964. The  $J-V$  characteristics were measured using a Keithley 236 electrometer. The spectrum of the solar simulator had a mismatch of less than 25%; it was calibrated using a PV-measurement (PVM-154) mono-Si solar cell (NREL calibrated), and Si photo diode (Hamamatsu S1133) was employed to check the uniformity of the exposed area. AM 1.5G (ASTM G173)<sup>[126]</sup> light intensity was calibrated through thermopile and PV-measurement. The mismatch factor (M) of 1.34 was obtained by taking the PVM-154 as the reference cell. The PVM-154

combined with KG-5 filter (350–700 nm passed, Newport) was used to simulate a reference solar cell exhibiting spectral responsivity from 350 to 700 nm. Reported efficiencies are the averages obtained from four devices prepared on each substrate. The external quantum efficiency (EQE) was measured using a Keithley 236 electrometer coupled with an Oriel Cornerstone 130 monochromator. The light intensity at each wavelength was calibrated using an OPHIR 71580 diode. Hole-only devices, used to investigate the hole transport in polymer/**PCBM**, were fabricated following the same procedure presented above, except that the top electrode was replaced with gold (Au; 100 nm). Electron-only devices were fabricated by spin-coating the active layer on top of glass/Ag (100 nm) followed by evaporation of the Al (100 nm) top electrode. The  $J$ - $V$  curve was measured using a Keithley 236 electrometer under inert condition.

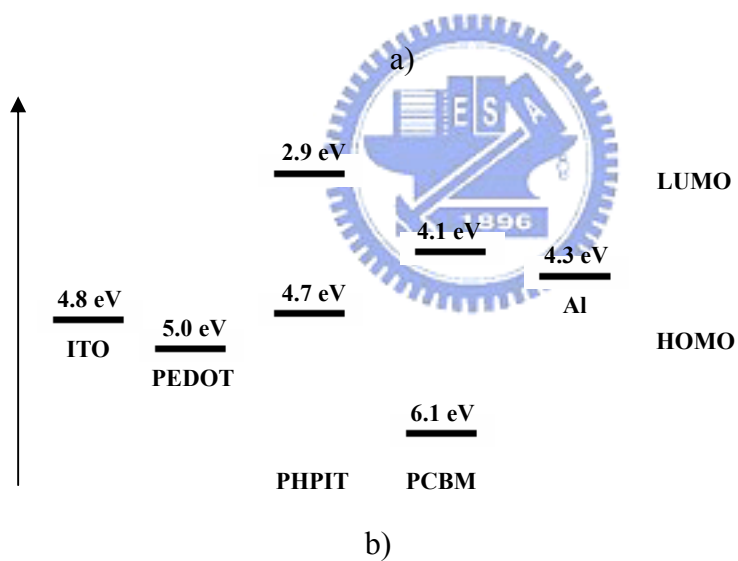
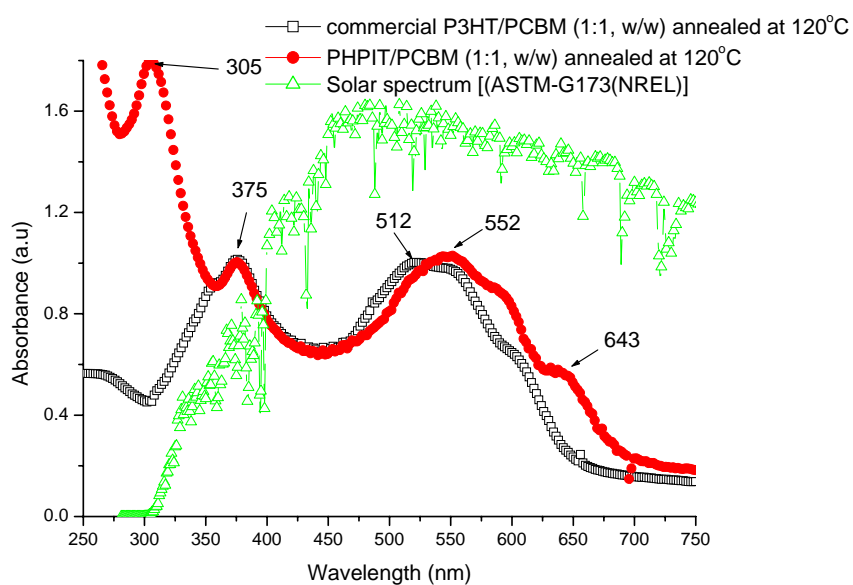


### 4-3. Results and Discussion

Figure 4-1 displays the UV–Vis spectra of **PHPIT/PCBM** (1:1, w/w) and the **P3HT/PCBM** (1:1, w/w) solid film obtained after annealing at 120 °C for 30 min, as well as cyclic voltammogram (CV) bandgap data for **PHPIT**, PEDOT, **PCBM**, Al, and ITO. The peak at 305 nm was caused by the presence of conjugated phenanthrenyl-imidazole moieties that were not fully coplanar with the polythiophene chain because of steric hindrance. The maximum absorption ( $\lambda_{\text{max}}$ ) at ca. 512 nm for the **P3HT/PCBM** thin film resulted from  $\pi$ – $\pi^*$  transitions. The annealed **PHPIT/PCBM** film exhibits a red-shifted  $\pi$ – $\pi^*$  transition peak at 552 nm and two additional absorption peaks at 596 and 641 nm, indicating that a phase separated structure developed after annealing at 120 °C. The area under the spectrum in the visible absorption range (400–750 nm) for **PHPIT/PCBM** after annealing at 120 °C for 30 min was 11% higher than that of the annealed **P3HT/PCBM**. The optical bandgap of **PHPIT** was ca. 1.85 eV, which is close to the cyclic voltammogram (CV) bandgap (1.80 eV), with the highest occupied molecular orbital at ca. 4.70 eV and the lowest unoccupied molecular orbital at ca. 2.90 eV. We detected no photoluminescence from the **PHPIT** film, suggesting that charge transfer from the photoexcited polythiophene backbone to the electron-withdrawing phenanthrenyl-imidazole side chains was sufficiently rapid to compete with radiative

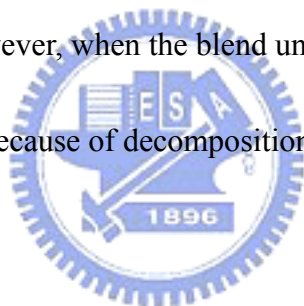


recombination of the excitons.<sup>[118, 127]</sup>



**Figure 4-1.** a) UV–Vis spectra of **P3HT/PCBM** as cast and **PHPIT/PCBM** annealed at 120 °C in the solid state, and the solar spectrum. b) CV bandgap data for **PHPIT**, **PEDOT**, **PCBM**, **Al**, and **ITO**.

Figure 4-2 displays the photocurrents of diodes having the structure ITO/PEDOT:PSS/polymer:PCBM (1:1, w/w)/Ca/Al that were illuminated at 100 mW/cm<sup>2</sup> under AM 1.5G, as well as their dark currents. Table 4-1 lists the short-circuit current densities ( $J_{sc}$ ), open-circuit voltages, and power conversion efficiencies of these heterojunction polymer solar cells. The value of  $J_{sc}$  for the device incorporating the PHPIT/PCBM blend improved to 11.3 mA/cm<sup>2</sup> from 8.3 mA/cm<sup>2</sup> after the annealing time at 120 °C was increased from 20 to 30 min, probably because of improved ordering of the blend structure. The value of  $J_{sc}$  of the device decreased to 7.8 mA/cm<sup>2</sup>, however, when the blend underwent thermal treatment at 120 °C for 45 min, probably because of decomposition of the polymer structure.



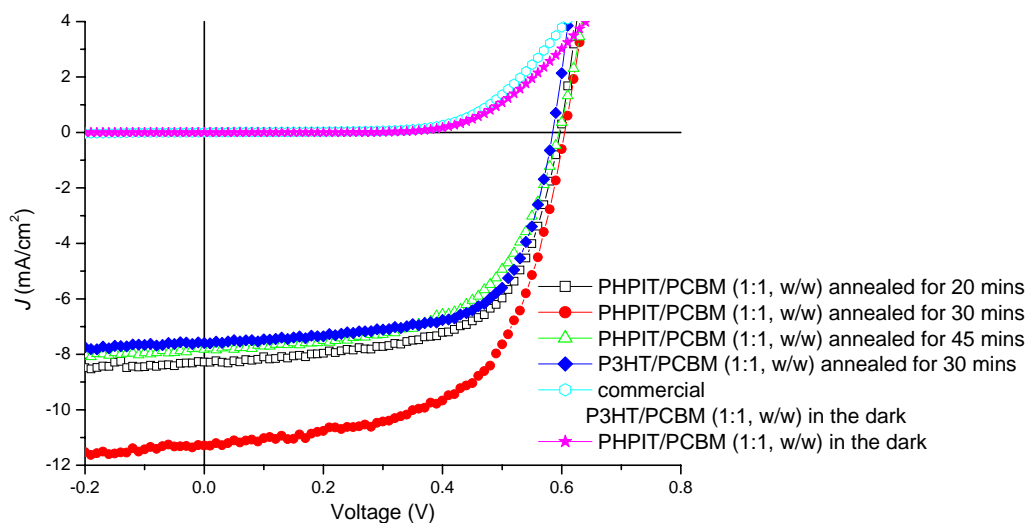


**Figure 4-2.** Current–voltage characteristics of illuminated (AM 1.5G, 100 mW/cm<sup>2</sup>)

polymer/PCBM (1:1, w/w) solar cells.

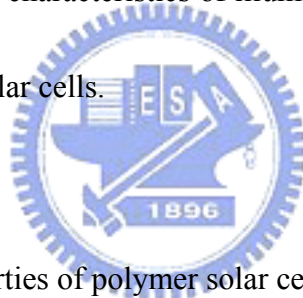
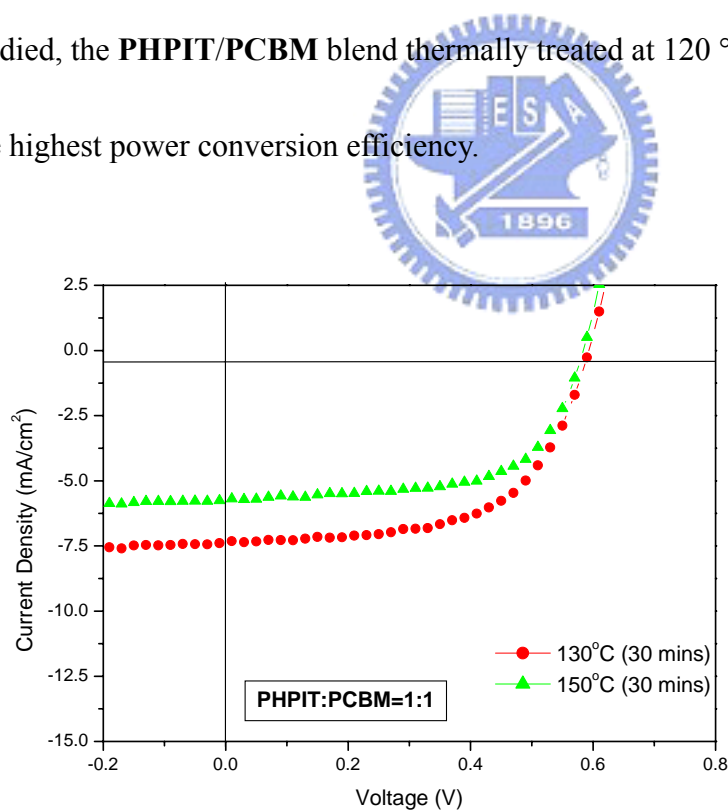


**Table 4-1.** Photovoltaic properties of polymer solar cells annealed at 120 °C for

various lengths of time and of **P3HT/PCBM** annealed at 120 °C for 30 min.

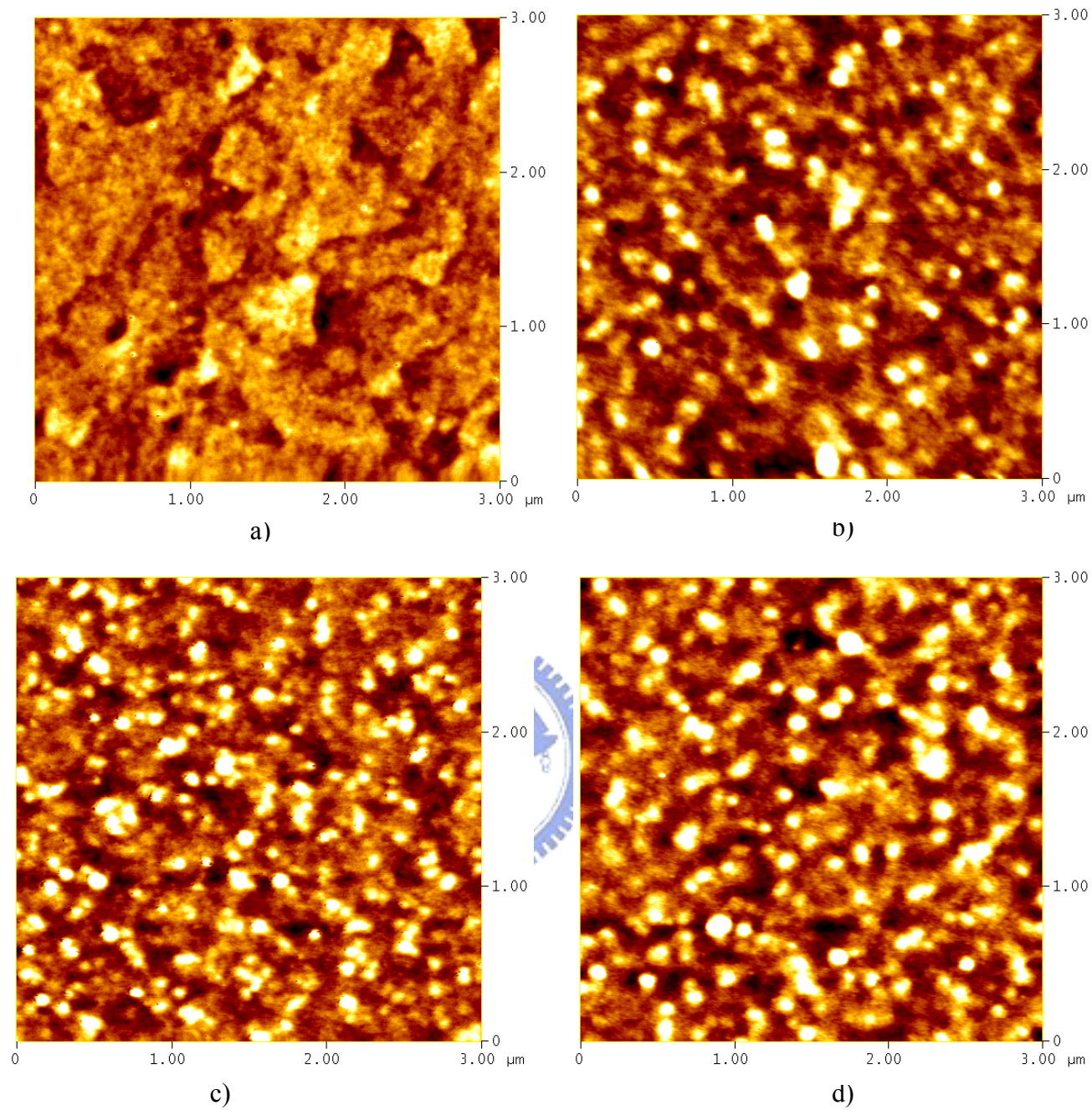
Blend annealing at 120 °C	$V_{oc}$ (V)	$J_{sc}$ (mA/cm <sup>2</sup> )	Fill Factor (%)	PCE (%)
<b>PHPIT/PCBM</b> (1:1, w/w) for 20 min	0.6	8.3	62	3.1
<b>PHPIT/PCBM</b> (1:1, w/w) for 30 min	0.61	11.3	60	4.1
<b>PHPIT/PCBM</b> (1:1, w/w) for 45 min	0.61	7.8	58	2.7
<b>P3HT/PCBM</b> (1:1, w/w) for 30 min	0.58	7.6	66	2.9

Figure 4-3 presents the device characteristics of the blends that we subjected to annealing at temperatures of 130 and 150 °C. The short-circuit current density ( $J_{sc}$ ) increased upon decreasing the annealing time, probably as a consequence of polymer decomposition.<sup>[128]</sup> Compared with our findings in a previous study, however, the fill factors were greater, because of improved solubility, when the trihexyl groups were present on the phenanthrenyl-imidazole moieties. The power conversion efficiencies were 2.6 and 2.1% for the devices incorporating samples annealed at 130 °C for 30 min and at 150 °C for 30 min, respectively; among all of the systems we studied, the **PHPIT/PCBM** blend thermally treated at 120 °C for 30 min exhibited the highest power conversion efficiency.



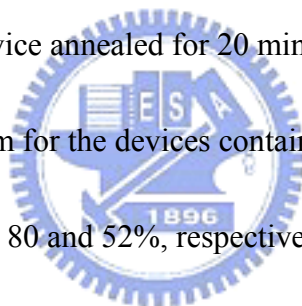
**Figure 4-3.** Photocurrents of diodes having the structure ITO/PEDOT:PSS/**PHPIT:PCBM** (1:1, w/w)/Ca/Al that were illuminated at AM 1.5G and 100 mW/cm<sup>2</sup> after annealing at various temperatures for 30 min.

From atomic force microscopy images (See Figure 4-4), we found that the root-mean-square roughness of the **PHPIT/PCBM** film (2.27 nm) annealed at 120 °C for 30 min was larger than those (1.94 and 1.76 nm) of the **PHPIT/PCBM** films annealed at 120 °C for 20 and 45 min. Hence, we suspect that the rough surface effectively reduced the charge-transport distance while providing a nanoscaled texture that further enhanced internal light absorption.<sup>[114b,129, 130b]</sup> The power conversion efficiency of the device incorporating **PHPIT/PCBM** increased dramatically to 4.1% from 3.1% when the annealed time at 120 °C was increased from 30 to 20 min, but it decreased to 2.7% when annealed for 45 min, presumably because of decomposition of the polymer.<sup>[115c, 130]</sup> We performed a control experiment in which we subjected commercially available high-molecular-weight **P3HT** (Mn = ca. 33,000 about 200 repeating units) to the same annealing conditions as those experienced by **PHPIT**. The power conversion efficiency of the device incorporating commercially available **P3HT** and **PCBM** was 2.9% (Figure 4-2). Thus, although thermal treatment at 120 °C for 30 min is optimal for **PHPIT/PCBM**, it is not necessarily the case for commercial **P3HT/PCBM**.



**Figure 4-4.** Atomic force microscopy (AFM) images of **PHPIT/PCBM** films a) as cast and annealed at 120 °C for b) 20, c) 30, and d) 45 min.

We investigated the photophysics of the devices incorporating the synthesized copolymers by determining their external quantum efficiencies (EQEs). Figure 4-5 displays the EQEs of the **PHPIT/PCBM** devices in which the blends were annealed at 120 °C for various annealing times. At wavelengths from 400 to 650 nm, the absolute EQEs of the device prepared from **PHPIT/PCBM** annealed at 120 °C for 30 min were ca. 20% higher than those of the corresponding blends annealed for 20 and 45 min. For example, the EQE at an incident wavelength of 400 nm for the device incorporating **PHPIT/PCBM** annealed at 120 °C for 30 min improved to 79% from 53% for the corresponding device annealed for 20 min device—an increase of 50%. The maximum EQEs at 460 nm for the devices containing **PHPIT** annealed at 120°C for 30 and 20 min device were 80 and 52%, respectively—a 53% increase for the former over the latter; at a much longer wavelength of 620 nm, the corresponding values were 48 and 30%, respectively—almost a 60% increase.



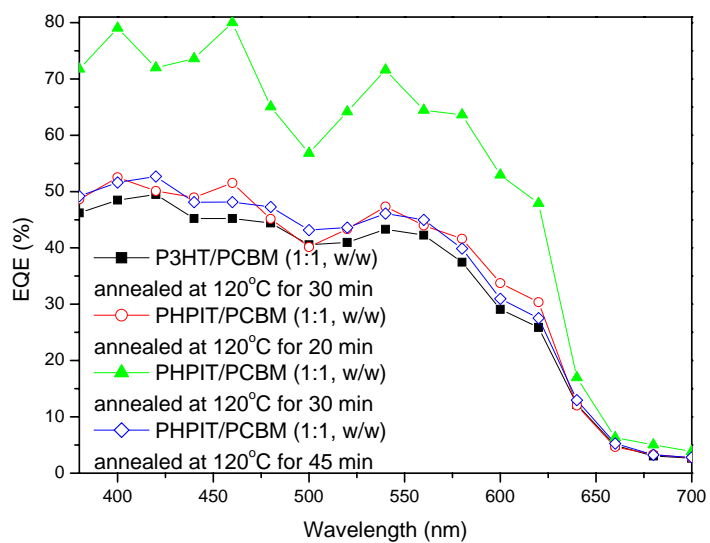


**Figure 4-5.** EQEs of devices containing polythiophene side-chain-tethered

hexylphenanthrenyl-imidazole/PCBM blends (1:1, w/w) annealed at 120 °C for

various times.

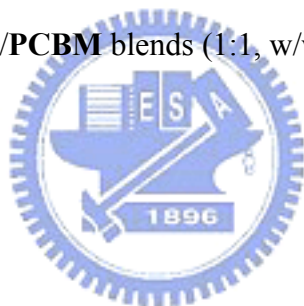
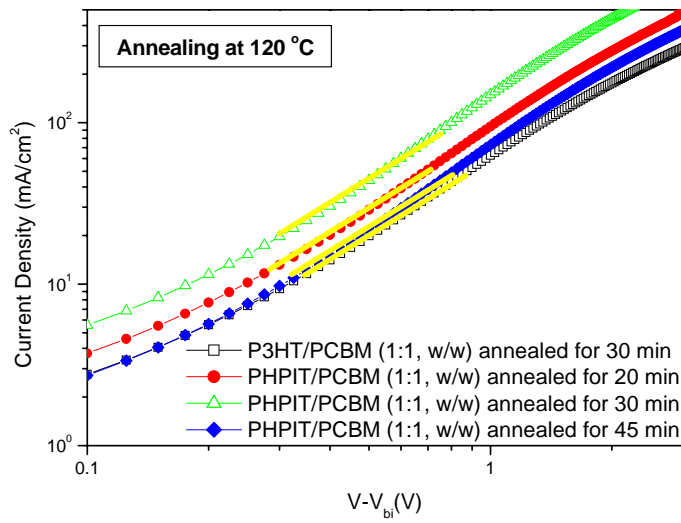




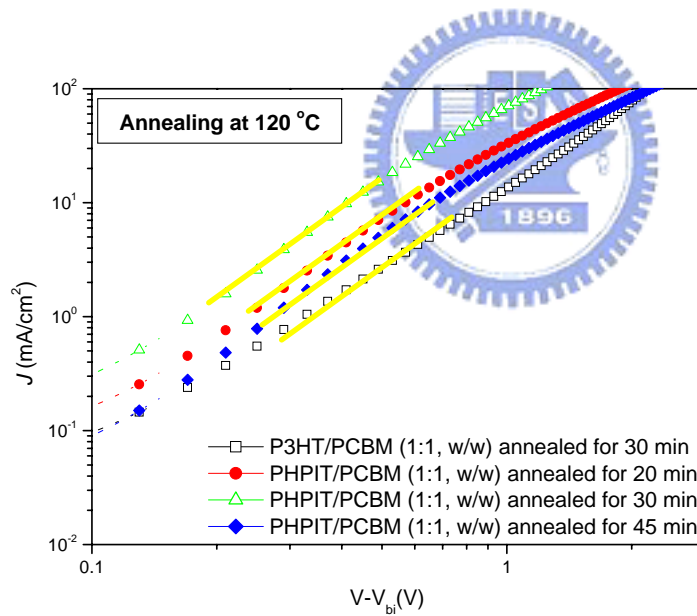
Figure 4-6 displays the dark  $J$ - $V$  curves for electron- and hole-dominated carrier devices. The electron and hole mobilities were determined by fitting the dark  $J$ - $V$  curves into the space-charge-limited current (SCLC) model for electron- and hole-dominated carrier devices based upon the equation

$$J = 9\varepsilon_0\varepsilon_r\mu_{h(e)}V^2/8L^3 \quad (1)$$

where  $\varepsilon_0$  is the permittivity of free space,  $\varepsilon_r$  is the dielectric constant of the polymer,  $\mu_{h(e)}$  is the hole (electron) mobility,  $V$  is the voltage drop across the device, and  $L$  is the polymer thickness.<sup>[131]</sup> Table 4-2 lists the hole mobilities, electron mobilities, and the ratio of hole and electron mobilities that are determined from Figure 4-6 and equation (1). We obtained hole mobilities for the **PHPIT/PCBM** system (from  $6.5 \times 10^{-6}$  to  $1.9 \times 10^{-5} \text{ cm}^2 \text{ V}^{-1} \text{ s}^{-1}$ ) that were ca. three to 10 times greater than that of the **P3HT/PCBM** system ( $1.8 \times 10^{-6} \text{ cm}^2 \text{ V}^{-1} \text{ s}^{-1}$ ) when both blends experienced the same thermal treatment. The device containing the **PHPIT/PCBM** blend annealed at 120 °C for 30 min exhibited the highest mobility, indicating that more-ordered **PHPIT/PCBM** films facilitate hole transport. Thus, the lowest electron-to-hole mobility ratio for the **PHPIT/PCBM** blend results in a highest photocurrent.<sup>[113b]</sup>



a)



b)

**Figure 4-6.** Dark  $J$ - $V$  curves for a) electron- and b) hole-dominated carrier devices incorporating **PHPIT/PCBM** (1:1, w/w) annealed at 120 °C for various times.

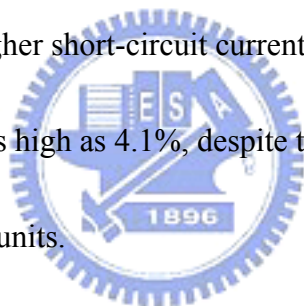
**Table 4-2.** Hole mobilities, electron mobilities, and hole-to-electron-mobility ratios of **P3HT/PCBM** annealed at 120 °C for 30 min and **PHPIT/PCBM** annealed at 120 °C for various lengths of time.

Blend annealing at 120 °C	Hole mobility ( $\mu_h$ , $\text{cm}^2/\text{Vs}$ )	Electron mobility ( $\mu_e$ , $\text{cm}^2/\text{Vs}$ )	$\mu_e/\mu_h$
<b>P3HT/PCBM</b> (1:1, w/w) for 30 min	$1.8 \pm 0.1 \times 10^{-6}$	$1.8 \pm 0.1 \times 10^{-5}$	10
<b>PHPIT/PCBM</b> (1:1, w/w) for 20 min	$9.0 \pm 0.3 \times 10^{-6}$	$2.6 \pm 0.1 \times 10^{-5}$	2.9
<b>PHPIT/PCBM</b> (1:1, w/w) for 30 min	$1.9 \pm 0.1 \times 10^{-5}$	$4.2 \pm 0.1 \times 10^{-5}$	2.2
<b>PHPIT/PCBM</b> (1:1, w/w) for 45 min	$6.5 \pm 0.1 \times 10^{-6}$	$2.1 \pm 0.1 \times 10^{-5}$	3.2



#### **4-4. Conclusions**

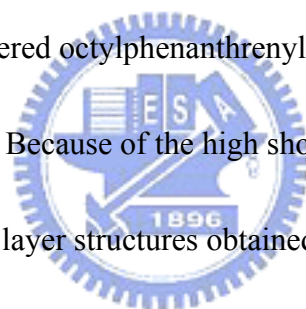
In summary, we have synthesized **PHPIT**, a new kind of intramolecular D–A side-chain-tethered hexylphenanthrenyl-imidazole polythiophene. The visible light absorption of the **PHPIT/PCBM** blend is enhanced by the presence of the electron-withdrawing hexylphenanthrenyl-imidazole. The EQE of the device was maximized when the **PHPIT/PCBM** blend experienced annealing at 120 °C for 30 min. The more-balanced electron and hole mobilities and the enhanced visible and internal light absorptions in the devices consisting of annealed **PHPIT/PCBM** blends both contributed to a much higher short-circuit current density, which in turn led to a power conversion efficiency as high as 4.1%, despite the fact that **PHPIT** is only comprised of ca. 20 repeating units.



## Chapter 5. Conclusions

In this dissertation, we synthesized a series of polythiophene derivatives to study their photovoltaic characteristics. First of all, we have used Grignard metathesis polymerization to successfully synthesize a series of regioregular polythiophene copolymers that contain electron-withdrawing and conjugated phenanthrenyl-imidazole moieties as side chains. The reduction in the bandgap energy in conjunction with the observed photoluminescence quenching indicates that rapid charge transfer occurred from the photoexcited polythiophene backbone through the phenanthrenyl-imidazole moieties to PCBM in the device. The much higher external quantum efficiency of the polythiophene-side-chain-tethered phenanthrenyl-imidazole device than that of pure poly(3-octylthiophene) device results in much higher short circuit current density. Due to the high short circuit current density obtained in the phenanthrenyl-imidazole presenting regioregular poly(3-octylthiophene), the power conversion efficiency improved dramatically to 2.80% for the copolymer containing 80 mol % phenanthrenyl-imidazole from 1.22% for pure poly(3-octylthiophene). Second, intramolecular donor-acceptor structures prepared by binding conjugated octylphenanthrenyl-imidazole moieties covalently onto the side chains of regioregular poly(3-hexylthiophene)s exhibit lowered bandgaps and enhanced electron transfer. The reduction in the bandgap energy in

conjunction with photoluminescence quenching indicates that rapid charge transfer occurred in the device from the photoexcited polythiophene backbone, through the octylphenanthrenyl-imidazole moieties, to the **PCBM** units. The ratios of the net electron transfer rate constant to the quenching rate constant at different wavelengths were much higher for the copolymer incorporating 90 mol% octylphenanthrenyl-imidazole moieties/**PCBM** than for **P3HT/PCBM**, indicating that electron transfer probability in the former case was greatly favored over that of the latter. The high external quantum efficiency of the device that incorporates the polythiophene-side-chain-tethered octylphenanthrenyl-imidazole results in its high short-circuit current density. Because of the high short-circuit current density as well as more organized active layer structures obtained for the octylphenanthrenyl-imidazole presenting regioregular poly(3-hexylthiophene), the power conversion efficiency improved dramatically to 3.45% for the copolymer containing 90 mol% octylphenanthrenyl-imidazole. Finally, we have synthesized **PHPIT**, a new kind of intramolecular D–A side-chain-tethered hexylphenanthrenyl-imidazole polythiophene. The visible light absorption of the **PHPIT/PCBM** blend is enhanced by the presence of the electron-withdrawing hexylphenanthrenyl-imidazole. The EQE of the device was maximized when the **PHPIT/PCBM** blend experienced annealing at 120 °C for 30 min. The



more-balanced electron and hole mobilities and the enhanced visible and internal light absorptions in the devices consisting of annealed **PHPIT/PCBM** blends both contributed to a much higher short-circuit current density, which in turn led to a power conversion efficiency as high as 4.1%, despite the fact that **PHPIT** is only comprised of ca. 20 repeating units.



## References

- [1] B. A. Gregg, *J. Phys. Chem. B* **2003**, *107*, 4688 – 4698.
- [2] C. W. Tang, *Appl. Phys. Lett.* **1986**, *48*, 183 – 184.
- [3] W. Ma, C. Yang, X. Gong, K. Lee, A. J. Heeger, *Adv. Funct. Mater.* **2005**, *15*, 1617.
- [4] G. Li, V. Shrotriya, J. Huang, Y. Yao, T. Moriarty, K. Emery, Y. Yang, *Nat. Mater.* **2005**, *4*, 864 – 868.
- [5] M. Reyes-Reyes, K. Kim, D. L. Carroll, *Appl. Phys. Lett.* **2005**, *87*, 083506.
- [6] J. Xue, B. P. Rand, S. Uchida, S. R. Forrest, *J. Appl. Phys.* **2005**, *98*, 124903.
- [7] J. Xue, B. P. Rand, S. Uchida, S. R. Forrest, *Adv. Mater.* **2005**, *17*, 66.
- [8] J. Xue, S. Uchida, B. P. Rand, S. R. Forrest, *Appl. Phys. Lett.* **2004**, *84*, 3013.
- [9] N. S. Sariciftci, D. Braun, C. Zhang, V. I. Srdanov, A. J. Heeger, G. Stucky, F. Wudl, *Appl. Phys. Lett.* **1993**, *62*, 585.
- [10] M. Granstrom, K. Petritsch, A. C. Arias, A. Lux, M. R. Andersson, R. H. Friend, *Nature* **1998**, *395*, 257.
- [11] P. Peumans, A. Yakimov, S. R. Forrest, *J. Appl. Phys.* **2003**, *93*, 3693.
- [12] J. J. M. Halls, C. A. Walsh, N. C. Greenham, E. A. Marseglia, R. H. Friend, S. C. Moratti, A. B. Holmes, *Nature* **1995**, *376*, 498.
- [13] G. Yu, A. J. Heeger, *J. Appl. Phys.* **1995**, *78*, 4510.



- [14] C. J. Brabec, N. S. Sariciftci, J. C. Hummelen, *Adv. Funct. Mater.* **2001**, *11*, 15.
- [15] R. Koeppe, N. S. Sariciftci, *Photochem. Photobiol. Sci.* **2006**, *5*, 1122.
- [16] *Photoinduced Electron Transfer* (Eds.: M. A. Fox, M. Chanon), Elsevier, Amsterdam, **1988**.
- [17] H. Hoppe, N. S. Sariciftci, *J. Mater. Res.* **2004**, *19*, 1924.
- [18] C. J. Brabec, A. Cravino, D. Meissner, N. S. Sariciftci, T. Fromherz, M. T. Rispens, L. Sanchez, J. C. Hummelen, *Adv. Funct. Mater.* **2001**, *11*, 374.
- [19] A. Gadisa, M. Svensson, M. R. Andersson, O. Inganäs, *Appl. Phys. Lett.* **2004**, *84*, 1609.
- [20] L. J. A. Koster, V. D. Mihailetschi, P.W. M. Blom, *Appl. Phys. Lett.* **2006**, *88*, 093511.
- [21] M. C. Scharber, D. Mühlbacher, M. Koppe, P. Denk, C. Waldauf, A. J. Heeger, C. J. Brabec, *Adv. Funct. Mater.* **2006**, *18*, 789.
- [22] B. C. Thompson, Y. G. Kim, T. D. McCarley, J. R. Reynolds, *J. Am. Chem. Soc.* **2006**, *128*, 12714.
- [23] C. Soci, I.-W. Hwang, D. Moses, Z. Zhu, D. Waller, R. Gaudiana, C. J. Brabec, A. J. Heeger, *Adv. Funct. Mater.* **2007**, *17*, 632.
- [24] K. M. Coakley, M. D. McGehee, *Chem. Mater.* **2004**, *16*, 4533.
- [25] S. Gunes, H. Neugebauer, N. S. Sariciftci, *Chem. Rev.* **2007**, *107*, 1324.

- [26] J. Hou, Z. Tan, Y. Yan, Y. He, C. Yang, Y. Li, *J. Am. Chem. Soc.* **2006**, *128*, 4911.
- [27] C. Winder, N. S. Sariciftci, *J. Mater. Chem.* **2004**, *14*, 1077.
- [28] C. J. Brabec, C. Winder, N. S. Sariciftci, J. C. Hummelen, A. Dhanabalan, P. A. van Hal, R. A. J. Janssen, *Adv. Funct. Mater.* **2002**, *12*, 709.
- [29] F. Zhang, K. G. Jespersen, C. Björström, M. Svensson, M. R. Andersson, V. Sundström, K. Magnusson, E. Moons, A. Yartsev, O. Inganäs *Adv. Funct. Mater.* **2006**, *16*, 667.
- [30] F. Zhang, W. Mammo, L. M. Andersson, S. Admassie, M. R. Andersson, O. Inganäs *Adv. Mater.* **2006**, *18*, 2169.
- [31] C. Shi, Y. Yao, Y. Yang, Q. Pei, *J. Am. Chem. Soc.* **2006**, *128*, 8980.
- [32] M. M. Wienk, M. G. R. Turbiez, M. P. Struijk, M. Fonrodona, R. A. J. Janssen, *Appl. Phys. Lett.* **2006**, *88*, 153511.
- [33] D. Mühlbacher, M. Scharber, M. Morana, Z. Zhu, D. Waller, R. Gaudiana, C. Brabec, *Adv. Mater.* **2006**, *18*, 2884.
- [34] H. A. M. van Mullekom, J. A. J. M. Vekemans, E. E. Havinga, E. W. Meijer, *Mater. Sci. Eng. R.* **2001**, *32*, 1.
- [35] A. Gadisa, F. Zhang, D. Sharma, M. Svensson, M. R. Andersson, O. Inganäs, *Thin Solid Films* **2007**, *515*, 3126.
- [36] L. M. Popescu, P. vanRt Hof, A. B. Sieval, H. T. Jonkman, J. C. Hummelen, *Appl.*

*Phys. Lett.* **2006**, 89, 213507.

[37] I. Riedel, E. von Hauff, J. Parisi, N. Martin, F. Giacalone, V. Dyakonov, *Adv.*

*Funct. Mater.* **2005**, 15, 1979.

[38] S. Backer, K. Sivula, D. F. Kavulak, J. M. J. Fréchet, *Chem. Mater.* **2007**, 19,  
2927.

[39] J. Roncali, *Chem. Rev.* **1997**, 97, 173.

[40] G. Zerza, M. C. Scharber, C. J. Brabec, N. S. Sariciftci, R. Gómez, J. L. Segura,  
Martín, N. V. I. Srdanov, *J. Phys. Chem. A.* **2000**, 104, 8315.

[41] a) C. Ego, D. Marsitzky, S. Becker, J. Zhang, A. C. Grimsdale, K. Müllen, J. D.

MacKenzie, C. Silva, R. H. Friend, *J. Am. Chem. Soc.* **2003**, 125, 437. b) J. Pei,

W. Yu, J. Ni, Y. Lai, W. Huang, A. J. Heeger, *Macromolecules* **2001**, 34, 7241.

[42] J. H. A. Smits, S. C. J. Meskers, R. A. J. Janssen, A. W. Marsman, D. M. D.

Leeuw, *Adv. Mater.* **2005**, 17, 1169.

[43] a) J. Liu, E. N. Kadnikova, Y. Liu, M. D. McGehee, J. M. J. Fréchet, *J. Am.*

*Chem. Soc.* **2004**, 126, 9486. b) J. Liu, T. Tanaka, K. Sivula, A. P. Alivisatos, J. M.

J. Fréchet, *J. Am. Chem. Soc.* **2004**, 126, 6550. c) A. M. Ramos, M. T. Rispens, J.

K. J. V. Duren, J. C. Hummelen, R. A. J. Janssen, *J. Am. Chem. Soc.* **2001**, 123,

6714. d) P. Schilinsky, U. Asawapirom, U. Scherf, M. Biele, C. J. Brabec, *Chem.*

*Mater.* **2005**, 17, 2175.

- [44] G. Yu, J. Gao, J. C. Hummelen, F. Wudl, A. J. Heeger, *Science* **1995**, 270, 1789.
- [45] W. U. Huynh, J. J. Dittmer, A. P. Alivisatos, *Science* **2002**, 295, 2425.
- [46] K. M. Coakley, M. D. McGehee, *Chem. Mater.* **2004**, 16, 4533.
- [47] T. J. Savenije, J. E. Kroeze, X. Yang, J. Loos, *Adv. Funct. Mater.* **2005**, 15, 1260.
- [48] Y. Liu, M. A. Summers, C. Edder, J. M. J. Fréchet, M. D. McGehee, *Adv. Mater.* **2005**, 17, 2960.
- [49] V. D. Mihaiketchi, H. Xie, B. D. Boer, L. J. A. Koster, P. W. M. Blom, *Adv. Funct. Mater.* **2006**, 16, 699.
- [50] J. Hou, Z. Tan, Y. Yan, Y. He, C. Yang, Y. F. Li, *J. Am. Chem. Soc.* **2006**, 128, 4911.
- [51] K. Sivula, Z. T. Ball, N. Watanabe, J. M. J. Fréchet, *Adv. Mater.* **2006**, 18, 206.
- [52] G. Li, V. Shortriya, J. Huang, Y. Yao, T. Moriarty, K. Emery, Y. Yang, *Nature Mater.* **2005**, 4, 864.
- [53] T. Erb, U. Zhokhavets, G. Gobsch, S. Raleva, B. Stühn, P. Schilinsky, C. Waldauf, C. J. Brabec, *Adv. Funct. Mater.* **2005**, 15, 1193.
- [54] K. M. Coakley, M. D. McGehee, *Chem. Mater.* **2004**, 16, 4533.
- [55] J. Roncali, *Chem. Rev.* **1997**, 97, 173.
- [56] S. Hotta, S. D. D. V. Rughooputh, A. J. Heeger, *Synth. Met.* **1987**, 22, 79.
- [57] a) R. D. McCullough, R. D. Lowe, M. Jayaraman, D. L. Anderson, *J. Org. Chem.*

- 1993**, 58, 904. b) M. C. Iovu, E. E. Sheina, R. R. Gil, R. D. McCullough,  
*Macromolecules* **2005**, 38, 8649. c) E. E. Sheina, S. M. Khersonsky, E. G. Jones,  
R. D. McCullough, *Chem. Mater.* **2005**, 17, 3317.
- [58] A. R. Murphy, J. Liu, C. Luscombe, D. Kavulak, J. M. J. Fréchet, R. J. Kline, M.  
D. McGehee, *Chem. Mater.* **2005**, 17, 4892.
- [59] M. Sato, T. Shimizu, A. Yamauchi, *Makromol. Chem.* **1990**, 191, 313.
- [60] M. Sato, H. Morii, *Macromolecules* **1991**, 24, 1196.
- [61] F. Giacalone, J. L. Segura, N. Martin, M. Catellani, S. Luzzati, N. Lupsac, *Org.*  
*Lett.* **2003**, 5, 1669.
- [62] C. Waldauf, P. Schilinsky, J. Hauch, C. J. Brabec, *Thin Solid Films* **2004**,  
451–452, 503.
- [63] M. C. Scharber, D. Mühlbacher, M. Kopper, P. Denk, C. Waldauf, A. J. Heeger, C.  
J. Brabec, *Adv. Mater.* **2006**, 18, 789.
- [64] J. Liu, Y. Shi, Y. Yang, *Adv. Funct. Mater.* **2001**, 11, 420.
- [65] W. Ma, C. Yang, X. Gong, K. Lee, A. J. Heeger, *Adv. Funct. Mater.* **2005**, 15,  
1617.
- [66] a) C. Ego, D. Marsitzky, S. Becker, J. Zhang, A. C. Grimsdale, K. Müllen, J. D.  
MacKenzie, C. Silva, R. H. Friend, *J. Am. Chem. Soc.* **2003**, 125, 437. b) J. Pei, W.  
Yu, J. Ni, Y. Lai, W. Huang, A. J. Heeger, *Macromolecules* **2001**, 34, 7241. c) F.



- Zhang, E. Perzon, X. J. Wang, W. Mammo, M. R. Andersson, O. Inganäs, *Adv. Funct. Mater.* **2005**, *15*, 745. d) O. Inganäs, M. Svensson, F. Zhang, A. Gadisa, N. K. Persson, X. Wang, M. R. Andersson, *Appl. Phys. A: Mater. Sci. Process.* **2004**, *79*, 31. e) M. Y. Chiu, U. S. Jeng, C. H. Su, K. S. Liang, K. H. Wei *Adv. Mater.* **2008**, *20*, 2573.
- [67] J. H. A. Smits, S. C. J. Meskers, R. A. J. Janssen, A. W. Marsman, D. M. D. Leeuw, *Adv. Mater.* **2005**, *17*, 1169.
- [68] G. Yu, J. Gao, J. C. Hummelen, F. Wudl, A. J. Heeger, *Science* **1995**, *270*, 1789.
- [69] W. U. Huynh, J. J. Dittmer, A. P. Alivisatos, *Science* **2002**, *295*, 2425.
- [70] K. M. Coakley, M. D. McGehee, *Chem. Mater.* **2004**, *16*, 4533.
- [71] T. J. Savenije, J. E. Kroeze, X. Yang, J. Loos, *Adv. Funct. Mater.* **2005**, *15*, 1260.
- [72] Y. Liu, M. A. Summers, C. Edder, J. M. J. Fréchet, M. D. McGehee, *Adv. Mater.* **2005**, *17*, 2960.
- [73] a) C. J. Brabec, N. S. Sariciftci, J. C. Hummelen, *Adv. Funct. Mater.* **2001**, *11*, 15.  
b) S. C. Ng, H.-F. Lu, H. S. O. Chan, A. Fujii, T. Laga, K. Yoshino, *Adv. Mater.* **2000**, *12*, 1122. c) Z. Bao, Z. Peng, M. E. Galvin, E. A. Chandross, *Chem. Mater.* **1998**, *10*, 1201. d) S. Son, A. Dodabalapur, A. J. Lovinger, M. E. Galvin, *Science* **1995**, *269*, 376.
- [74] a) T. Yoshihara, S. I. Druzhinin, K. A. Zachariasse *J. Am. Chem. Soc.* **2004**, *126*,

8535. b) A. Escosura, M. V. Martínez-Díaz, D. M. G. T. Torres, *J. Am. Chem. Soc.* **2006**, *128*, 4112. c) E. H. A. Beckers, S. C. J. Meskers, A. P. H. J. Schenning, Z. Chen, F. Würthner, P. Marsal, D. Beljonne, J. Cornil, R. A. J. J. Janssen, *Am. Chem. Soc.* **2006**, *128*, 649. d) A. M. Ramos, S. C. J. Meskers, E. H. A. Beckers, R. B. Prince, L. Brunsveld, R. A. J. Janssen, *J. Am. Chem. Soc.* **2004**, *126*, 9630. e) D. M. Guldi, A. Swartz, C. Luo, R. Gómez, J. L. Segura, N. Martin, *J. Am. Chem. Soc.* **2002**, *124*, 10875. f) P. Samorí, X. Yin, N. Tchebotareva, Z. Wang, T. Pakula, F. Jäckel, M. D. Watson, A. Venturini, K. Müllen, J. P. Rabe, *J. Am. Chem. Soc.* **2004**, *126*, 3567. g) V. Lemaire, M. Steel, D. Beljonne, J.-L. Brédas, J. Cornil, *J. Am. Chem. Soc.* **2005**, *127*, 6077. h) M. L. Kirk, D. A. Shultz, E. C. Depperman, C. L. Brannen, *J. Am. Chem. Soc.* **2007**, *129*, 1937. i) S. Handa, F. Giacalone, S. A. Haque, E. Palomares, N. Martin, J. R. Durrant, *Chem. Eur. J.* **2005**, *11*, 7440.
- [75] W. J. E. Beek, M. M. Wienk, R. A. J. Janssen, *Adv. Funct. Mater.* **2006**, *16*, 1112.
- [76] Z. Zhu, D. Waller, R. Gaudiana, M. Morana, D. Mühlbacher, M. Scharber, C. J. Brabec, *Macromolecules* **2007**, *40*, 1981.
- [77] a) Z. Tan, J. H. Hou, Y. J. He, E. Zhou, C. Yang, Y. F. Li, *Macromolecules* **2007**, *40*, 1868. b) A. Cravino, N. S. Sariciftci, *J. Mater. Chem.* **2002**, *12*, 1931. c) A. Cravino, G. Zerza, M. Maggini, S. Bucella, M. Svewnsson, M. R. Andersson, H. Neugebauer, N. S. Sariciftci, *Chem. Commun.* **2000**, *24*, 2487. d) A. Marcos

Ramos, M. T. Rispens, J. C. Hummelen, R. A. J. Janssen, *Synth. Met.* **2001**, *119*, 171. e) F. Zhang, M. Svensson, M. R. Andersson, M. Maggini, S. Bucella, E. Menna, O. Inganäs, *Adv. Mater.* **2001**, *13*, 1871. f) A. Marcos Ramos, M. T. Rispens, J. K. J. Van Duren, J. C. Hummelen, R. A. J. Janssen, *J. Am. Chem. Soc.* **2001**, *123*, 6714. g) F. Giacalone, N. Martin, *Chem. Rev.* **2006**, *106*, 5136. h) X. Wang, E. Perzon, F. Oswald, F. Langa, S. Admassie, M. R. Andersson, O. Inganäs, *Adv. Funct. Mater.* **2005**, *15*, 1665. i) X. J. Wang, E. Perzon, J. L. Delgado, P. de la Cruz, F. Zhang, F. Langa, M. R. Andersson, O. Inganäs, *Appl. Phys. Lett.* **2004**, *85*, 5081.

[78] V. D. Mihaiketchi, H. Xie, B. D. Boer, L. J. A. Koster, P. W. M. Blom, *Adv. Funct. Mater.* **2006**, *16*, 699.



[79] J. Hou, Z. Tan, Y. Yan, Y. He, C. Yang, Y. F. Li, *J. Am. Chem. Soc.* **2006**, *128*, 4911.

[80] K. Sivula, Z. T. Ball, N. Watanabe, J. M. J. Fréchet, *Adv. Mater.* **2006**, *18*, 206.

[81] a) G. Li, V. Shrotriya, Y. Yao, Y. Yang, *J. Appl. Phys.* **2005**, *98*, 043704. b) G. Li, V. Shrotriya, J. Huang, Y. Yao, T. Moriarty, K. Emery, Y. Yang, *Nat. Mater.* **2005**, *4*, 864.

[82] T. Erb, U. Zhokhavets, G. Gobsch, S. Raleva, B. Stühn, P. Schilinsky, C. Waldauf, C. J. Brabec, *Adv. Funct. Mater.* **2005**, *15*, 1193.



[83] I. Riedel, E. V. Hauff, J. Parisi, N. Martin, F. Giacalone, V. Dyakonov, *Adv. Funct.*

*Mater.* **2005**, *15*, 1979

[84] Y.-T. Chang, S.-L. Hsu, M.-H. Su, K.-H. Wei, *Adv. Funct. Mater.* **2007**, *17*, 3326.

[85] a) R. D. McCullough, R. D. Lowe, M. Jayaraman, D. L. Anderson, *J. Org. Chem.*

**1993**, *58*, 904. b) M. C. Iovu, E. E. Sheina, R. R. Gil, R. D. McCullough,

*Macromolecules* **2005**, *38*, 8649. c) E. E. Sheina, S. M. Khersonsky, E. G. Jones, R.

D. McCullough, *Chem. Mater.* **2005**, *17*, 3317.

[86] L.-Y. Luo, C.-F. Lo, C.-Y. Lin, I.-J. Chang, E. W.-G. Diau, *J. Phys. Chem. B* **2006**,

*110*, 410.

[87] American Society for Testing and Materials (ASTM) standard G173, “ Standard

Tables for Reference Solar Spectrum Irradiance: Direct Normal and

Hemispherical on 37° Tilted Surface.”

[88] A. R. Murphy, J. Liu, C. Luscombe, D. Kavulak, J. M. J. Fréchet, R. J. Kline, M.

D. McGehee, *Chem. Mater.* **2005**, *17*, 4892.

[89] J. Roncali, *Chem. Rev.* **1997**, *97*, 173.

[90] F. Giacalone, J. L. Segura, N. Martin, M. Catellani, S. Luzzati, N. Lupsac, *Org.*

*Lett.* **2003**, *5*, 1669.

[91] B. Valeur, *Molecular Fluorescence-Principles and Application*, 2nd Edn.;

Wiley-VCH: New York, 2002; pp. 172–173.

- [92] A. Matsuse, S. Takeuchi, K. Yoshino, T. Kobayashi, *Chem. Phys. Lett.*, **1998**, 288, 165.
- [93] J. G. Müller, J. M. Lupton, J. Feldmann, U. Lemmer, M. C. Scharber, N. C. Sariciftci, C. J. Brabec, U. Scherf, *Phys. Rev. B* **2005**, 72, 195208.
- [94] C. Waldauf, P. Schilinsky, J. Hauch, C. J. Brabec, *Thin Solid Films* **2004**, 451–452, 503.
- [95] V. Shrotriya, G. Li, Y. Yao, T. Moriarty, Y. Yang, K. Emery, *Adv. Funct. Mater.* **2006**, 16, 2016.
- [96] K. Emery, Handbook of Photovoltaic Science and Engineering, Eds: A. Luge, S. Hegedus, Wiley, Chichester, UK 2003, CH16.
- [97] a) P. Schilinsky, U. Asawapirom, U. Scherf, M. Biele, C. J. Brabec *Chem. Mater.* **2005**, 17, 2175. b) W. Ma, J. Y. Kim, K. Lee, A. J. Heeger *Macromol. Rapid Commun.* **2007**, 28, 1776.
- [98] A. Pivrikas, N. S. Sariciftci, G. Juška, R. Osterbacka *Prog. Photovolt: Res. Appl.* **2007**, 15, 677.
- [99] M. C. Scharber, D. Mühlbacher, M. Kopper, P. Denk, C. Waldauf, A.J. Heeger, C. J. Brabec, *Adv. Mater.* **2006**, 18, 789.
- [100] J. Liu, Y. Shi, Y. Yang, *Adv. Funct. Mater.* **2001**, 11, 420.
- [101] C. Shi, Y. Yao, Y. Yang, Q. Pei, *J. Am. Chem. Soc.* **2006**, 128, 8980.

- [102] W. Ma, C. Yang, X. Gong, K. Lee, A. J. Heeger, *Adv. Funct. Mater.* **2005**, *15*, 1617.
- [103] S. Berson, R. D. Bettignies, S. Bailly, S. Guillerez, *Adv. Funct. Mater.* **2007**, *17*, 1377.
- [104] a) C. Ego, D. Marsitzky, S. Becker, J. Zhang, A. C. Grimsdale, K. Müllen, J. D. MacKenzie, C. Silva, R. H. Friend, *J. Am. Chem. Soc.* **2003**, *125*, 437. b) J. Pei, W. Yu, J. Ni, Y. Lai, W. Huang, A. J. Heeger, *Macromolecules* **2001**, *34*, 7241. c) F. Zhang, E. Perzon, X. J. Wang, W. Mammo, M. R. Andersson, O. Inganäs, *Adv. Funct. Mater.* **2005**, *15*, 745. d) O. Inganäs, M. Svensson, F. Zhang, A. Gadisa, N. K. Persson, X. Wang, M. R. Andersson, *Appl. Phys. A: Mater. Sci. Process.* **2004**, *79*, 31. e) F. Zhang, M. Svensson, M. R. Andersson, M. Maggini, S. Bucella, E. Menna, O. Inganäs, *Adv. Mater.* **2001**, *13*, 1871. f) A. Marcos Ramos, M. T. Rispens, J. K. J. Van Duren, J. C. Hummelen, R. A. J. Janssen, *J. Am. Chem. Soc.* **2001**, *123*, 6714. g) F. Giacalone, N. Martin, *Chem. Rev.* **2006**, *106*, 5136. h) X. Wang, E. Perzon, F. Oswald, F. Langa, S. Admassie, M. R. Andersson, O. Inganäs, *Adv. Funct. Mater.* **2005**, *15*, 1665. i) X. J. Wang, E. Perzon, J. L. Delgado, P. de la Cruz, F. Zhang, F. Langa, M. R. Andersson, O. Inganäs, *Appl. Phys. Lett.* **2004**, *85*, 5081. j) M. Y. Chiu, U. S. Jeng, C. H. Su, K. S. Liang, K. H. Wei, *Adv. Mater.* **2008**, *20*, 2573. k) J. Huang, G. Li and Y. Yang,

- Adv. Mater.* **2008**, *20*, 415. l) R. J. Tseng, R. Chan, V. C. Tung, Y. Yang, *Adv. Mater.* **2008**, *20*, 435.
- [105] J. H. A. Smits, S. C. J. Meskers, R. A. J. Janssen, A. W. Marsman, D. M. D. Leeuw, *Adv. Mater.* **2005**, *17*, 1169.
- [106] G. Yu, J. Gao, J. C. Hummelen, F. Wudl, A. J. Heeger, *Science* **1995**, *270*, 1789.
- [107] a) W. U. Huynh, J. J. Dittmer, A. P. Alivisatos, *Science* **2002**, *295*, 2425. b) J. Liu, E. N. Kadnikova, Y. Liu, M. D. McGehee, J. M. J. Fréchet, *J. Am. Chem. Soc.* **2004**, *126*, 9486. c) J. Liu, T. Tanaka, K. Sivula, A. P. Alivisatos, J. M. J. Fréchet, *J. Am. Chem. Soc.* **2004**, *126*, 6550.
- [108] K. M. Coakley, M. D. McGehee, *Chem. Mater.* **2004**, *16*, 4533.
- [109] T. J. Savenije, J. E. Kroeze, X. Yang, J. Loos, *Adv. Funct. Mater.* **2005**, *15*, 1260.
- [110] Y. Liu, M. A. Summers, C. Edder, J. M. J. Fréchet, M. D. McGehee, *Adv. Mater.* **2005**, *17*, 2960.
- [111] V. D. Mihaiketchi, H. Xie, B. D. Boer, L. J. A. Koster, P. W. M. Blom, *Adv. Funct. Mater.* **2006**, *16*, 699.
- [112] J. Hou, Z. Tan, Y. Yan, Y. He, C. Yang, Y. F. Li, *J. Am. Chem. Soc.* **2006**, *128*, 4911.
- [113] K. Sivula, Z. T. Ball, N. Watanabe, J. M. J. Fréchet, *Adv. Mater.* **2006**, *18*, 206.
- [114] a) G. Li, V. Shrotriya, Y. Yao, Y. Yang, *J. Appl. Phys.* **2005**, *98*, 043704. b) G. Li,

- V. Shrotriya, J. Huang, Y. Yao, T. Moriarty, K. Emery, Y. Yang, *Nat. Mater.* **2005**, *4*, 864. c) G. Li, Y. Yao, H. Yang, V. Shrotriya, G. Yang, Y. Yang, *Adv. Funct. Mater.* **2007**, *17*, 1636.
- [115] a) T. Erb, U. Zhokhavets, G. Gobsch, S. Raleva, B. Stühn, P. Schilinsky, C. Waldauf, C. J. Brabec, *Adv. Funct. Mater.* **2005**, *15*, 1193. b) J. Y. Kim, K. Lee, N. E. Coates, D. Moses, T.-Q. Nguyen, M. Dante, A. J. Heeger, *Science* **2007**, *317*, 222. c) W. Ma, C. Yang, X. Gong, K. Lee, A. J. Heeger, *Adv. Funct. Mater.* **2005**, *15*, 1617. d) M. Reyes-Reyes, K. Kim, D. L. Carrolla, *Appl. Phys. Lett.* **2005**, *87*, 83506.
- [116] I. Riedel, E. V. Hauff, J. Parisi, N. Martin, F. Giacalone, V. Dyakonov, *Adv. Funct. Mater.* **2005**, *15*, 1979.
- [117] a) C. J. Brabec, N. S. Sariciftci, J. C. Hummelen, *Adv. Funct. Mater.* **2001**, *11*, 15. b) S. C. Ng, H.-F. Lu, H. S. O. Chan, A. Fujii, T. Laga, K. Yoshino, *Adv. Mater.* **2000**, *12*, 1122. c) Z. Bao, Z. Peng, M. E. Galvin, E. A. Chandross, *Chem. Mater.* **1998**, *10*, 1201.
- [118] a) Y.-T. Chang, S.-L. Hsu, M.-H. Su, K.-H. Wei, *Adv. Funct. Mater.* **2007**, *17*, 3326. b) Y.-T. Chang, S.-L. Hsu, M.-H. Su, K.-H. Wei, T.-A. Singh, E. W.-G. Diao, *Adv. Funct. Mater.* **2008**, *18*, 2356.
- [119] Z. Zhu, D. Waller, R. Gaudiana, M. Morana, D. Mühlbacher, M. Scharber, C. J.

- Brabec, *Macromolecules* **2007**, *40*, 1981.
- [120] J. I Nakamura, K. Murata, K. Takahashi, *Appl. Phys. Lett.* **2005**, *87*, 132105.
- [121] A. C. Arango, L. R. Johnson, V. N. Bliznyuk, Z. Schlesinger, S. A. Carter, H.-H. Hörhold, *Adv. Mater.* **2000**, *12*, 1689.
- [122] M. M. Mandoc, L. J. A. Koster, P. W. M. Blom, *Appl. Phys. Lett.* **2007**, *90*, 133504.
- [123] B. C. Thompson, J. M. J. Fréchet, *Angew. Chem. Int. Ed.* **2008**, *47*, 58.
- [124] a) E. H. A. Beckers, S. C. J. Meskers, A. P. H. J. Schenning, Z. Chen, F. Würthner, P. Marsal, D. Beljonne, J. Cornil, R. A. J. Janssen, *J. Am. Chem. Soc.* **2006**, *128*, 649. b) A. M. Ramos, S. C. J. Meskers, E. H. A. Beckers, R. B. Prince, L. Brunsveld, R. A. J. Janssen, *J. Am. Chem. Soc.* **2004**, *126*, 9630.
- [125] a) R. D. McCullough, R. D. Lowe, M. Jayaraman, D. L. Anderson, *J. Org. Chem.* **1993**, *58*, 904. b) M. C. Iovu, E. E. Sheina, R. R. Gil, R. D. McCullough, *Macromolecules* **2005**, *38*, 8649. c) E. E. Sheina, S. M. Khersonsky, E. G. Jones, R. D. McCullough, *Chem. Mater.* **2005**, *17*, 3317.
- [126] American Society for Testing and Materials (ASTM) standard G173, *Standard Tables for Reference Solar Spectrum Irradiance: Direct Normal and Hemispherical on 37° Tilted Surface*.
- [127] F. Giacalone, J. L. Segura, N. Martin, M. Catellani, S. Luzzati, N. Lupsac, *Org.*

- Lett.* **2003**, *5*, 1669.
- [128] C. Waldauf, P. Schilinsky, J. Hauch, C. J. Brabec, *Thin Solid Films* **2004**, *451–452*, 503.
- [129] S. Berson, R. D. Bettignies, S. Bailly, S. Guillerez, *Adv. Funct. Mater.* **2007**, *17*, 1377.
- [130] a) F. Padinger, R. S. Rittberger, N. S. Sariciftci, *Adv. Funct. Mater.* **2003**, *13*, 85.  
b) L. H. Nguyen, H. Hoppe, T. Erb, S. Günes, G. Gobsch, N. S. Sariciftci, *Adv. Funct. Mater.* **2007**, *17*, 1071.
- [131] a) P. W. M. Blom, M. J. M. de Jong, M. G. van Munster, *Phys. Rev. B* **1997**, *55*, R656. b) C. Goh, R. J. Kline, M. D. McGehee, *Appl. Phys. Lett.* **2005**, *86*, 122110. c) C. Melzer, E. J. Koop, V. D. Mihailetschi, P. W. M. Blom, *Adv. Funct. Mater.* **2004**, *14*, 865. d) V. R. Nikitenko, H. Heli, H. V. Seggern, *J. Appl. Phys.* **2003**, *94*, 2480. e) P. W. M. Blom, M. J. M. D. Jong, J. J. M. Vlegaar, *Appl. Phys. Lett.* **1996**, *68*, 3308. f) V. D. Mihailetschi, J. Wildeman, P. W. M. Blom, *Phys. Rev. Lett.* **2005**, *94*, 126602.

## Publications

**Yao-Te Chang**, So-Lin Hsu, Ming-Hsin Su, Kung-Hwa Wei “Intramolecular Donor–Acceptor Regioregular Poly(hexylphenanthrenyl-imidazole thiophene) Exhibits Enhanced Hole Mobility for Heterojunction Solar Cell Applications” *Advanced Materials*, **2009**, Accepted. (SCI ; IF:8.191)

**Yao-Te Chang**, So-Lin Hsu, Guan-Yu Chen, Ming-Hsin Su, Thounaojam Avinash Singh, Eric Wei-Guang Diao, Kung-Hwa Wei “Intramolecular Donor-Acceptor Regioregular Poly(3-hexylthiophene)s Presenting Octylphenanthrenyl-Imidazole Moieties Exhibit Enhanced Charge Transfer for Heterojunction Solar Cell Applications” *Advanced Functional Materials*, **2008**, *18*, 2356. (SCI ; IF 7.496)

**Yao-Te Chang**, So-Lin Hsu, Ming-Hsin Su, Kung-Hwa Wei Soluble Phenanthrenyl-Imidazole-Presenting Regioregular Poly(3-octylthiophene) Copolymers having Tunable Bandgaps for Solar Cell Applications, *Advanced Functional Materials*, **2007**, *17*, 3326. (SCI ; IF 7.496)

Siao-Wei Yeh, **Yao-Te Chang**, Chia-Hung Chou, Kung-Hwa Wei “Effect of Surface-Hydroxylated CdS Nanoparticles on the Morphological Transformation of Polystyrene-*block*-Poly(ethylene oxide) Thin Films” *Macromolecular Rapid Communications*, **2004**, *25*, 1679. (SCI ; IF 3.383)

**Yao-Te Chang**, Ching-Fong Shu, Chyi-Ming Leu, Kung-Hwa Wei “Synthesis and characterization of hyperbranched aromatic poly(ether imide)s with terminal amino groups” *Journal of Polymer Science: Part A: Polymer Chemistry*, **2003**, *41*, 3726. (SCI ; IF 3.529)

**Yao-Te Chang** and Ching-Fong Shu “Synthesis of hyperbranched aromatic poly(amide-imide): Copolymerization of B' B-2 monomer with A(2) monomer” *Macromolecules*, **2003**, *36*, 661. (SCI ; IF 4.411)

Leu Chyi-Ming, **Chang Yao-Te**, Wei Kung-Hwa “Synthesis and dielectric properties of polyimide-tethered polyhedral oligomeric silsesquioxane (POSS) nanocomposites via POSS-diamine” *Macromolecules*, **2003**, *36*, 9122. (SCI ; IF 4.411)

Chyi-Ming Leu, **Yao-Te Chang**, and Kung-Hwa Wei “Polyimide-Side-Chain Tethered Polyhedral Oligomeric Silsesquioxane Nanocomposites for Low-Dielectric Film Applications” *Chem. Mater.* **2003**, *15*, 3721. (SCI ; IF 4.883)



Chyi-Ming Leu, **Yao-Te Chang**, and Ching-Fong Shu “Synthesis and Characterization of Dendritic Poly(ether imide)s” *Macromolecules*, **2000**, *33*, 2855. (SCI ; IF 4.411)

## Patents

**Inventor:** KH Wei and **Yao-Te Chang**

**Title:** Soluble phenanthrenyl imidazole for photo-electrical conversion of solar cell.  
**Status:** US/Taiwan Patent application.

**Inventor:** KH Wei and **Yao-Te Chang**

**Title:** Intramolecular Donor-Acceptor Regioregular Poly(3-hexylthiophene)s Presenting Octylphenanthrenyl-Imidazole Moieties Exhibit Enhanced Charge Transfer for Heterojunction Solar Cell Applications.

**Status:** US/Taiwan Patent application.

**Inventor:** KH Wei and **Yao-Te Chang**

**Title:** Intramolecular Donor–Acceptor Regioregular Poly(hexylphenanthrenyl-imidazole thiophene) Exhibits Enhanced Hole Mobility for Heterojunction Solar Cell Applications.

**Status:** US/Taiwan Patent application.



## 學經歷資料

- 姓名：張耀德
- 性別：男
- 生日：民國 67 年 7 月 18 日，雲林人
- 聯絡電話：(學校) 03-5731771 (手機) 0921179430
- 通訊地址：新竹市大學路 1001 號  
國立交通大學材料與工程研究所  
永久地址：雲林縣林內鄉林南村 15 鄰中華巷 18 號



## 學歷

---

博士候選人：國立交通大學材料科學與工程學研究所	2002, 9 ~ 2009, 2
研究所：國立交通大學應用化學研究所	2000, 9 ~ 2002, 6
大學：國立交通大學應用化學系	1996, 9 ~ 2000, 6

## 專長

---

- 有機太陽能(solar cell)光電材料：
  1. 新穎之材料高分子設計及合成。
  2. 異質介面之有機太陽能元件製備。
- 有機/無機奈米複合材料：
  1. 低介電聚醯胺(PI)/無機物奈米複合材料。
  2. 低介電聚醯胺(PI)材料之設計與合成。
  3. 樹枝狀高分子材料之設計與合成。
  4. 高分支狀高分子材料之設計與合成。

### ■ 分析儀器操作：

真空手套箱(Dry Box)、Spin coater, 蒸鍍機, UV-Cleaner、元件封裝機、穿透式電子顯微鏡(TEM)、原子力顯微鏡(AFM)、拉曼光譜儀、紅外線光譜儀(FT-IR)、XRD、核磁共振光譜儀(Varian NMR and Bruker NMR)、微差掃描卡計(DSC)、熱重量分析儀(TGA)、質譜儀(Mass)、流變儀、凝膠滲透儀(GPC)、微光光譜儀(UV-Vis)、螢光光譜儀(PL)、循環伏安計(CV)、薄膜測厚儀( $\alpha$ -step)、奈米壓痕機(NIP)。